

CHEMICAL REVIEWS

Nanoscale Strategies for Light Harvesting

Simanta Kundu and Amitava Patra*

Department of Materials Science, Indian Association for the Cultivation of Science, Jadavpur, Kolkata 700032, India

ABSTRACT: Recent advances and the current status of challenging light-harvesting nanomaterials, such as semiconducting quantum dots (QDs), metal nanoparticles, semiconductor–metal heterostructures, π -conjugated semiconductor nanoparticles, organic–inorganic heterostructures, and porphyrin-based nanostructures, have been highlighted in this review. The significance of size-, shape-, and composition-dependent exciton decay dynamics and photoinduced energy transfer of QDs is addressed. A fundamental knowledge of these photophysical processes is crucial for the development of efficient light-harvesting systems, like photocatalytic and photovoltaic ones. Again, we have pointed out the impact of the metal-nanoparticle-based surface energy transfer process for developing light-harvesting systems. On the other hand, metal–semiconductor hybrid nanostructures are found to be very promising for photonic applications due to their exciton–plasmon interactions. Potential light-harvesting systems based on dye-doped π -conjugated semiconductor polymer nanoparticles and self-assembled structures of π -conjugated polymer are highlighted. We also discuss the significance of porphyrin-based nanostructures for potential light-harvesting systems. Finally, the future perspective of this research field is given.



CONTENTS

1. Introduction	712	5.2. Dye-Encapsulated π -Conjugated Semiconductor Nanoparticles	735
2. Basic Aspects of Energy Transfer Process in Nanoscale Systems	714	5.3. Self-Assembled π -Conjugated Semiconductor Nanostructures	737
3. QD-Based Light-Harvesting Systems	716	5.4. π -Conjugated Semiconductor Nanoparticle–QD Hybrid Systems	739
3.1. Decay Dynamics of QDs	716	6. Porphyrin-Based Functional Nanosystems for Light Harvesting	739
3.1.1. Kinetic Model for Decay Dynamics	716	6.1. Self-Assembled Porphyrin Nanostructures	740
3.1.2. Impact of QDs' Size	717	6.2. Porphyrin Composite Systems	741
3.1.3. Impact of QDs' Shape	718	7. Conclusions and Outlook	742
3.1.4. Alloy QDs	719	Author Information	743
3.1.5. Impact of QDs' Surface	720	Corresponding Author	743
3.2. QD-Based Energy Transfer Systems	721	Notes	743
3.2.1. Kinetic Model for QD-Based Energy Transfer	722	Biographies	743
3.2.2. Energy Transfer Based on Shape-, Size-, and Composition-Dependent QDs	722	Acknowledgments	743
3.3. QD-Based Light-Harvesting Applications	724	References	743
3.3.1. QD-Based Solar Cells	724		
3.3.2. Basic Aspects of Photocatalysis and H ₂ Generation	726		
4. Metal-Nanoparticle-Based Light-Harvesting Systems	726	1. INTRODUCTION	
4.1. Metal-Nanoparticle-Based Energy Transfer	729	The development of strategies for efficient conversion of solar energy to renewable energy is a challenging and active area of research nowadays. The most well-known process for natural solar energy conversion to chemical energy is photosynthesis, where solar light is absorbed by antenna complexes in the outer region followed by multistep photoinduced energy transfer from the antenna to the reaction center to produce chemical energy. ^{1–6} During photosynthesis, protein–pigment complexes initially absorb photons, which induce an excited electronic	
4.2. Energy Transfer between Confined Dye and Metal Nanoparticles	731		
4.3. Metal Nanoparticle– π -Conjugated Semiconductor Hybrid	732		
4.4. Metal Nanoparticle–Inorganic Semiconductor Heterostructures	732		
5. Basic Aspects of π -Conjugated Semiconductor Nanoparticles	734	Special Issue: Light Harvesting	
5.1. Exciton Dynamics of π -Conjugated Semiconductor Nanoparticles	735	Received: January 18, 2016 Published: August 5, 2016	

state (exciton) of the complexes. Then, multistep cascade energy transfer occurs among the chlorophyll molecules and subsequently transfers to the reaction center for chemical transformations.^{7–9} The chlorophyll molecule acts as a bridging linker between chloroplast pigments and the reaction centers (RCs). The efficient antenna system should have very high molar extinction coefficient, excellent photostability, and the ability to transfer its energy. Considering these issues, several strategies have been undertaken to design artificial light-harvesting systems by using dendrimers,^{10–18} organogels,^{17–19} porphyrin arrays/assemblies,^{20–25} biopolymer assemblies,^{26–31} and organic–inorganic hybrid materials.^{32–35} Dendrimers are found to be ideal, mimicking light-harvesting systems where light energy is captured by peripheral chromophores and the energy subsequently transferred to the core via energy transfer.

In addition to that, inorganic nanocrystals have aroused increasing attention in the design of nanoscale-based light-harvesting systems in the past few years. Semiconducting quantum dots (QDs) are found to be promising light-harvesting materials because of their size-, shape-, and composition-dependent electronic properties, high stability, and exciton generation after photoexcitation.^{36,37} The major challenge in nanoscience is to design nanomaterials with tailored properties and to understand their functionality at fundamental levels. The most ambitious and challenging light-harvesting nanomaterials are QDs, metal nanoparticles, semiconductor–metal heterostructures, π -conjugated semiconductor nanoparticles, organic–inorganic heterostructures, and porphyrin-based nanostructures (Figure 1). Here, we are

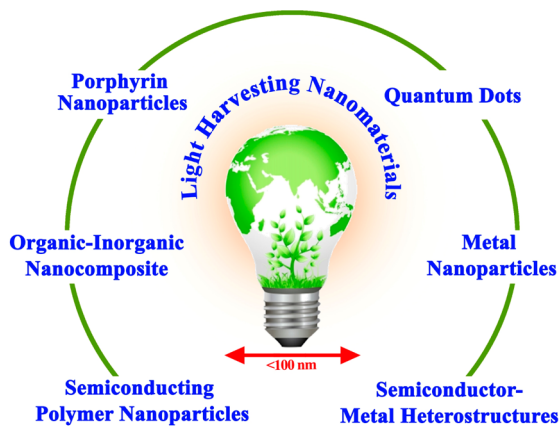


Figure 1. Various nanoscale light-harvesting systems.

highlighting the recent advances and important issues of nanoparticle-based light-harvesting systems, even though this field has grown significantly fast during the past decade.

An overview of the recent understanding of photoinduced processes, such as exciton dynamics, charge transfer, and photoinduced energy transfer, during the interaction of light with antenna materials, like semiconductor quantum dots, metal nanoparticles, π -conjugated semiconductor polymer nanoparticles, and porphyrin aggregates, is illustrated in this review. Most fundamental photophysical processes, i.e., exciton formation and recombination via radiative and nonradiative relaxation, charge separation through migration of electron and hole in a specific direction, and photoexcited energy transfer, are important for understanding and developing efficient light-

harvesting systems (Figure 2). Here, we review possible strategies for designing nanoscale light-harvesting systems and the outline of this discussion is as follows:

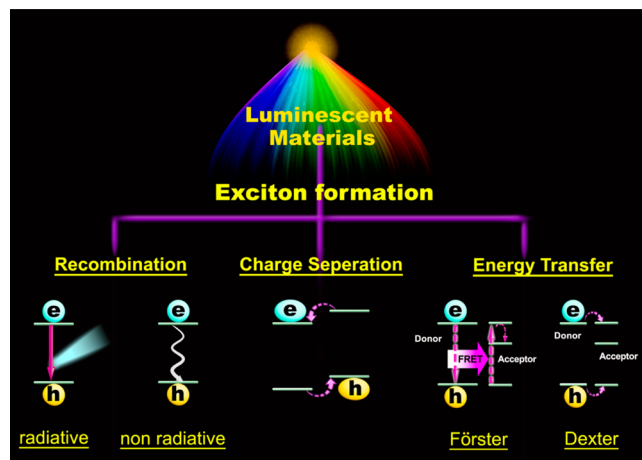


Figure 2. Schematic representation of excitonic processes within luminescent materials.

(1) Recently, semiconductor quantum dots (QDs) are considered the most used luminescent nanomaterials because they can generate light after photoexcitation and the emission wavelength can be tuned by adjusting their size and shape (Figure 3). Therefore, significant attention has been given to

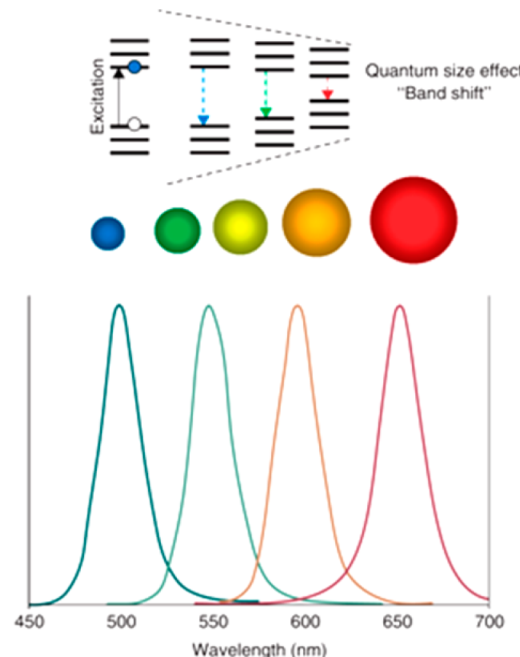


Figure 3. Schematic representation of size-dependent tunable optical properties of QDs due to quantum confinement. Reprinted with permission from ref 41. Copyright 2010 Wiley-Blackwell.

utilizing QDs for developing a new generation of light-harvesting materials, because they are able to generate exciton after photoexcitation. Semiconductor quantum dots exhibit tunable optical properties due to the quantum confinement effect, which eventually controls the charge carrier dynamics and tailors the properties of nanocrystals.^{38–41} Considering the

significance of light-harvesting systems based on semiconductor quantum dots,^{42–47} the knowledge of the size-, shape-, composition-, and surrounding-environment-dependent exciton dynamics and energy transfer is crucial to develop efficient systems for photovoltaic and photocatalysis applications. In the QD-based energy transfer process, a fundamental understanding of photophysical interactions between excited states of QDs with dye molecules and of the distribution of dye molecules around QDs is required because these are the governing factors for QD-based energy transfer.

(2) Considerable attention has been paid to understand the energy transfer between an excited molecule and a nearby metal particle for developing new light-harvesting systems. The molecule's orientation relative to the particle surface influences the radiative (fluorescence) rate of the fluorophore, which controls the energy transfer process. Here, we discuss the design of porous-material-based light-harvesting systems where the surface energy transfer between confined dye in porous materials with Au nanoparticles follows a $1/d^4$ distance dependence. Recent results reveal that π -conjugated polymer/metal nanoparticle hybrid nanostructures are promising materials for light harvesting due to the exciton–plasmon interaction. In particular, metal–semiconductor hybrids offer the modification of electronic properties due to the exciton–plasmon interaction, which leads to a change in the optical responses. Again, the knowledge of the ultrafast photoinduced charge separation in hybrid nanoparticles is important for designing new heterostructures for photocatalysis, photovoltaic, and nonlinear applications.

(3) Another potential strategy for developing a new generation of light-harvesting system is the use of π -conjugated semiconductor polymer nanoparticles because of their semiconductor-like properties, large absorption cross section, high fluorescence efficiency, and easy processing method. A large variety of energy acceptors can overlap with π -conjugated semiconductor polymer because of their broad emission spectra. In this section, the photophysical phenomena of conjugated polymer nanoparticles are discussed, and the roles of the exciton dynamics, rotational dynamics of the dye, and the energy transfer of single or multiple fluorophore-encapsulated π -conjugated semiconducting nanoparticles are highlighted.^{48,49} An effort to develop tunable and white light emission by controlling the energy transfer rate inside the nanoparticles by varying the concentration of multiple fluorophores has been discussed. Furthermore, the importance of self-assembled structures of π -conjugated polymer for light-harvesting applications has been addressed. Finally, we will discuss the importance of the energy transfer, charge transfer, and interfacial charge transfer in hybrid nanostructures of π -conjugated polymers and inorganic nanoparticles for developing promising light-harvesting devices.

(4) Another strategy for light-harvesting systems is the application of self-assembled porphyrin aggregates (H- and J-aggregation) where the aggregated structures are formed due to hydrogen bonding, π – π stacking, electrostatic interactions, van der Waals forces, etc. It is evident that J-aggregates are known to mimic the light-harvesting antenna complexes of chlorophyll because π electronic coupling enhances the coherent electronic delocalization. We discuss the photophysical properties of aggregated porphyrin structures, efficient photoinduced energy transfer, the singlet oxygen (${}^1\text{O}_2$) generation from porphyrin aggregates and their photocatalytic behavior. The design of porphyrin–quantum dot hybrid materials and their photo-

physical properties are illustrated for promising light-harvesting systems.

2. BASIC ASPECTS OF ENERGY TRANSFER PROCESS IN NANOSCALE SYSTEMS

Förster resonance energy transfer (FRET) is an important process in light-harvesting systems where photons are absorbed by antenna materials and subsequently the excited state energy is transferred to a suitable acceptor. This process plays a decisive role in natural solar energy conversion in light-harvesting systems. This is a nonradiative excited state energy transfer process from the donor molecule (D) to an acceptor molecule (A) in the ground state (Figure 4) and it depends on

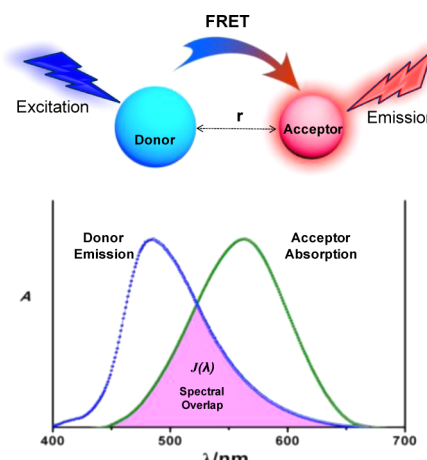


Figure 4. Energy transfer between donor–acceptor and the spectral overlap between the emission spectrum of donor and the absorption spectrum of the acceptor.

the distance between donor and acceptor molecules. The overlap between the emission spectrum of the donor and the absorbance spectrum of acceptor is an essential requirement for the efficient energy transfer. The mechanism of this energy transfer process in light-harvesting systems is now well-studied.^{50–52} The point-dipole approximation is used for weak and strong excitonic couplings, and the energy transfer rate is calculated on the basis of the interactions between the transition dipoles of donor and acceptor. However, Förster's method may fail if the excitations on the chain are delocalized in the conjugated molecular system where the line-dipole approximation is used for calculating excitation transfer rates more precisely than point-dipole approximation.⁵³ For the conjugated polymer nanoparticle, it is the part of the polymer with conjugated double bonds. If the size of this part is comparable or larger than the edge-to-edge distance between the conjugated parts of the nanoparticles, then line-dipole approaches may be considered. In the Dexter method, the energy transfer is a very short range process compared to the Förster method, which is a long-range process. The rate of energy transfer is given by Förster theory

$$k_T(r) = \frac{1}{\tau_D} \left(\frac{R_0}{r} \right)^6 \quad (1)$$

where the lifetime of the donor is τ_D in the absence of the acceptor, and the Förster distance is R_0 , the distance at which the transfer rate $k_T(r)$ is equal to the decay rate of the donor in

the absence of the acceptor. The Förster distance (R_0) is defined as

$$R_0 = 9.78 \times 10^3 [\kappa^2 n^{-4} Q_D J(\lambda)]^{1/6} \text{ (in } \text{\AA}) \quad (2)$$

where the quantum yield of donor in the absence of acceptor is Q_D , the refractive index of the medium is n , and the orientation factor is κ^2 , which is defined as

$$\begin{aligned} \kappa^2 &= (\cos \theta_T - 3 \cos \theta_D \cos \theta_A)^2 \\ &= (\sin \theta_D \sin \theta_A \cos \varphi - 2 \cos \theta_D \cos \theta_A)^2 \end{aligned} \quad (3)$$

where the angle between the emission transition dipole of the donor and the absorption transition dipole of the acceptor is θ_T , the angles between these dipoles are θ_D and θ_A , and the angle between the planes of the donor and acceptor is φ . For collinear and parallel transition, $\kappa^2 = 4$, and $\kappa^2 = 1$ for parallel dipoles and $\kappa^2 = 0$ for perpendicularly oriented dipoles. The magnitude of $\kappa^2 = 2/3$ for randomized donor and acceptor molecules. The overlap integral between donor emission spectrum and acceptor absorption spectrum is $J(\lambda)$, which is given by

$$J(\lambda) = \frac{\int_0^\infty F_D(\lambda) \epsilon_A(\lambda) \lambda^4 d\lambda}{\int_0^\infty F_D(\lambda) d\lambda} \quad (4)$$

$F_D(\lambda)$ is the corrected fluorescence intensity of the donor in the wavelength range from λ to $\lambda + \Delta\lambda$, with the total intensity normalized to unity; $\epsilon_A(\lambda)$ is the extinction coefficient of the acceptor at λ ; and the units of $J(\lambda)$ are $M^{-1} \text{ cm}^{-1} \text{ nm}^4$, if λ is in nm. The efficiency of energy transfer can be calculated after knowing the value of R_0 . The efficiency of energy transfer (E) is defined as

$$E = \frac{k_T(r)}{\tau_D^{-1} + k_T(r)} \quad \text{or} \quad E = \frac{R_0^6}{r^6 + R_0^6} \quad (5)$$

In the case of a QD-based energy transfer process, the size of a QD is larger than that of an organic dye; thus, multiple acceptors (n) can interact with a single donor, and such a multiple donor–acceptor system enhances the efficiency and the sensitivity. Thus, the efficiency of energy transfer can be written as

$$E = \frac{n R_0^6}{n R_0^6 + r_n^6} \quad (6)$$

From the photoluminescence study, the energy transfer efficiency can be measured by using the relative fluorescence intensity of the donor (F_D) in the absence of the acceptor and the fluorescence intensity of the donor (F_{DA}) in the presence of the acceptor, which is given as

$$E = 1 - \frac{F_{DA}}{F_D} \quad (7)$$

From the decay time measurement, the energy transfer efficiency can be measured by using the decay time of the donor (τ_D) in the absence of the acceptor and the decay time of the donor (τ_{DA}) in the presence of the acceptor, which is given as

$$E = 1 - \frac{\tau_{DA}}{\tau_D} \quad (8)$$

The fundamental knowledge of the energy transfer process in the nanoscale system is essential because the efficiency of the energy transfer depends on the number of acceptor molecules attached to the surface of QDs, which eventually depends on the size, shape, and composition of the QDs. The limitation of the FRET process is that this method can be used for measuring the distance between donor and acceptor only up to 80 Å. In the case of densely packed films of QDs, the point-dipole approximation is not valid because the point-dipole approximation is valid when the size of the QD is less than the distance between the donor and acceptor (d). In the case of thin films of quantum dots, the important issues for the breakdown of the point-dipole approximation are thin-film geometries, the dielectric constant, and the integral over the spatial distribution of the donor plane. In densely packed films of QDs, the interaction between QDs is increased and the distance is shorter than the center-to-center distance.⁵⁶ The incorporation of the dipole distribution into the FRET theory is used to calculate the energy transfer rate in the case of close-packed films of QDs.

Recently, understanding the surface energy transfer (SET) phenomena between an excited molecule and a nearby metal particle is a burgeoning area of research for potential applications.^{57,58} Compared with the R^{-6} -distance-dependent FRET process, the “surface energy transfer” process depends on the R^{-4} distance from the molecule to the surface of the metal, where the spectral overlap between donor emission and the acceptor absorption spectrum is not required. For a metal nanoparticle, the free conduction electrons of the metal travel near or perpendicular to the metal surface and then they interact strongly with the donor molecule.⁵⁸ Considering the Fermi golden rule approximation, the energy transfer rate (k_{ET}) is related to the square dependence of the excitonic coupling. According to the Persson model, the surface energy transfer rate is given by

$$k_{SET} = \frac{1}{\tau_D} \left(\frac{d_0}{d} \right)^4 \quad (9)$$

where the lifetime of the donor in the absence of the acceptor is τ_D , and the distance between the donor and acceptor is d . The distance d_0 is calculated by using the model

$$d_0 = \left(\frac{0.225 c^3 \Phi_{dye}}{\omega_{dye}^2 \omega_F k_F} \right)^{1/4} \quad (10)$$

where d_0 is the distance at which the dye transfers energy and spontaneously emits, the quantum efficiency of the dye is ϕ_{dye} , the frequency of the donor electronic transition is ω , the Fermi frequency is ω_F , and Fermi wave vector of the metal is k_F .⁵⁸ Using $\omega = 3.6 \times 10^{15} \text{ s}^{-1}$, $\omega_F = 8.4 \times 10^{15} \text{ s}^{-1}$, $k_F = 1.2 \times 10^8 \text{ cm}^{-1}$, and $c = 3 \times 10^{10} \text{ cm s}^{-1}$, the d_0 value is calculated. The radiative rate enhances⁵⁹ at very close distances (<10 Å), whereas the energy transfer takes place at intermediate distances (20–300 Å).^{57,58} Thus, the general form of the quantum efficiency of energy transfer is given by

$$\Phi_{ET} = \frac{1}{1 + \left(\frac{r}{r_0} \right)^n} \quad (11)$$

where $n = 6$ for dipole–dipole energy transfer (FRET) and $n = 4$ for dipole–surface energy transfer (SET). The advantage of the SET process is its capability to measure longer distances

than the typical Forster distances because it is R^{-4} distance dependence.^{57–63}

3. QD-BASED LIGHT-HARVESTING SYSTEMS

The generation of an exciton by absorption of light and the subsequent funneling of the excitation energy by electron/charge transfer depend on the size, shape, and composition of the QDs and the surface properties of the QDs, ligands, etc., which are the important issues in light-harvesting systems.^{64–83} Here, we point out the influence of such parameters on the relaxation dynamics and FRET of QDs.

3.1. Decay Dynamics of QDs

Exciton dynamics on nanoscale systems often provide an insight into fundamental electronic properties of nanoscale systems, which are found to be related to size, shape, and composition. Recent findings reveal that several processes, like Auger recombination,^{84,85} carrier trapping at QD defect states/surface states,^{86,87} charge transfer into a ligand-based orbital,⁸⁸ and relaxation to the ground state,⁸⁹ are involved in semiconducting nanocrystal photoexcitation dynamics (Figure 5) that eventually control the overall performance of light-

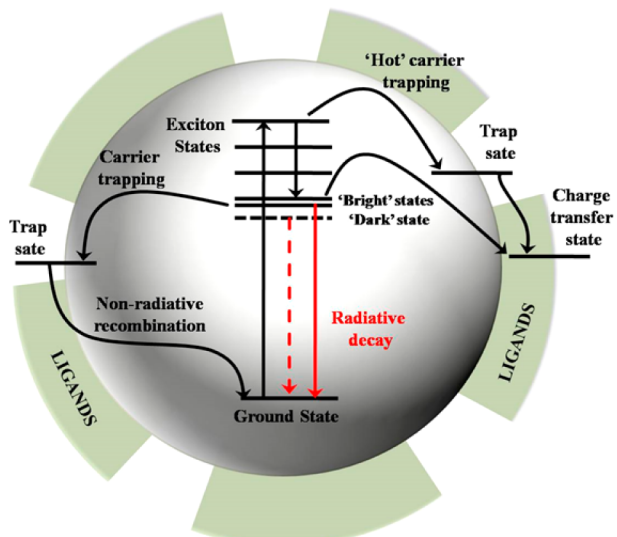


Figure 5. Schematic diagram of several processes involved in semiconducting nanocrystal photoexcitation dynamics. Reprinted with permission from ref 70. Copyright 2010 Royal Society of Chemistry.

harvesting systems. The local environment^{90–92} (e.g., sample inhomogeneities, ligand exchange) of the QDs also controls the relaxation process.

A detailed understanding of the charge carrier dynamic of QDs is required for developing an efficient light-harvesting system. Pioneering work has been done by El-Sayed's group on the fundamental understanding of electron–hole dynamics in semiconductor nanoparticles by using ultrafast spectroscopy, and they reported the dependence of relaxation dynamics on the size, shape, and composition of nanocrystals.^{93–96} An excellent review on the excitons in various nanoscale systems, like conjugated polymers, aggregated molecules, QDs, and carbon-based materials, was written by Scholes and Rumbles.⁹⁷ To exploit these QDs in light-harvesting applications, emphasis is given to a high-level understanding of the decay dynamics of QDs by using time-resolved spectroscopy.^{98–102} Jones and

Scholes have illustrated an in-depth knowledge of the interactions of exciton states with surface-localized states, the surrounding environment, the attached ligands, and the extent of ligand coverage.⁷⁰ Using transient absorption and time-resolved photoluminescence spectroscopy, Chuang and Burda have analyzed the carrier relaxation dynamics, including carrier multiplication, trapping, and interfacial carrier transfer of semiconducting nanoparticles.¹⁰³ Zhang and co-workers have also investigated the fundamental photophysical processes, such as ultrafast electron dynamics, and the charge carrier dynamics of semiconductor nanocrystals to find out potential applications of QDs. Thus, the knowledge of the important processes, like charge carrier dynamics, charge separation, and recombination at the interface of QDs, is extremely important for fabrication of efficient light-harvesting devices,^{104–109} and it is evident that different radiative and nonradiative processes are involved in carrier relaxation process in a wide time scale range. Here, we have highlighted the importance of the size, shape, and composition in the exciton dynamics of semiconducting nanocrystals.

3.1.1. Kinetic Model for Decay Dynamics. On the basis of several relaxation processes, a few kinetic models are proposed to illustrate the photoexcited decay dynamics of QDs that is required for quantitative estimation of different relaxation processes.^{65,86,110–113} The Perrin model, Poisson distribution, and binomial distribution of quenchers are used to analyze the decay dynamics of QDs. A stochastic model based on the Poisson distribution of the charge carrier dynamics in QDs has been proposed by Hilczer and Tachiyia.¹¹⁴ Al Salman and co-workers have proposed a model based on a stochastic ground-state dipole moments approximation.¹¹⁰ A model based on the Poisson distribution of quenchers is being used to analyze the decay curves of QD nanocrystals to understand the relaxation dynamics.^{115,116} Later on, Pansu and co-workers used the binomial distribution of quenchers for the analysis of decay curves of QD nanocrystals to reveal the mechanism of relaxation pathways.¹¹⁷ We have developed a stochastic kinetic model (Figure 6) to understand the relaxation dynamics of

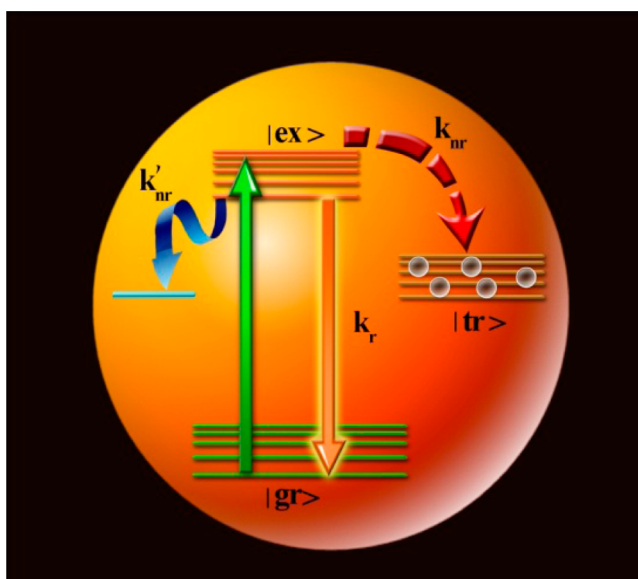


Figure 6. A proposed model for different relaxation processes and their rates in semiconductor nanocrystals. Reprinted from ref 116. Copyright 2012 American Chemical Society.

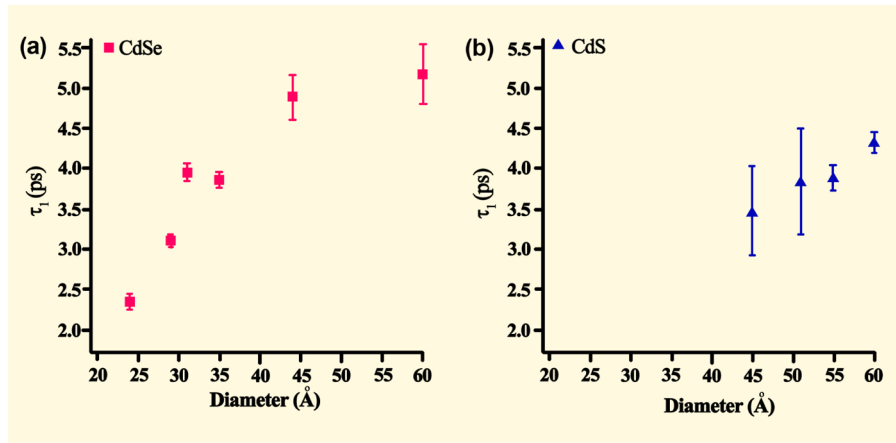


Figure 7. The relation between the short-lived component of fluorescence (τ_1) and the size of (a) CdSe and (b) CdS QDs. Reprinted from ref 122. Copyright 2008 American Chemical Society.

QDs at room temperature,^{115,116} where ground state, excited state, and trap state are represented as $|gr\rangle$, $|ex\rangle$, and $|tr\rangle$, respectively. All the possible radiative and nonradiative processes occurring on the time scale of nanoseconds are considered in this model. The rate due to the radiative recombination is designated as k_r , and the nonradiative rate due to the trapping of charge carriers in each trap state is k_{nr} . The rate due to the luminescence quenching process of the QD local environment is designated as k_{nr}' . The number of trap states participating in the charge carrier trapping process and the number of quenchers surrounding the QDs are n_t and n_t' , respectively. A Poisson distribution of the number of trap states present on the surface of the semiconductor QDs is¹¹⁸

$$\Phi(n) = (m^n / n!) \exp(-m) \quad (12)$$

where the average value is m . The averaged decay curve of the excited semiconductor QD is derived as¹¹⁶

$$I_t = I_0 \sum_{n_t=0}^{\alpha} \sum_{n_t'=0}^{\alpha} \Phi(n_t) \Phi(n_t') \exp[-(k_r + n_t k_{nr} + n_t' k_{nr}')] t \quad (13)$$

The final equation after simplification is

$$I_t = I_0 \exp\{-k_r t - m_t [1 - \exp(-k_{nr} t)] - m_t' [1 - \exp(-k_{nr}' t)]\} \quad (14)$$

where the average number of trap states participating in the charge carrier trapping process and the average number of quenchers surrounding the QDs are m_t and m_t' , respectively.

In QD-based solar cells, QDs are attached to a metal oxide, where the rapid electron injection from QD to metal oxide leads to charge separation and enables light harvesting.¹¹⁹ To improve the performance of QD-based solar cells, hole trapping is an important occurrence that blocks hole injection. Recently, Žídek et al.¹²⁰ have proposed the statistical trap model, based on three possibilities: trap creation without recovery, trap creation and recovery, and trap creation with an upper limit for trap number accommodated in a QD. A deeper understanding of hole trapping may be required to improve device performance. Trapping can be suppressed by making a core–shell structure, which will influence on the performance of the solar cell. A correlation has been drawn between ultrafast carrier

dynamics and solar cell efficiency, and analysis reveals that optimum shell thickness increases the solar cell efficiency.¹²¹

3.1.2. Impact of QDs' Size. Here, we discuss the influence of particle size on relaxation dynamics, which eventually controls the overall efficiency of the challenging devices. Recent findings reveal that electron–hole wave function overlapping is found to be increased with reduction in the QDs size.⁶⁸ The short-lived component of fluorescence decay time (Figure 7a,b) at the band edge is found to be increased upon increasing the size of CdSe and CdS QDs from 23 to 60 Å.¹²² Actually, the electron–hole exchange interaction influences the decay kinetics of QDs, which eventually depends on the size of the QDs.^{123,124} Further, Yagi et al.¹²⁵ have described the size-dependent relaxation dynamics of CdS QDs and it is found that the fast decay component is increased upon decreasing the size of QDs because of the surface states are decreased in larger QDs. It is also evident that the relaxation decay of photoexcited QDs is influenced by the densities of surface and interior trap states of QDs. It is reported that the radiative recombination rate and the number of surface traps are found to be decreased upon increasing the size of QD.⁷⁵ The nanoradiative surface trap state is found to be related to the size of the nanocrystals because the surface reconstruction process occurs during the nanocrystals' growth.⁷⁵ Recently, considerable attention has been paid to understand the size effect on relaxation dynamics of QDs in the presence of graphene because graphene–semiconductor hybrids are found to be promising materials for solar energy conversion and optoelectronic devices.^{126–129} The enhancement of photocurrent occurs due to the efficient electron transfer from QD to graphene upon photoexcitation in the grapheme–QDs hybrid materials. Krishnamurthy and Kamat¹²⁶ have studied the size-dependent electron transfer process between CdSe QDs and graphene oxide for light energy conversion, and the electron transfer rate constant is decreased upon increasing the size of the QDs. Zhu et al. have also reported that the electron transfer process from photoexcited QDs to graphene is enhanced in sandwiched hybrid QD–graphene nanofilms.¹²⁷ However, the size-dependent decay dynamics of QDs in the presence of graphene oxide is not fully understood. In recent work, a graphene oxide–CdTe QD composite was designed by electrostatic attachment of positively charged CdTe QDs to negatively charged graphene oxide (GO), where the number of available sites on the QDs and the mean fractional surface

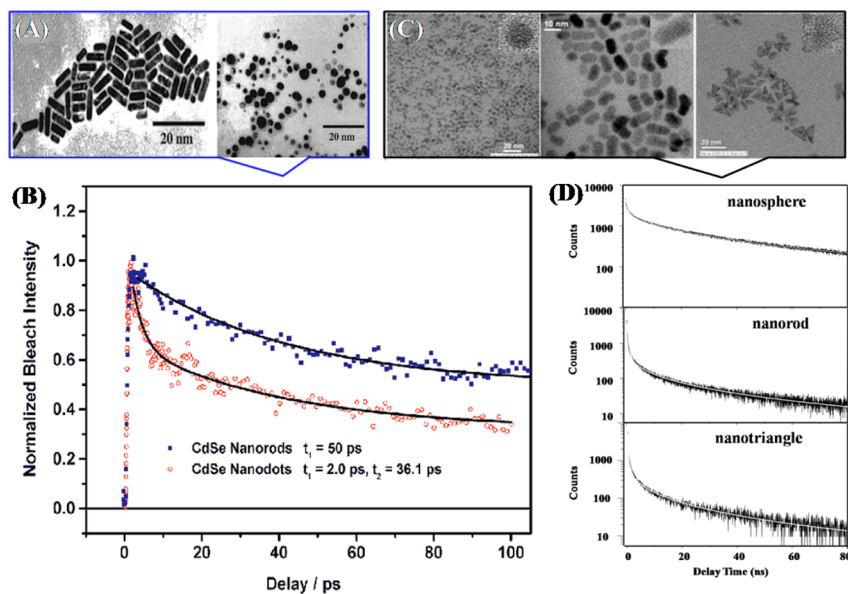


Figure 8. (A) TEM images of CdSe nanorods and CdSe nanodots and (B) decay kinetics of the CdSe nanorods and nanodots at 585 nm wavelength (at the band gap). Reprinted from ref 96. Copyright 2001 American Chemical Society. (C) TEM images of different shapes of QDs and (D) decay curves of different shapes of CdS (nanspheres, nanorods, and nanotriangles). Reprinted from ref 115. Copyright 2011 American Chemical Society.

coverage of the QDs on the GO sheet are dependent on the size of the QDs.¹²⁸ To understand the decay kinetics of QDs in the QD–GO composite system, we assume a binomial distribution of the number of available QD sites and the mean fractional surface coverage of QD on the GO sheet, and we have developed a kinetic model which is

$$A_m = \binom{N}{m} (\theta)^m (1 - \theta)^{N-m} \quad (15)$$

where the probability of finding a QD attached to the GO sheet through m sites is A_m , N is the number of available sites on the QD surface through which the GO sheet is attached, and the mean fractional surface coverage of QD by GO sheet is θ . With an increase of the QD size, the average numbers of available sites increased and the mean fractional surface coverage and the total quenching rate decreased. Finally, it is found that the electron transfer rate decreased upon increasing the size of QDs from 2.4 to 4.8 nm.¹²⁸ A similar study also found that the energy transfer depends on the size of the QDs in graphene–CdSe QD composites.¹²⁹ Analysis of this study definitely reveals that the size of the QDs has a significant impact on the performance of the light-harvesting system.

3.1.3. Impact of QDs' Shape. In this section, we are focusing on the impact of shape on the relaxation dynamics of QDs because exciton size depends on the shape of QDs, which controls the exciton dynamics.¹³⁰ An interesting finding reveals that the exciton shape varies with changing the shape of the particles due to a change in their symmetry;¹³¹ thus, exciton dynamics should vary with changing the shape. It is reported that a longer recombination lifetime is observed in the case of rod-shaped CdS nanocrystals (NCs) than for spherical ones.¹³² The reduced optical phonon coupling during the recombination process of carriers is the reason for the longer lifetime. Due to the lowering of symmetry in the rods, the electron–hole relaxation dynamic of nanorod samples is different from that of nanodot samples, and the carrier relaxation dynamics of nanorods (50 ps) at the band gap state are faster than that of nanodots (2 and 36.1 ps) (Figure 8A,B).⁹⁶ Generally,

multiexponential decay is observed for different shapes of QDs, and the components of lifetime are not easy to extract in the case of three- and four-exponential decay. To resolve this issue, the stretched exponential¹³³ decay based on the Kohlrausch–William–Watts (KWW) function is commonly used, which is given below:

$$I(t) = a \exp[-(t/\tau_0)^\beta] \quad (16)$$

A stretched exponential is used to estimate the average lifetime for heterogeneity of the sample, where the stretching exponent is β and β tends toward 1 for a homogeneous system. To extract multiple exponentials from a stretched exponential fit, inverse Laplace transforms are used. Sometimes, the above stretched exponential is modified by addition of a fast initial single exponential when the initial decay is too fast, and the modified stretched exponential function^{130,134} is

$$I(t) = b \exp(-t/\tau_0) + a \exp[-(t/\tau_0)^\beta] \quad (17)$$

The decay times evidently decrease (from 13.6 to 2.9 ns) upon changing particles from spherical (symmetrical) to nonspherical (asymmetrical).¹¹⁵ Analysis reveals that the stretching exponent (β) decreases from spherical to anisotropic shaped QDs (from 0.4 to 0.27), indicating a broader distribution than for symmetrically shaped QDs. It is further revealed that the radiative recombination rate is higher in spherical particles than asymmetrical particles because the exciton size and shape change the radiative rates of QDs. Figure 8C,D represents the TEM images and the decay curves of different shapes (nanspheres, nanorods, and nanotriangle) of CdS QDs.¹¹⁵ Attached ligands and the extent of ligand coverage have a strong influence on surface-localized states and radiationless processes, including carrier trapping at NC defects and charge transfer to surface ligands. It is evident that the carrier relaxation dynamics of differently shaped CdS NCs can be modified by the passivating ligands. Some correlation may exist between the number of surface states and the size or the surface area of nanocrystals. It is reported that the average total surface area of CdS QDs is 120.7 nm² (considering that the average

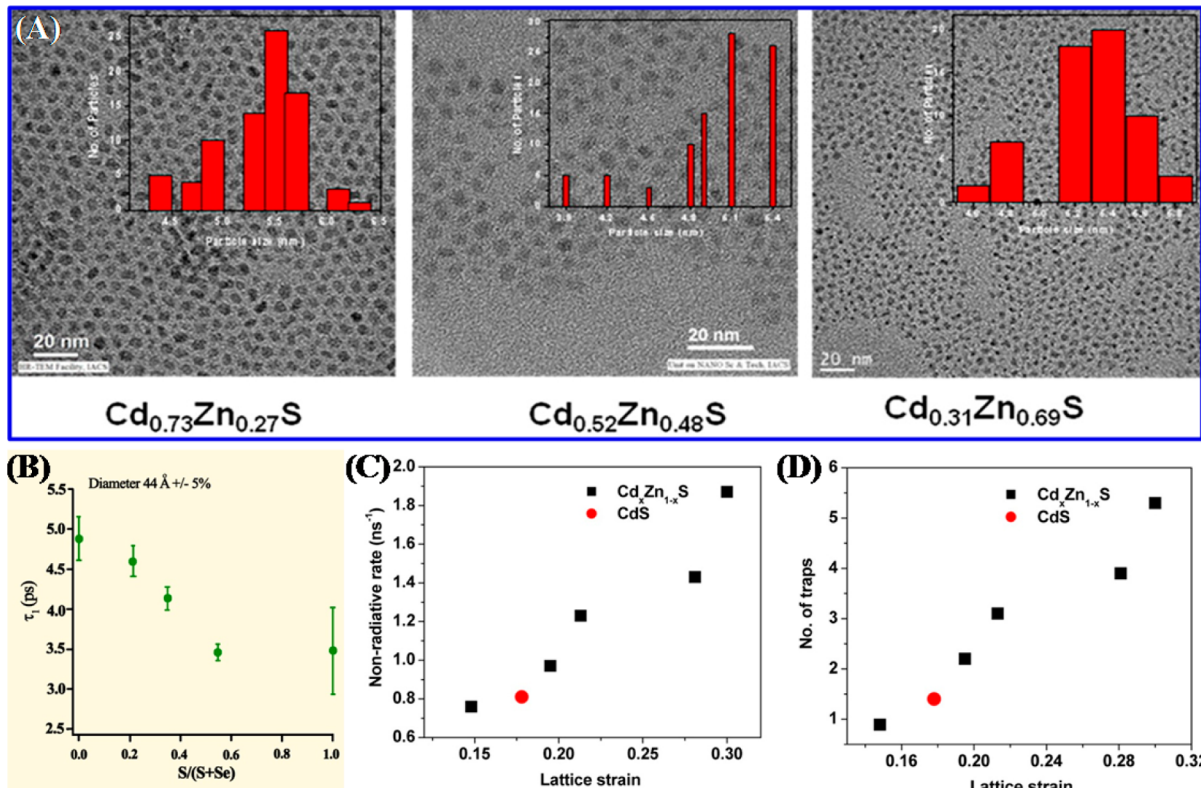


Figure 9. (A) TEM images of Cd_xZn_{1-x}S alloy QDs with three different compositions showing the size distribution in the inset. Reprinted from ref 116. Copyright 2012 American Chemical Society. (B) A plot of short-lived decay time (τ_1) versus the composition of CdS_xSe_{1-x}QDs. Reprinted from ref 122. Copyright 2008 American Chemical Society. (C) A plot of the nonradiative relaxation rates with lattice strain and (D) the number of trap states with lattice strain of alloy QDs. Reprinted from ref 116. Copyright 2012 American Chemical Society.

diameter of a nanosphere is 3.1 nm), the surface area is 692.06 nm² for CdS nanorods (considering that the average length of a nanorod is 13.2 nm and the average diameter of a nanorod is 5.8 nm), and the surface area is 62.56 nm² for nanotriangles (considering that the average side length of a nanotriangle is 8.5 nm).¹¹⁵ To avoid the contribution of ligands and unreacted reaction precursors, the same washing procedure is used for these different shapes of CdS nanoparticles (nanosphere, nanorod, and nanotriangle). However, it is not easy to compare the influence of the size and surface areas on the relaxation dynamics of CdS nanoparticles, as the shape of NCs is different. To better understand the relaxation dynamics of different shapes of CdS nanocrystals, a kinetic model is developed to quantify the radiative and nonradiative relaxation pathways, which includes the average number of surface trap states, the luminescence quenching rate due to surface trap states, and the rate due to nonradiative recombination from trap state to ground state. The average number of surface traps (m_t) changes with the shape of the particles, and the values are 11.2, 21.9, and 34.5 for CdS nanosphere, nanorod, and nanotriangle, respectively, indicating that the surface curvature of nanocrystals plays an important role in the relaxation processes of shaped nanocrystals.¹¹⁵ The low photoluminescence (PL) quantum yield for nonspherical CdS QDs is explained by the presence of a large number of surface traps on nonspherical CdS QDs. A recent finding reveals that the knowledge of decay dynamics of shaped QDs would be beneficial for developing an efficient light-harvesting system.

3.1.4. Alloy QDs. Here, we point out the impact of semiconductor alloy QDs (AB_xC_{1-x}) on the decay dynamics

because alloy QDs exhibit composition-dependent optical properties that are useful for photovoltaic, nonlinear, and solar cell applications. Interestingly, alloy QDs are found to exhibit lattice strain due to the difference in the lattice constants of their constituents, which influences the carrier relaxation of alloy nanocrystals. The excited state lifetime of colloidal ternary alloy QDs was discussed by various groups.^{77,122,135} It is evident from the ultrafast spectroscopic study that the relaxation dynamics of alloy QDs depends on the composition and that the short-lived decay component is due to both radiative and nonradiative relaxation.^{136,137} Nie and co-workers¹³⁸ have pointed out that the lattice strain of core–shell QDs influences the photophysical properties of QDs because lattice strain controls the location of charge carriers and modulates the exciton lifetimes. It is seen from TEM images that the Cd_xZn_{1-x}S alloy QDs (Figure 9A) are spherically (5.4 ± 0.4 nm) shaped, indicating that the polarization has no influence on it. It is evident that the shape of Cd_xZn_{1-x}S alloy QDs has no influence on the radiative and nonradiative relaxation processes.¹¹⁶ The formation of an intermixing crystal structure of Cd_xZn_{1-x}S ternary alloy QDs occurs due to the substitution of Cd²⁺ by Zn²⁺ or vice versa and the composition of Cd_xZn_{1-x}S alloy QDs modifies the lattice strain. For the homogeneous Cd_xZn_{1-x}S QDs alloy structure, a nearly linear relationship of the Cd mole fraction with the lattice constant “ a ” is observed.¹¹⁶ Similar results were obtained by Zhong and co-workers¹³⁹ for Zn_xCd_{1-x}S alloy QDs, where the lattice parameter c decreases linearly with increasing Zn content. The existence of lattice strain in alloy compounds is reported by many other groups.^{140–142} The difference in the bond lengths

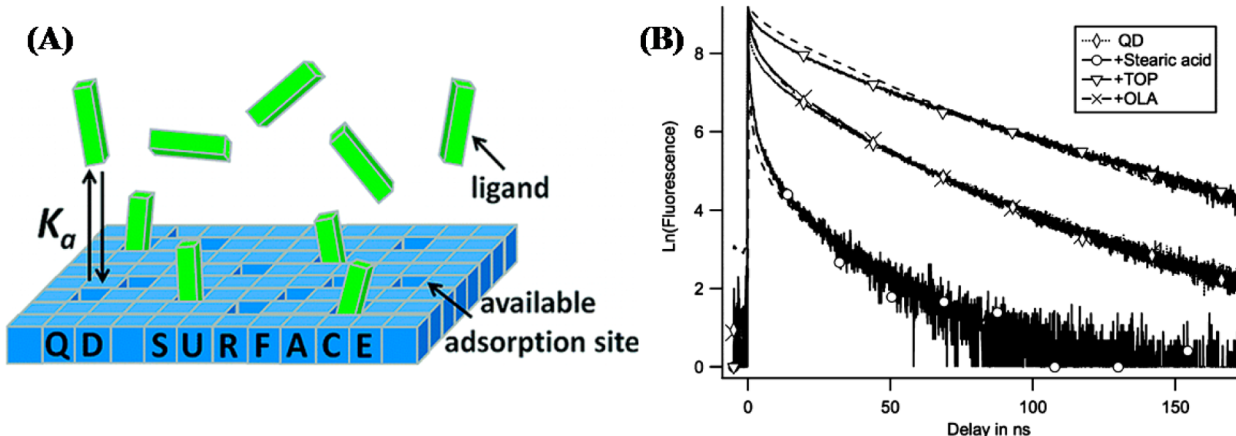


Figure 10. (A) A schematic diagram of the adsorption equilibrium of solution-phase CdS QDs and acid-derivatized viologen ligands for quenching of the photoluminescence of the QDs by V^{2+} . Reprinted from ref 155. Copyright 2012 American Chemical Society. (B) Fluorescence decay curves of (\diamond) CdSe QDs at a concentration 20 $\mu\text{mol}/\text{L}$, (\circ) with stearic acid (final concentration of added stearic acid 0.25 mol/L), (∇) with TOP (1.1 mol/L), and (\times) with oleylamine (OLA) (1.5 mol/L). Reprinted from ref 117. Copyright 2012 American Chemical Society.

of Cd–S and Zn–S and the sizes of Cd^{2+} and Zn^{2+} induce the lattice strain in $\text{Cd}_x\text{Zn}_{1-x}\text{S}$ QD. It is reported by Fancey et al.¹⁴³ that the shortening of decay time with increasing lattice strain occurred in InGaAsP/InP heterostructures, indicating that the lattice strain plays an important role in the relaxation process. Again, the lattice strain increases the nonradiative recombination rate that is associated with defects at the interfaces due to mismatch of lattice constants. The compressive strain of ZnS nanocrystals has been reported by Gilbert et al.¹⁴⁵ As we know, the photoluminescence quantum efficiency is controlled by the radiative and nonradiative rates, and it is reported that the lattice strain influences the radiative and nonradiative rates.^{144,145} Veilleux et al.¹⁴⁶ have reported that the exciton lifetimes of colloidal QDs are controlled by the lattice strain. Their analysis revealed that the lattice-mismatch-induced strain is responsible for a greater number of defects, which causes nonradiative recombination. Ultrafast spectroscopic studies confirmed that the surface trap states play an important role in the band edge recombination in $\text{CdS}_x\text{Se}_{1-x}$ alloy QDs. A correlation was drawn between the short- and long-lived decay components with the composition (Figure 9B) of QDs.¹²² We have seen that the radiative and nonradiative relaxation rates are increased upon decreasing the Cd mole fraction in $\text{Cd}_x\text{Zn}_{1-x}\text{S}$ alloy QDs.¹¹⁶ The radiative relaxation rate, nonradiative relaxation rate, and number of trap states are quantified by using a stochastic model of carrier relaxation dynamics,¹¹⁶ and the radiative, nonradiative relaxation rate and the number of trap states are found to be increased with increasing the lattice strain of the alloy QDs (Figure 9C,D). It is found that lattice strain can modify the radiative relaxation rate (k_r), the nonradiative relaxation rate (k_{nr}), and the number of trap states (m_t) of alloy $\text{Cd}_x\text{Zn}_{1-x}\text{S}$ QDs, because lattice strain creates a number of trap states, which will influence the relaxation dynamics.¹¹⁶ A restriction of QD-based solar cell is the existence of surface traps, which block the hole injection and that can be overcome by using core–shell QDs to reduce the number of surface trap states, which is useful for solar cell applications.¹⁴⁷ The crucial factors in QD-based solar cell are hole trapping and hole injection, and it is seen that hole injection enhances the conversion efficiency up to 17% in p-type CdSe QD photocathodes.¹⁴⁸ Recently, Zheng et al.¹⁴⁹ have distinguished the hole injection and hole trapping process

by an ultrafast spectroscopic study, and it was found that the overall hole injection efficiency is enhanced in core–shell QDs. The electron and hole dynamics of core–shell QDs were investigated, and analysis revealed that the solar cell efficiency depends on the shell thickness.¹²¹ This study clearly indicates that trap states play an important role in solar energy conversion applications.

3.1.5. Impact of QDs' Surface. Besides the size, shape, and composition of QDs, ligands, surface reconstruction, solvent, and surface atoms of QDs play big roles in controlling the radiative and nonradiative relaxation rates of decay dynamics of QDs.^{150–152} It is evident that the surface reconstruction induces the electronic state degeneracy because of symmetry breaking of the QDs.¹⁵⁰ An ultrafast fluorescence upconversion spectroscopic study revealed that the exciton dynamics of CdSe QDs are strongly influenced by surface morphology, which leads to an increase in the radiative decay efficiency. A previous study highlighted the influence of capping ligands on the carrier relaxation dynamics of QDs.¹⁵³ Koole et al. have described the ligand exchange kinetics on QD surface and extract the quenching rate, exchange rate of ligands.¹⁵⁴ Weiss and co-workers have monitored the photoluminescence quenching of QDs and studied the absorption equilibrium of acid-derivatized viologen ligands (V^{2+}) (Figure 10A).¹⁵⁵ They pointed out that the surface structure of the QDs depends on their concentration. The dilution of QDs enhances the disaggregation and subsequently desorption of the native ligands, which influences the available adsorption sites per QD. It was seen that the available adsorption sites per QD increased up to 37-fold. Again, the length of the ligand influenced the rate of the photoinduced electron transfer process in QD/poly(viologen) assemblies.¹⁵⁶ Pansu and co-workers¹¹⁷ have studied the influence of dilution and the nature of ligands on the decay kinetics of trioctylphosphine (TOP)-capped CdSe QDs and reported that fluorescence quenching occurs due to removal of TOP ligands by dilution and that the fluorescence is regained upon addition of TOP ligands (Figure 10B). They analyzed the fluorescence quenching by using a binomial distribution model, and analysis revealed that the quenching sites and quenching rate are influenced by ligands. The ligands and surrounding environments of QDs have considerable influence on the

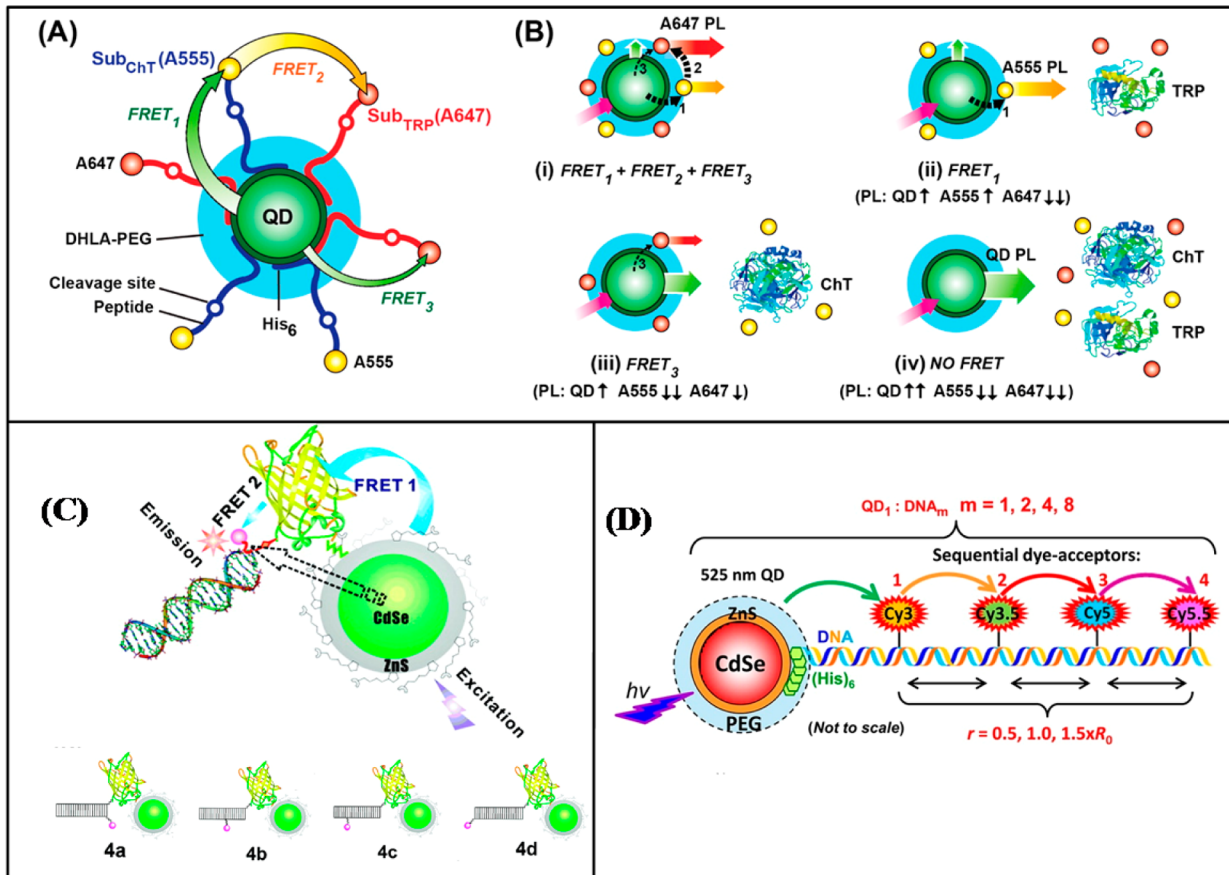


Figure 11. (A) A QD-based energy transfer system composed of CdSe/ZnS QDs, Alexa Fluor 555 (AF555), and Alexa Fluor 647 (AF647) dyes. (B) PL intensity changes from the three emitters, such as QD and AF555 and AF647 dyes. Reprinted from ref 166. Copyright 2012 American Chemical Society. (C) Schematic presentation of the QD-enhanced yellow fluorescent protein (EYFP)-Atto647 dye system. Position of the terminal acceptor, Atto647 (pink sphere), with varying DNA as shown in structures 4a–4d. Reprinted from ref 167. Copyright 2008 American Chemical Society. (D) Schematic of a central QD donor assembled with a peptide–DNA photonic wire. The inter-fluorophore distances vary as a function of $0.5R_0$, $1.0R_0$, and $1.5R_0$ distances. Reprinted from ref 168. Copyright 2013 American Chemical Society.

relaxation dynamics of QDs, which eventually influence the device fabrication.

3.2. QD-Based Energy Transfer Systems

Here, we discuss the importance of QD-based energy transfer, which has significant impacts on light harvesting, bioimaging, tagging, and multiplexing because of several advantages of QDs, such as their narrow emission band and broad excitation band.^{90,157,158} Recent findings revealed that the energy transfer between QDs and dye is a $1/d^6$ -distance-dependent FRET process. In QD-based energy transfer, multiple acceptors could interact with one QD, because a QD is larger than an organic dye, which enhances FRET efficiency.¹⁵⁹ To make efficient light-harvesting systems, the main requisite is the presence of donor and acceptor molecules where energy transfer occurs either by FRET or Dexter energy transfer, depending on the distance between them. Scholes and co-workers¹⁶⁰ have examined the energy transfer and the electronic coupling between QDs and chlorophyll molecules based on transition densities. Significant energy transfer efficiency (90%) is reported for the CdSe/ZnS core–shell nanocrystal/Rhodamine B dye system.¹⁶¹ By using ultrafast spectroscopy, Lian and co-workers¹⁶² have studied the exciton quenching process of QD in the presence of Rhodamine B dye and found that quenching due to the electron transfer process is 84%, whereas the energy transfer process is 16%. Ultrafast spectroscopic study is very

essential for understanding the electron or energy transfer process. The well-known biological scaffolds deoxyribonucleic acid (DNA), ribonucleic acids (RNA), and more rigid peptide nucleic acids (PNA) are being developed as efficient light-harvesting systems because of their sufficient stiffness over a persistent length of ~ 50 nm.^{163,164} Medintz et al.¹⁶⁵ have reported the resonance energy transfer from CdSe/ZnS core–shell QDs to fluorescent protein molecules and observed a 60% and 22% energy transfer efficiency for QD (emission at 510 nm)–yellow fluorescent protein (YFP) conjugate and QD (emission at 550 nm)–mCherry conjugate, respectively. An energy transfer efficiency of 98% was found for multi-chromophore b-phycoerythrin (b-PE)–QDs complexes because of multiple acceptor chromophores within b-PE and the relatively large cross-section of b-PE toward QDs. Analysis revealed that energy transfer is controlled by the size of the QDs and the nature of the dye molecule. A system was designed where a central QD was attached to two different peptides, and each peptide was labeled with one of two fluorescent dyes, Alexa Fluor 555 (AF555) or Alexa Fluor 647 (AF647), to explore the energy transfer between the QD and the attached dye.¹⁶⁶ It is found that less energy transfer occurs from QDs to AF647 and moderate transfer efficiency is found when it is relayed via AF555 to AF647 (Figure 11A,B). When ssDNA and yellow fluorescent protein (YFP) are adsorbed on the surface of CdSe/ZnS core–shell QDs and Atto647 dye

molecules are tagged with complementary ssDNA to form a dsDNA strand, another QD-based efficient energy transfer system is created.¹⁶⁷ This Atto647 is tagged at different positions of the complementary ssDNA to tune the distance between dye and protein or QDs. FRET is observed from QDs to YEP and finally toward Atto647. It is found that the efficiency of energy transfer decreases from ~60% to ~5% upon increasing the distance between QDs and Atto647 (Figure 11C), indicating the distance-dependent energy transfer. An elegant light-harvesting system has been designed by Spillmann et al.,¹⁶⁸ where a CdSe/ZnS core–shell is surrounded by a photonic wire of cyanine dyes in dsDNA. Four-step-cascade energy transfer is observed from QD toward four different dyes (Cy3, Cy3.5, Cy5, and Cy5.5), which are placed at $0.5R_0$, $1.0R_0$, and $1.5R_0$ intervals, on dsDNA (Figure 11D). Dennis and Bao¹⁶⁹ have designed fluorescent protein–QD pairs for an efficient energy transfer system where the acceptor protein molecules are attached to the QD surface via polyhistidine coordination, and 90% quenching of QD fluorescence was found.

3.2.1. Kinetic Model for QD-Based Energy Transfer. In this section, we address the kinetics of the energy transfer process and examine the distribution of dye molecules around QDs in QD–dye assemblies to develop efficient light harvesting in nanoscale systems. In the QD-based energy transfer process, size and shape are important parameters to control the distribution of dye molecules around QDs, because the size and shape of QDs are finite and the size of QDs is relatively larger than that of the dye molecules. Thus, the kinetics of energy transfer varies with changing the distribution of acceptor molecules around QDs. Recently, we have developed a stochastic model based on the interaction between the excited state of QDs and dye molecules to understand the kinetics of energy transfer from differently shaped QDs to dye molecules.¹⁷⁰ This model (Figure 12) allows us to estimate the number of dye molecules attached to the surface of a QD.⁷⁰

According to the kinetic model, the photoexcited QDs follow the processes

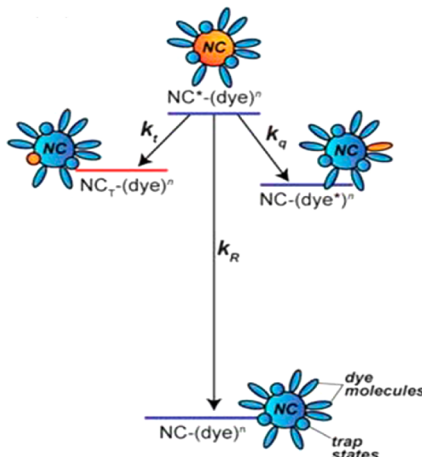


Figure 12. A four-states model of kinetics of energy transfer from QDs to dye molecules. Reprinted with permission from ref 70. Copyright 2010 Royal Society of Chemistry.



The excited-state QD is denoted as QD_n^* , where n is the attached number of dye molecules. QD_n represents n number of dye molecules attached to ground-state QD. The decay constant (k_0) represents a unimolecular process for the excited state donor in the absence of acceptor molecules. The rate constant (k_q) is for the energy transfer per one dye molecule. During the excitation of a QD with n number dye molecules, the rate constant of the excited state decay of QD is given by $k_0 + nk_q$, and nk_q is the total energy transfer rate constant. In this model, we have assumed that the distribution of the number of dye molecules attached to one QD follows a Poisson distribution (eq 12), and the ensemble averaged decay curve of the excited QD is given by^{44,170}

$$I(t,m) = I_0 \sum_{n_t=0}^{\alpha} \Phi(n) \exp[-(k_0 + nk_q)t] = I_0 \exp\{-k_0 t - m[1 - \exp(-k_q t)]\} \quad (20)$$

where m is the mean number of dye molecules attached to one QD. The above kinetic model was developed on the basis of the Tachiya¹⁷¹ model of luminescence quenching in micelles. Here, we have considered the existence of some unidentified traps on the surface of the QDs along with the acceptor dye molecules. In the absence and presence of dye molecules, the fluorescence decay curves of the excited state of QD are given by eqs 21 and 22. Again, considering the Poisson distribution of the number of unidentified traps on the surface of the QD, with m_t being the average number of unidentified traps, the equations are given below:

$$I(t,0) = I_0 \exp\{-k_0 t - m_t[1 - \exp(-k_{qt} t)]\} \quad (21)$$

$$I(t,m) = I_0 \exp\{-k_0 t - m_t[1 - \exp(-k_{qt} t)] - m[1 - \exp(-k_q t)]\} \quad (22)$$

The rate constant of quenching by unidentified traps is k_{qt} , which may be different from that (k_q) by dye molecules. The radiative rate constant, trapping rates, and energy transfer rate^{44,170} are calculated by using eq 22, which matches well with the experimental data, indicating that this kinetic model is extremely important to understand the kinetics of energy transfer and to quantify the number of attached acceptors with a single QD. A suitable kinetic model is important to understand the distribution of acceptor molecules around QDs to develop efficient light-harvesting systems.

3.2.2. Energy Transfer Based on Shape-, Size-, and Composition-Dependent QDs. The attachment of a number of acceptor fluorophores with an individual particle depends on the surface area of the QD, which is dependent on its size and shape.^{172–177} Recently, the shape-dependent resonance energy transfer between CdS quantum dots (QD)/quantum rods (QR) and dye molecules was determined by using steady state and time-resolved spectroscopy.¹⁷⁰ Analysis revealed that the efficiency of energy transfer from QD or QR to dye molecules depends on the donor/acceptor ratio (Figure 13A,B). Using a stochastic kinetic model, the decay curves of CdS QD/QR in the absence and presence of dye molecules were analyzed by using eq 22 to understand the shape-dependent energy transfer.¹⁷⁰ It is interesting to note that the average number of dye molecules (m) attached to the surface of a QD depends

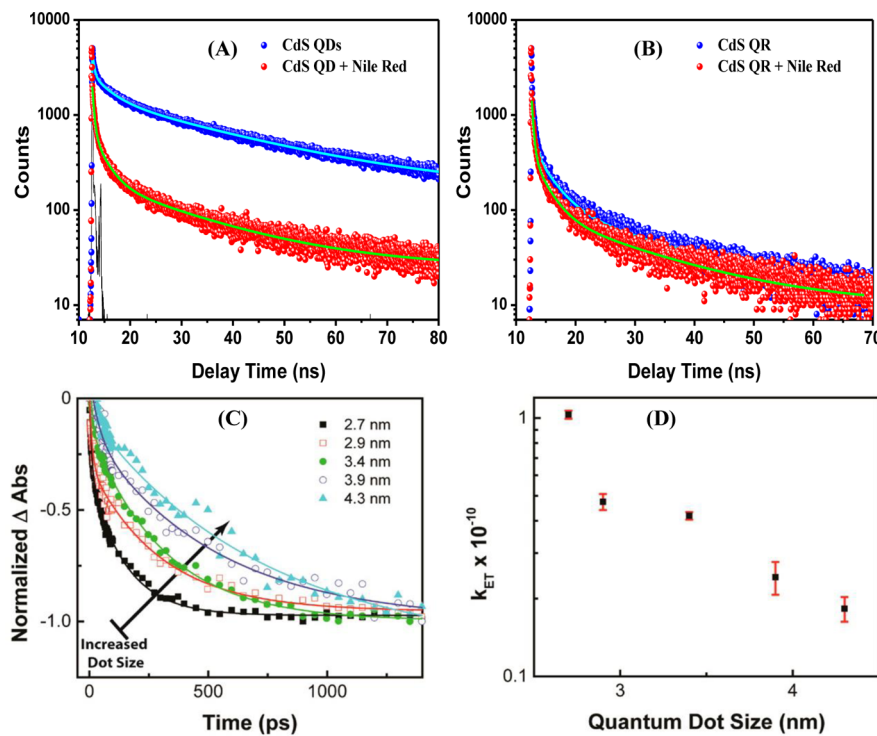


Figure 13. (A) Time-resolved fluorescence decay curves of CdS QDs and (B) CdS QRs in the presence and absence of Nile Red dye. Reprinted with permission from ref 176. Copyright 2008 Wiley-VCH Verlag GmbH & Co. KGaA. (C) Kinetic traces of the bleach growth of squaraine dye (at 648 nm) with changing the size of the QD. (D) Rate of energy transfer is plotted against the size of the QD. Reprinted from ref 179. Copyright 2014 American Chemical Society.

on the concentration of dye molecules and the shape of the QD. The shape of the QD also controls the equilibrium constant of bound and unbound dye during energy transfer. It is to be noted that not all dye molecules are involved during the energy transfer process. The fractions of dye molecules attached to QDs vary with the changing shape and size of the QDs, and the remaining fraction of the unattached dye molecules remains in the solution. It is seen that the larger surface area of a QR accommodates more dye molecules than a QD;¹⁷⁰ as a result, the energy transfer rate constant of QRs per one dye molecule is higher than that of QDs. Again, Hardzei et al.¹⁷⁵ have investigated the energy transfer from CdSe/ZnS core–shell QDs or nanorods (NRs) to Alexa Fluoro 647 organic dye molecules and revealed that the energy transfer efficiency of NRs is different from that of QDs.

Dayal et al.¹⁷⁸ have highlighted the influence of the size of QDs on the energy transfer efficiency in CdSe QD–phthalocyanine conjugate systems. A nonlinear dependence of energy transfer is observed in the case of smaller-sized QDs, and a linear dependence is observed in the case of larger-sized QDs, which may be due to the involvement of surface states in the energy transfer process.¹⁷⁸ It is known that spectral overlap between the emission band of the donor and the absorbance band of the acceptor would play a role in the efficiency of energy transfer. In the case of QD-based energy transfer, the overlap integral can be tuned by changing the size of the QD, which eventually influences the energy transfer efficiency. It is reported that the spectral overlap between the emission band of the QD and the absorbance band of squaraine dye decreases with decreasing QD size, which controls the energy transfer efficiency.¹⁷⁹ This study definitely demonstrated the size-dependent energy transfer between CdSe QDs and dye. Figure 13C represents the decay curves of the bleach growth of

different QD sizes, and Figure 13D shows that the rate of energy transfer decreases upon changing the size of the QDs. Another example is given of the energy transfer between CdSe QDs and Nile Red dye, where the distribution of dye molecules around the QD varies with a change in the size of the QD.⁴⁴ A stochastic kinetic model has been used to analyze the decay profiles of CdSe QDs in the absence and presence of Nile Red dye molecules, and the kinetic data match well with the FRET data. Analysis revealed that the average number of dye molecules attached to one QD increases with an increase in the size,⁴⁴ which is explained by the size-dependent energy transfer. Analysis of the size-dependent energy transfer revealed that the size of QDs controls their PL shifting, the change of spectral overlap, and the average number of dye molecules attached to one QD, and all these parameters eventually control the efficiency of energy transfer. In our opinion, knowledge of the exact number of acceptor molecules participating in an energy transfer process is important when designing efficient QD-based light-harvesting systems.

Like the size and shape of QDs, the composition of QDs influences the efficiency of the energy transfer, because the efficiency of energy transfer depends on the spectral overlap between the emission band of the donor and the absorbance band of the acceptor. PL shifting is observed upon changing the composition of alloy QDs, which influences the overlap integral. Therefore, it is expected that the alloy QDs are promising for developing QD-based light-harvesting materials. The PL quenching and the shortening of the decay time of $\text{Cd}_x\text{Zn}_{1-x}\text{S}$ alloy QDs in the presence of dye molecules confirm the efficient energy transfer from $\text{Cd}_x\text{Zn}_{1-x}\text{S}$ alloy QDs to Nile Red dye molecules.¹⁸⁰ In such cases, the energy transfer efficiency value varies with composition because the overlap integral of alloy QDs changes with the composition of QDs.

The average distances between QDs and dye molecules can be calculated by considering single donor and multiple acceptor participation during the energy transfer process. Analysis of this study revealed that the size, shape, and composition of QDs play a significant role in the control of the energy transfer process, and such knowledge will help us to develop new and challenging light-harvesting systems based on QDs. In our opinion, a future area of research may focus on the design of assembled structures of QDs–metal nanoparticles, QDs–graphene, etc. to develop promising QD-based light-energy-harvesting and solar cell applications.^{181,182}

3.3. QD-Based Light-Harvesting Applications

It is well-acknowledged that semiconducting nanomaterials are being used for photovoltaics and photocatalysis applications using solar energy conversion. In the case of photovoltaic applications, photocurrent generation occurs due to charge migration of photogenerated electrons and holes of semiconductor nanoparticles toward opposite electrodes. However, the photogenerated electrons and holes of semiconductor nanoparticles are used for reduction and oxidation reactions to facilitate chemical conversion in the case of photocatalysis. A schematic representation of QD-based photovoltaic and photocatalysis is given in Figure 14.

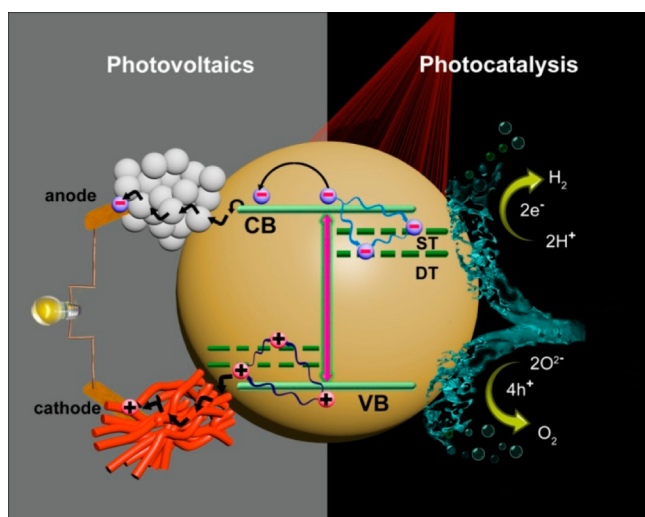


Figure 14. Schematic representation of basic aspects of QD-based photovoltaics and photocatalysis.

3.3.1. QD-Based Solar Cells. The capturing of incident light energy and the transportation of the photogenerated charge to the external circuit are the basic aspects for the development of high-performance QD-based photovoltaic devices. The device performance critically depends on the band offset, carrier mobility, trap density, and diffusion length of the carriers in the QD film. Several review articles on QD-based solar cells exist in the literature.^{183–191} Here, we have highlighted the important roles of size, shape, and composition in the QD-based solar cells efficiency.

3.3.1.1. Effect of QDs' Size on Solar Cell Efficiency. Recent findings revealed that the size of the QDs influences the photocurrent and fill factor, and these decrease with an increase of the size of QD because the larger particle size facilitates the inter-particle charge transfer.^{192,193} Again, Law and coauthors¹⁹² have demonstrated that the electron and hole mobilities are increased upon increasing the QD diameter

(Figure 15A). The increment of electron mobility with an increase of the particle diameter of CdSe also has been observed by Kang et al.¹⁹⁴ Again, it is reported that smaller-sized QDs exhibit greater charge injection rates with less visible light absorption ability. However, larger particles have better absorption ability in the visible region and less electron injection ability.¹⁹³ Thus, devices can be designed that stack QDs with different band gaps¹⁹⁵ to improve the efficiency by increasing solar light absorption as well as retaining higher charge injection. Another strategy to enhance the device performance is funneling of energy toward layers of QDs with different diameters by using graded band gap materials, as shown in Figure 15B.¹⁹⁶ This design not only facilitates the movement of photoelectrons from their generation point toward the electrodes, but also enhances the absorption of different wavelengths of light. Recently, a tandem heterojunction QDs solar cell was used to increase the energy harvesting from the sun, because a tandem solar cell is designed to use different sizes of PbS QDs (Figure 15C).¹⁹⁷ It is reported that the electron injection rate of small-sized QDs is higher than that of the large-sized QDs in QD-sensitized solar cells (QDSSCs).¹⁸⁴ In the CdSe/TiO₂ system, the electron transfer rate increases as the conduction band energy of QDs increases with decreasing QD size, which enhances the injection of electrons into a photoelectrode (Figure 15D).¹⁹⁸ Analysis suggested that the efficient solar-to-electricity conversion depends on the size of the QDs and the optical absorption wavelength.

3.3.1.2. Alloy and Core–Shell QDs. Another potential strategy is to design QD-based solar cells by using alloy or core–shell QDs to improve the efficiency,^{199–201} because the band gap of ternary and quaternary alloy systems is more narrow than that of binary alloy.^{202,203} The successive ionic layer adsorption and reaction (SILAR) technique is used to design QDSSCs. It was reported that alloy CdSe_xS_{1-x} QDs were used for QDSSCs devices, and the maximum energy conversion efficiency was achieved by changing of the ratio of sulfur (S) to selenium (Se) to control the band gap and the light absorption of CdSe_xS_{1-x} QDs.²⁰⁴ The limitation of the alloy QDs in the light-harvesting applications is the generation of a small photocurrent, because of the relatively short absorption edge wavelength (<700 nm). To improve the efficiency of QDs, extended absorption in the spectral region is required.^{205,206} CdSe_xTe_{1-x} alloy QDs exhibit extended absorption up to the near-infrared (NIR) region, and this QD improves the efficiency of the device up to 6.36%.²⁰⁵ The enhanced photocurrent generation of alloy CdSeTe QDs (Figure 16) is comparable with that of individual CdTe or CdSe QDs.²⁰⁵

Another strategy is to fabricate a device based on core–shell QDs to improve the solar cells efficiency, because core–shell QDs improve the light absorption and reduce the defect states by surface passivation. The effects of size and shell thickness influence the charge transfer rates.^{147,207,208} Type II core–shell QDs have been explored for photovoltaic applications, including ZnSe/CdS,^{209,210} CdS/CdSe,^{211–214} CdTe/CdS,²¹⁵ and CdTe/CdSe.^{216,217} Bawendi's group has recently engineered the band alignment of the quantum dot layers in a room-temperature-fabricated solution-processed ZnO/PbS quantum dot solar cell. They achieved an efficiency of 8.55%, and the performance of unencapsulated devices remained unchanged for over 150 days of storage in air.²¹⁸ An energy conversion efficiency of 3.17% is achieved by using CdSe_xS_{1-x}/

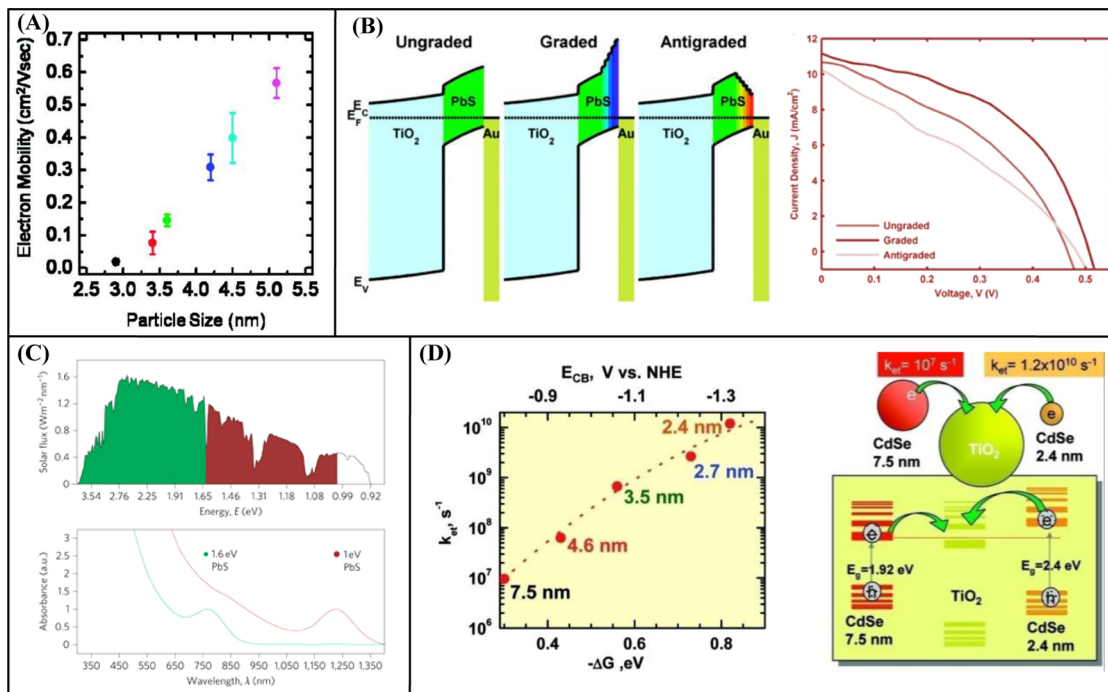


Figure 15. (A) Size-dependent electron mobility of CdSe QDs. Reprinted with permission from ref 194. Copyright 2010 American Chemical Society. (B) Spatial band diagrams of ungraded, graded (quantum funnel), and antigraded QD solar cells. The plot shows J - V performance under AM 1.5 conditions of the ungraded, graded (quantum funnel), and antigraded devices. Reprinted with permission from ref 196. Copyright 2011 American Chemical Society. (C) Spectral utilization (top) and absorption spectra (bottom) of different sizes of PbS QD. Reprinted with permission from ref 197. Copyright 2011 Nature Publishing Group. (D) The left plot shows the electron transfer rate constant versus the energy difference between the conduction bands. The right scheme illustrates the mechanism of electron transfer from CdSe QDs to TiO_2 nanoparticles. Reprinted with permission from ref 198. Copyright 2007 American Chemical Society.

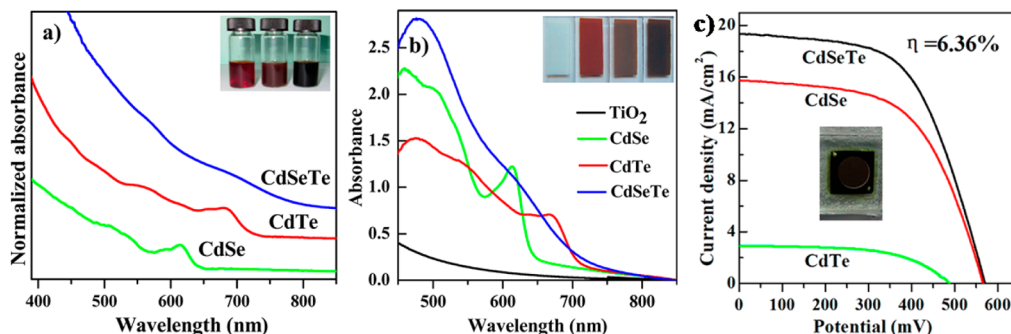


Figure 16. Absorbance spectra of binary CdSe and CdTe and ternary CdSeTe QDs in solution (a) and in film (b). The J - V plot (c) shows an enhanced photocurrent for the ternary CdSeTe QDs. Reprinted with permission from ref 205. Copyright 2013 American Chemical Society.

CdSe core–shell QDSSCs, which is much higher compared to a solar cell utilizing only $\text{CdSe}_{x}\text{S}_{1-x}$ QDs. The improved efficiency is due to enhanced absorption and reduced recombination in the core–shell QDs.²⁰⁴ The efficiency of QD-sensitized solar cells is reported to be enhanced after surface coating of CuInS_2 QDs with a ZnS layer²¹⁹ due to enhanced light absorption. The shell of QDs suppresses the hole traps and blocks the hole injection into the electrolyte. By combining the knowledge of the hole trapping¹²¹ and electron injection¹⁴⁷ into metal oxide, Abdellah et al. demonstrated how the shell thickness influences the solar cell efficiency, and they illustrated the electron and hole dynamics as a function of the shell thickness. They reported that the $\text{Cd}_{1-x}\text{Zn}_x\text{Se}_{1-y}\text{S}_y$ gradient core–shell QDs system having a shell thickness of 1.3 nm enhances the efficiency of the solar cells by 2.5 times compared to the core-only case. Zheng et al.¹⁴⁹ have reported

enhanced hole injection efficiency by passivation of surface traps of core–shell QDs in p-type QD solar cells. In addition to surface modifications, doping of QDs may be another technique to improve the solar cell efficiency.²²⁰

3.3.1.3. Trap State of QDs and Surface Ligands. The carrier diffusion length is of paramount importance to device performance, as the charge carrier transport relies solely on the diffusion process. The diffusion length is found to be influenced by the carrier mobility and carrier lifetime, which are crucial factors in device performance.^{189,221,222} Again, the defects in the band gap can act as recombination centers²²³ or trap states, which reduce the photocarrier populations, thereby limiting the diffusion length and carrier lifetime. Theoretical modeling indicates that the carrier lifetime is short when the trap density is high (Figure 17a). Similarly, the diffusion length of the film is increased (Figure 17b) when the trap density is reduced.²²¹

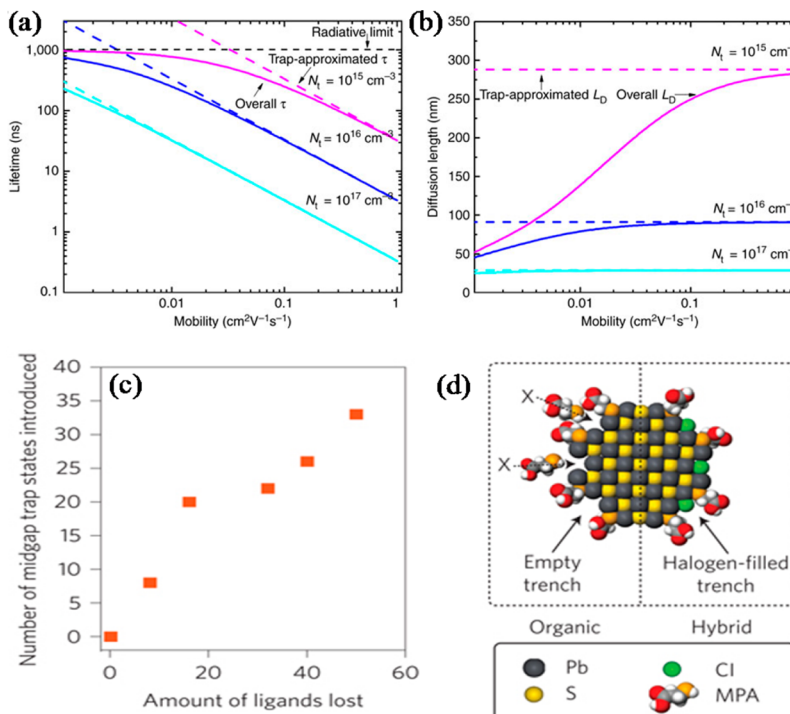


Figure 17. (a) Theoretical relationship between the trap density and carrier lifetime. (b) Theoretical relationship between the diffusion length and carrier mobility. Reprinted with permission from ref 221. Copyright 2014 Nature Publishing Group. (c) Plot of the number of midgap trap states with the amount of ligands lost from the quantum dot surface. (d) Schematic representation of a QD with organic passivation (left) and the hybrid passivation (right). Reprinted with permission from ref 225. Copyright 2012 Nature Publishing Group.

Defects can also reduce the quasi-Fermi level splitting range under illumination, which leads to lower open-circuit voltage. Thus, the control over the defect states is essential for improving device performance.²²⁴ Such defects are normally caused by the loss of surface ligands during the ligand exchange process.²²⁵ Figure 17c shows the plot of a correlation of the number of midgap trap states with the amount of ligand lost. The number of trap states increase with the number of “missing” ligands. The presence of unreacted precursors or excess surfactants is essential for stabilizing the colloidal quantum dot solution; however, they act as an insulating medium around the QDs and they slow down the charge transfer in solar cells.^{156,226–228} The partial or full exchange of primary ligands by short, conductive ligands will dramatically improve the device performance. Short thiol molecules are found to be effective for reducing recombination in CdTe and PbSe.^{229,230} Several metal chalcogenide complex (MCC) ligands like $\text{In}_2\text{Se}_4^{2-}$,^{231,232} Cu_7S^{4-} ,^{231,233} AsS_3^{3-} ,²³⁴ $\text{Sn}_2\text{S}_6^{4-}$,^{235,236} and $\text{Sn}_2\text{Se}_6^{4-}$ ²³⁵ have been successfully used for surface modification as small and conductive ligands. In solar cells based on QD–metal oxide, the linker molecule plays a crucial role in the relaxation channel. The recent development of a single atom surface passivation technique improves the extraction of current in a solar cell by reducing the deep trap states.²³⁷ It is now well-known that the trap states are reduced significantly by passivation.²²⁵ Figure 17d shows the cross-section of a PbS QD with mercaptopropanoic acid (MPA) (left) and the passivation by both MPA and halides (right).²²⁵ The passivation approach leads to improved photovoltaic performance with an efficiency of 7%.²²⁵ Thus, the knowledge of surface defects of QDs is important to develop an efficient QD-based system.²³⁸ A photonic enhancement has been utilized to increase further absorption in a given thickness of

light-absorbing material. Surface plasmon resonance, in which localized collective electron oscillations occur near a metal–dielectric interface or at the surface of a metal nanoparticle, has been used to improve QD solar cell performance.²³⁹ Further discussion will take place in the section 4 (Metal-Nanoparticle-Based Light-Harvesting Systems).

3.3.2. Basic Aspects of Photocatalysis and H₂ Generation. Photocatalysis is a mimicking of the natural photosynthesis system where solar energy directly converts to chemical energy. After the discovery of photocatalytic water splitting by Fujishima and Honda,²⁴⁰ significant emphasis has been given to develop semiconductor-based light-harvesting systems for degradation of hazardous substances, water splitting for hydrogen fuel, and photocatalytic conversion of CO₂ to energy-rich hydrocarbon fuels. Semiconducting QDs are used for chemical transformation by photon energy because electrons of the valence band (VB) are promoted to the conduction band (CB) and positive holes are left in the VB upon photoexcitation of QDs, and water molecules are reduced by the electrons and oxidized by the holes to form H₂ and O₂, respectively, during water splitting. Thus, the knowledge of the band gap and the conduction and valence band levels is important to develop efficient semiconductor photocatalyst materials for water splitting. For QD-based photocatalysis, the bottom level of the conduction band of QDs should be more negative than the redox potential of H⁺/H₂ (0 V vs NHE), and the top level of the valence band of QDs should be more positive than the redox potential of O₂/H₂O (1.23 V) for water splitting. The band levels of various common semiconductor materials are given in Figure 18A.²⁴¹ Thus, the solar light is harvested by QD photocatalysts to facilitate chemical conversions like hydrogen generation, oxygen evolution, CO₂ fixation reactions, and hazardous materials degradation. The

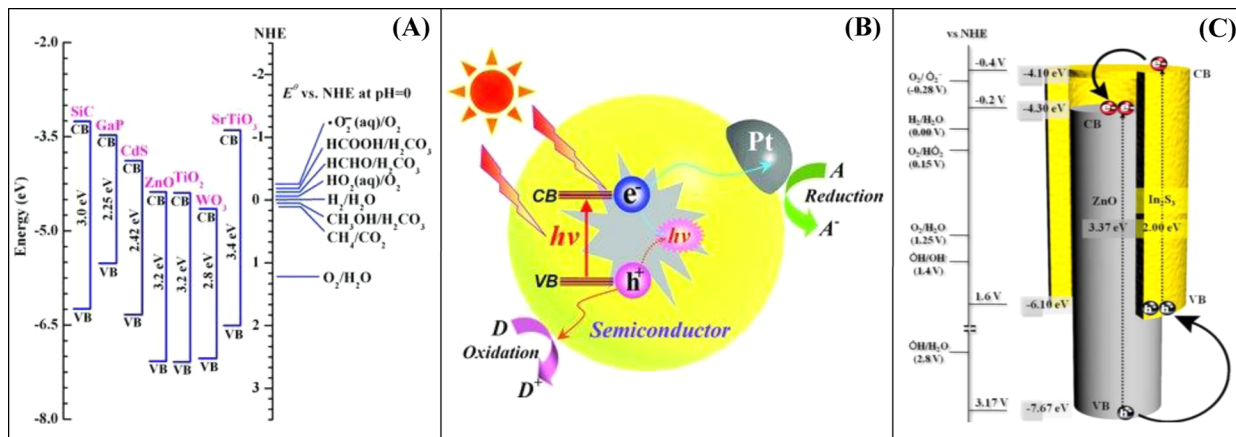
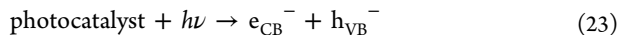


Figure 18. (A) Energy levels diagram of various semiconducting materials with respect to redox couples in water. (B) Schematic representation of the photocatalytic process of semiconductor materials. Reprinted with permission from ref 241. Copyright 2012 Wiley-VCH Verlag GmbH & Co. KGaA. (C) Effective charge separation in a type II core–shell ZnO/In₂S₃ heterostructure semiconductor for visible-light photocatalysis. Reprinted with permission from ref 246. Copyright 2013 American Chemical Society.

processes within the QDs can be summarized by the following equations:



A large number of semiconducting nanoparticles (NPs), including metal oxides, chalcogenides, heterostructures, and core–shell nanoparticles, are being used for photocatalytic applications.^{241–244} Wide band gap semiconductors like TiO₂ have proven to be better catalysts than the low band gap semiconductor CdS mainly due to photostability and photo-corrosion issues. However, the low band gap materials are more responsive to the solar spectrum and more efficient in visible solar light harvesting. In addition to pure semiconductor nanomaterials, use of metal–semiconductor heterostructures and core–shell materials is a potential strategy to improve the photocatalysis efficiency.^{245–247} Considering new-generation catalysts, light absorbing antenna materials are coupled with redox active reaction centers for the efficient charge separation. The deposition of noble metals (Au, Ag, Pd, and Ag) on the surface of semiconductors increases the lifetime of the electron–hole pair and causes efficient charge separation.^{248,249}

The electrons are enriched in the noble metal, and the hole remains confined within the semiconductor nanoparticle, which produces a potential difference that enhances the catalytic efficiency. By utilizing these strategies, heterostructures are designed for efficient catalysis, photocatalytic H₂ production, and CO₂ fixation (Figure 18B). The fast recombination of photogenerated electrons and holes and the low efficiency in the visible range of the solar spectrum are the drawbacks of the application of semiconductor nanomaterials to photocatalysis. To overcome this problem, type II core–shell nanomaterials (Figure 18C) are used for effective injection of photogenerated electrons from shell into core, which led to reduced recombination between electron–hole pairs of core–shell nanomaterials.²⁴⁶ However, both the electrons and holes are confined in the core in type I core–shell heterostructures, whereas the electrons and holes are separated between the core

and the shell in type II structures. This will give rise to a significant increase in the exciton lifetime, which is preferable for photocatalysis applications.

TiO₂ nanoparticles having a large band gap (3.2 eV) are commonly used for H₂ generation where 4% solar light is being used.^{241,250–255} The efficiency of the photoreaction is limited because the most intense visible light of the solar spectrum is not effectively used for the catalysis. Therefore, another strategy is to use low band gap semiconductor materials (CdS and CdSe nanoparticles, etc.)^{256–258} for visible light photocatalytic H₂ generation. Several visible light capturing semiconducting nanomaterials, i.e., heterostructures, alloys, and core–shell nanostructures such as TiO₂–CdS, TiO₂–Pt, CdS–Pt, Zn_{1-x}Cd_xS, Cu(OH)₂/TiO₂, Cu₂MoS₄, CdS–PdX, NiO_x–SrTiO₃, reduced graphene oxide–Zn_{1-x}Cd_xS, MoS₂–graphene/TiO₂, CdS–graphene–Pt, TiO₂–CdS–Pt, CdSe–MoS₂, Fe₃O₄, Co₃O₄, are found to be effective for efficient H₂ generation.^{251,259–267} In addition to these systems, the use of two-dimensional (2D) semiconductor nanostructures is another strategy for hydrogen generation. Among them, few-layer and single-layer MoS₂ and MoSe₂ have been widely used as a catalyst for electrochemical, photoelectrochemical, and photocatalytic H₂ generation from water^{268–271} because the conduction band minimum is situated well above the H₂O reduction potential.^{272–274} It is also evident from theoretical studies that the edge sites of MoS₂²⁷⁵ and vacancy defects²⁷⁶ are active in the hydrogen evolution reaction (HER). Thus, the large density of exposed edges of the sheetlike structure is responsible for the improvement of the activity. It was reported recently that the activity of the 1T form of MoS₂ much higher (600 times) than that of the few-layer 2H form of MoS₂.²⁷⁷ Figure 19a shows the time-dependent H₂ evolution from the 2H and 1T forms of MoSe₂ under visible light.²⁷⁸ The activity of MoSe₂ is found to be higher than that of MoS₂, which can be explained by the work function and binding of hydrogen at the edge site. Here, the work function of MoSe₂ is less than that of MoS₂, and the binding of hydrogen to Se is weaker than to S at the edge sites. The composites of MoS₂ with CdS,^{270,279} CdSe,²⁶¹ and TiO₂²⁸⁰ and dye sensitization with (Ru(bpy)₃)²⁶⁸ and eosin²⁸¹ are found to be promising for the HER. A composite with graphene is another material used to improve HER activity by effective enhancement of charge separation.²⁶⁹

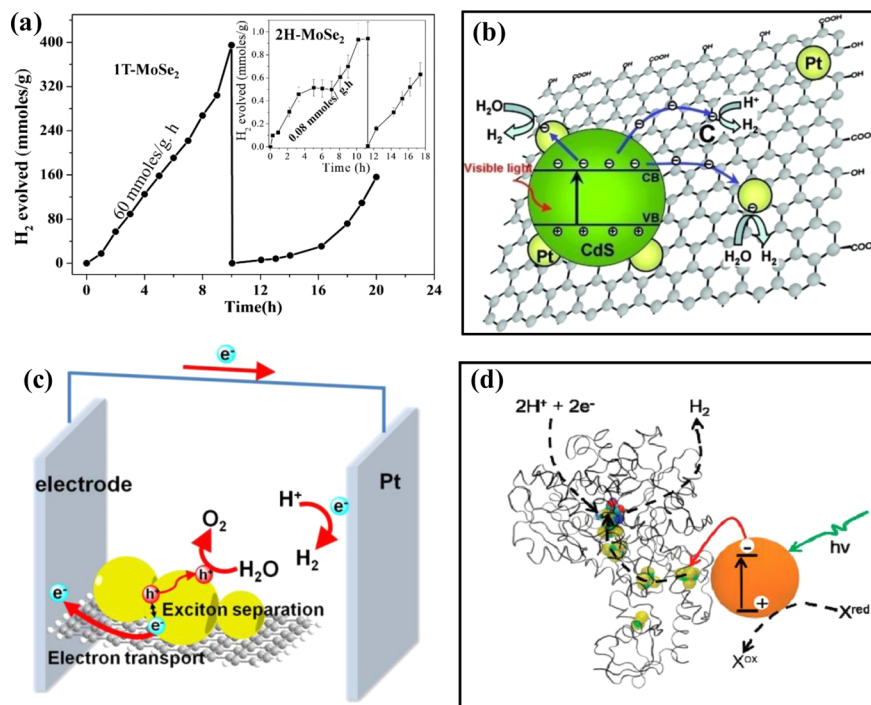


Figure 19. (a) Time-dependent H_2 evolution by 1T- and 2H-MoSe₂ under visible light. Reprinted with permission from ref 278. Copyright 2014 American Institute of Physics. (b) Schematic representation of the charge separation and electron transfer process in graphene–QDs composite. Reprinted with permission from ref 286. Copyright 2011 American Chemical Society. (c) Schematic diagram of a photochemical system where graphene acts as a channel for photogenerated electrons of QDs during H_2 generation. Reprinted with permission from ref 291. Copyright 2013 Elsevier BV. (d) A scheme for light-driven H_2 production by the nc-CdTe:H₂ase complex. Here, X represents a sacrificial hole scavenger. Reprinted with permission from ref 299. Copyright 2010 American Chemical Society.

A composite of few-layer 2H-MoS₂ with nitrogen-containing graphene exhibits enhanced photocatalytic activity due to the enhance charge separation in the composite materials.²⁷⁷ It is reported that graphene is extensively used to develop composite systems with semiconducting nanomaterials, such as TiO₂,^{282–285} CdS,^{286–289} and Cu₂O,²⁹⁰ for improved photocatalytic efficiency. Figure 19b represents the charge separation and electron transfer process in a graphene–QD composite.²⁹¹ Figure 19c represents the schematic diagram of a photochemical system where graphene acts as channel for photogenerated electrons during H_2 generation. The metal–semiconductor hybrid systems are also found to yield a significant amount of H_2 by effective charge separation.^{292,293} Amirav and Alivisatos²⁹⁴ have employed a platinum-tipped CdS rod with an embedded CdSe multicomponent nanoheterostructure for efficient photocatalytic hydrogen production because this system facilitates efficient long-lasting charge carrier separation. The quantum efficiency of 20% at 450 nm was revealed with long duration of catalytic activity. In another study, they showed that manipulating photoinduced charge-transfer rate and prolonging charge-separation lifetime, on the time scale of 10^{-7} s, might be sufficient for significant improvement of the catalytic efficiency.²⁹⁵ Amirav and his co-workers achieved 27% quantum efficiency of hydrogen generation using CdSe@CdS rods decorated with a single Pt catalyst.²⁹⁶ In a similar work, Bar-Sadan and co-workers have found that the cocatalyst composed of Au@(Au/Pd alloy) at the tip of CdSe@CdS-seeded rods was superior for hydrogen production.²⁹⁷ By manipulation of charge carriers dynamics, Kalisman et al. have found 100% photon-to-hydrogen production efficiency, under visible-light illumination, using Pt-tipped CdSe@CdS rods.²⁹⁸ This observation has opened up

a new avenue for the prospects of water splitting and solar-to-fuel energy conversion by using QDs.

To mimic the natural catalysts, semiconducting QDs coupled with natural enzymes are being used for catalytic hydrogen production. For example, King and co-workers have described a biomimetic approach for coupling [FeFe]-hydrogenase from *Clostridium acetobutylicum* to CdTe nanocrystals.²⁹⁹ Upon illumination with visible light, the electron transfer occurs from CdTe to the enzyme, which leads to H_2 production, and the quantum yield of H_2 generation is 9% ($\lambda = 532$ nm) (Figure 19d). Similarly, the complex of a synthetic mimic of [FeFe]-hydrogenase and 3-mercaptopropanoic acid capped CdTe QDs was used for the H_2 evolution reaction.³⁰⁰ Greene et al. have reported higher activity for the CdTe QD–[NiFe]-hydrogenase system than for the Ru(bpy)₃²⁺–[NiFe]-hydrogenase system, indicating the effective light harvesting by the CdTe QDs.³⁰¹ Brown et al. have reported 20% quantum yield of H_2 production with CdS nanorod–[FeFe] hydrogenase complexes under illumination of 405 nm light.³⁰² In our opinion, more emphasis should be given to designing QD-based systems for H_2 generation and trying to understand the basic mechanism by using ultrafast spectroscopy.

Beside H_2 evolution, the oxygen evolution reaction by water splitting has attracted recent interest, and several systems have been developed to mimic the oxidation of water by utilizing a Mn₄O₅Ca cluster in the protein.^{303,304} Recently, Maitra et al. have reported that the Mn and Co oxides of spinel and perovskite structures are efficient for photocatalytic oxygen evolution.³⁰⁵ Crystalline polymorphs of manganese oxides have been recently used for photocatalytic oxygen evolution, and it was found that Mn₂O₃ and Mn₃O₄ are most active due to the presence of Mn^{III} (d^4) in edge-sharing octahedral with longer

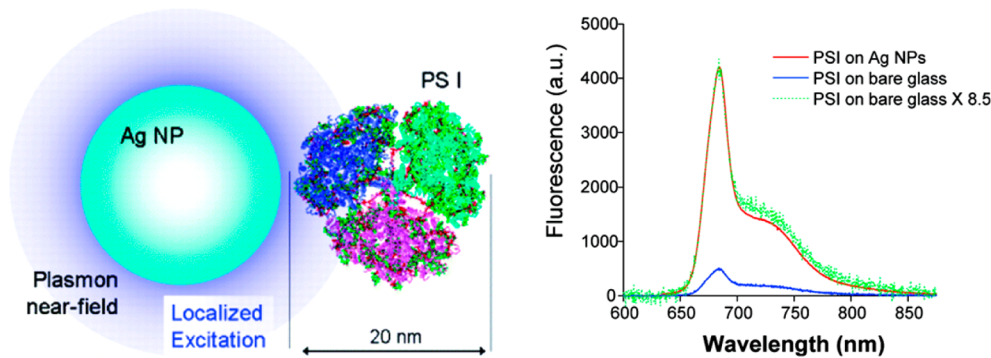


Figure 20. Enhanced fluorescence for a PSI thin film shown by comparing the PSI fluorescence emission occurring with a single individual Ag NP (red trace) with the PSI thin film fluorescence emission on a bare glass substrate (blue trace). Reprinted with permission from ref 323. Copyright 2011 American Chemical Society.

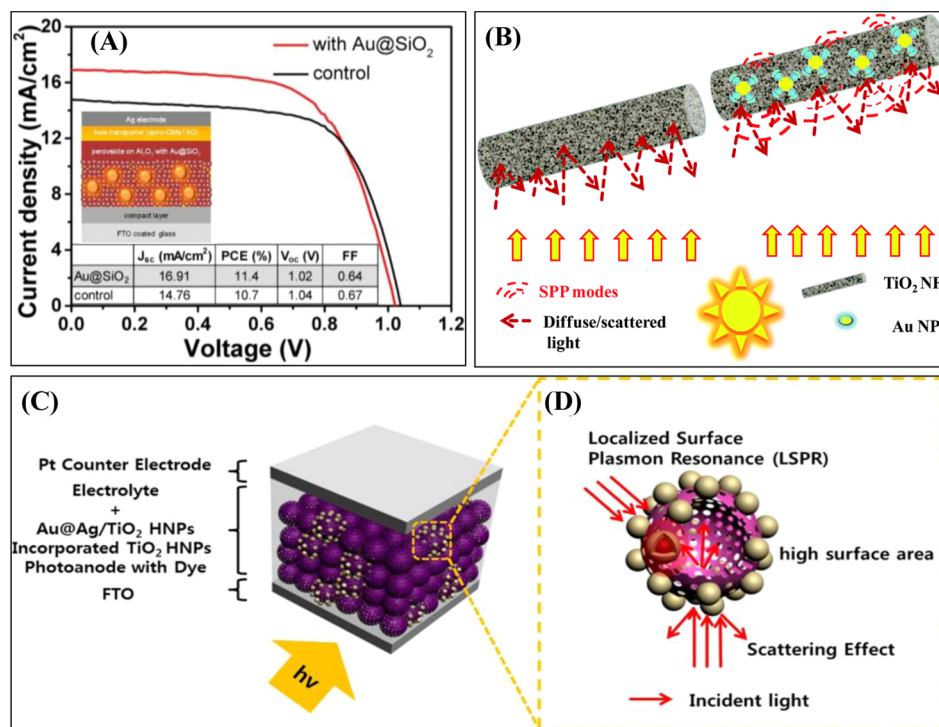


Figure 21. (A) Illustration of device structure incorporating core–shell $\text{Au}@\text{SiO}_2$ nanoparticles, and representative J – V curves for Al_2O_3 -only and $\text{Au}@\text{SiO}_2$ -incorporated devices measured under AM1.5 simulated sunlight (100 mW/cm² irradiance). Reprinted with permission from ref 326. Copyright 2013 American Chemical Society. (B) Mechanism of light harvesting of TiO_2 nanofibers and TiO_2 – Au nanofibers in the presence of the surface plasmon–polariton (SPP) modes of Au nanoparticles. Reprinted with permission from ref 336. Copyright 2014 Royal Society of Chemistry. (C and D) Schematic illustrations of a photoanode from a TiO_2 -HNP-based DSSC incorporating $\text{Au}@\text{Ag}/\text{TiO}_2$ hetero-nanoparticles. Reprinted with permission from ref 339. Copyright 2015 American Chemical Society.

Mn–O bonds than Mn^{IV} (d³).³⁰⁶ Photocatalytic conversion of CO₂ is an important issue to solve the problems related to global warming due to the green house effect of CO₂. A few review articles highlighted various catalysts involved in CO₂ conversion.^{307–309} The semiconducting QDs hybrid systems recently emerged as the new catalyst for photocatalytic reduction of CO₂. TiO₂ has been most widely used as the catalyst for CO₂ reduction. Heterostructures of TiO₂ with low band gap semiconductors such as CdSe, PbS, Bi₂S₃, and metal nanoparticles are suitable for the photocatalytic reduction of CO₂.^{310–314} Semiconducting QDs act as sensitizers in these heterostructures, where the injection of electrons to the TiO₂ conduction band occurs upon photoexcitation and enhances the photocatalytic CO₂ reduction activity.³¹⁰ The trans-

formation pathway is complicated and the conversion efficiency is very low because the reduction of CO₂ requires several electron transfers for the successful conversion. Thus, it reveals that a fundamental understanding of the electron transfer process is required to develop efficient systems for mimicking photosynthesis.

4. METAL-NANOPARTICLE-BASED LIGHT-HARVESTING SYSTEMS

In this section, we discuss the importance of plasmonic metal nanoparticles for developing challenging light-harvesting materials for energy generation.^{315–317} It is well-established that localized surface plasmon resonance (LSPR) of metal nanoparticles (Ag, Au, Pt) enhances light concentration around

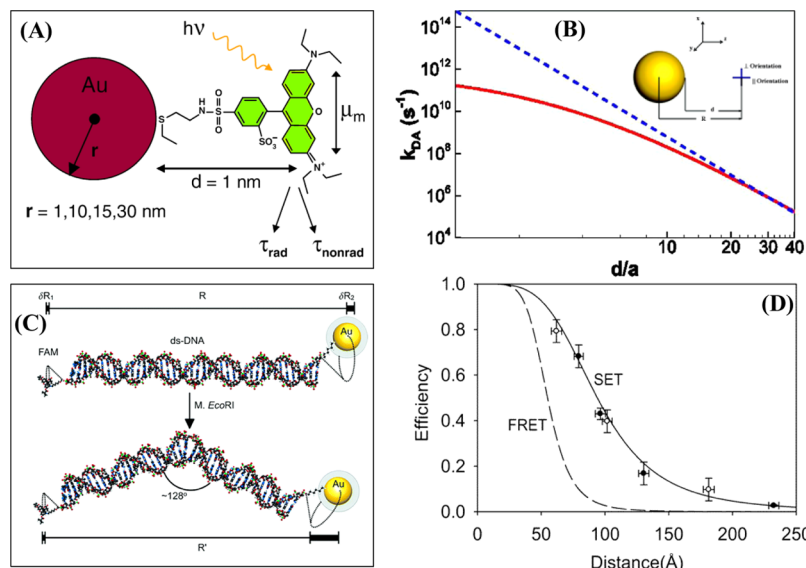


Figure 22. (A) The radiative and nonradiative rate of Au attached to a lissamine dye molecule upon changing the radii of the nanoparticle from 1 to 30 nm. Reprinted with permission from ref 59. Copyright 2002 American Physical Society. (B) The distance dependence of the rate of energy transfer (k_{DA}) calculated using full the Coulomb interaction (solid line) and the dipole–dipole approximation (Förster theory) (dashed line) for the parallel orientation for a nanoparticle of size 3.0 nm. Reprinted with permission from ref 353. Copyright 2006 American Institute of Physics. (C) Schematic representation of the energy transfer from fluorescein (FAM) dye to Au nanoparticle ($d = 1.4 \text{ nm}$). (D) Plots of energy transfer efficiency versus distance between FAM and Au. The dashed line represents the theoretical FRET efficiency, while the solid line represents the theoretical SET efficiency. Reprinted with permission from ref 357. Copyright 2005 American Chemical Society.

metal nanoparticles.³¹⁸ Köhler and his co-workers have reported Au nanoparticle plasmon induced fluorescence enhancement of photosynthetic pigment protein light-harvesting 2 (LH2) complexes.³¹⁹ Their study revealed that the fluorescent protein emission enhances upon excitation of the protein near Au plasmon resonance, whereas excitation beyond the plasmon resonance has no effect on the fluorescence. Mackowski and co-workers also have reported that the complex 2 of purple bacteria improves the light-harvesting properties in the presence of metal nanoparticles. Interestingly, the distance-dependent enhancement of the LH2 complex has been investigated and it was revealed that the maximum enhancement occurs when the separation layer between the LH2 complex and the metal nanoparticle is 12 nm.^{320–322} Kim et al. have used Ag nanoparticles to enhance light harvesting in cyanobacterial photosystem I trimer complexes (PSI).³²³ They observed 5–20-fold fluorescence enhancement of PSI complexes adjacent to Ag NPs due to efficient light collection and subsequent localized surface plasmon excitation of PSI (Figure 20). Analysis suggested that the orientation of the molecule plays an important role in the light-harvesting system of Fenna–Matthews–Olson complex (FMO) in the presence of gold nanoparticles.³¹⁸ Thus, metal-nanoparticle-based enhancement of fluorescence of natural light-harvesting proteins opens up new possibilities for biohybrid light-harvesting systems.

On the other hand, metal nanoparticles are being used to enhance the efficiency of solar cell and photocatalysis. Kim et al. have fabricated an organic solar cell by incorporating plasmonic Ag nanoparticles to improve the photocurrent density due to the strong interaction between electromagnetic field strength and the surface plasmons.³²⁴ Surface-enhanced absorption of solar light was found to enhance the photocurrent of Au-decorated Si nanowire.³²⁵ It was reported³²⁶ that the device performance of a solar cell based on perovskites (Figure 21A) improves because of the reduction of exciton

binding energy in the presence of metal nanoparticles. Several recent reports describe the importance of metal nanoparticles on the performance of dye-sensitized solar cells (DSSCs).^{327–334} It was found that metal nanoparticles improve the efficiency of TiO₂-based dye-sensitized solar cells because plasmonic nanoparticles transfer photoexcited electrons to the TiO₂ conduction band and extract the electrons from the dye molecules which efficiently blocking the holes. Li et al.³³⁵ have reported a 41% increase of the light-to-electricity conversion yield upon loading Au nanoparticles inside the inverse opal TiO₂ film. They have designed a system where a photonic crystal (TiO₂) is coupled with a plasmonic nanoparticle (Au) to improve the power conversion. A >25% increase in device efficiency of DSSCs has been found by Naphade et al.³³⁶ when plasmonic Au nanoparticles are used in the TiO₂ fibers (Figure 21B). The enhanced light harvesting by Au-NP-loaded TiO₂ nanofibers was revealed due to plasmon–polariton modes at the Schottky junctions in the Au:TiO₂ system. It was reported that the power conversion efficiency increases from 5.91% to 8.43% upon incorporation of Ag-encapsulated Au nanorods (Au@Ag NRs) into TiO₂ DSSCs due to efficient charge separation at the hot spot of the nanostructures.³³⁷ Similarly, an enhancement of the power conversion efficiency has been observed by Wang and his co-workers³³⁸ when they used a concave cubic Au core and a shell of TiO₂ nanoparticles as the light-harvesting layer. To enhance light-harvesting efficiency, TiO₂ hollow nanoparticles (HNP) were decorated with core-shell Au@Ag nanoparticles³³⁹ to enhance LSPR, large specific surface area, and efficient electron transfer (Figure 21C,D). A few hybrid plasmonic metal–semiconducting NPs are reported to improve the efficiency of photocatalysis.^{340–343} In presence of metal nanoparticles, the absorption cross section of semiconductors increases, which leads to increase the rate of catalysis because of injection of hot electrons from metal nanoparticles to the conduction band of the semiconducting

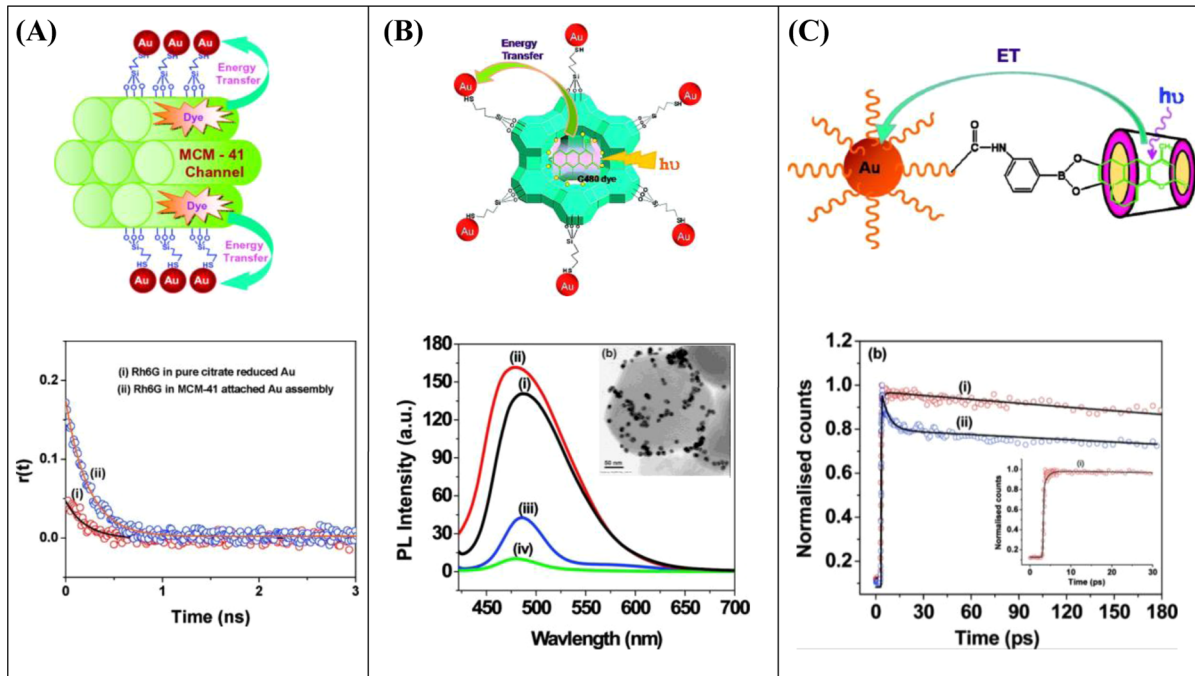


Figure 23. (A) Rhodamine 6G (R6G) dye encapsulated by mesoporous silica with Au nanoparticles attached to the mesoporous matrix used to study energy transfer, and the lower panel shows fluorescence anisotropy decay curves of R6G dye in the presence of Au NPs. Reprinted with permission from ref 374. Copyright 2010 American Chemical Society. (B) A system of dye encapsulated in zeolite with Au attachment for light harvesting, and the lower panel shows the emission spectra of C480 dye (curve i) in water, in zeolite dispersion (curve ii), in the presence of Au nanoparticles without zeolite (curve iii), and in the presence of Au nanoparticles on the surface of zeolite (curve iv) at $\lambda_{ex} = 405$ nm. The inset shows the TEM image of Au nanoparticles attached to zeolite. Reprinted with permission from ref 375. Copyright 2010 American Chemical Society. (C) A system of dye encapsulated in cyclodextrin with Au nanoparticle attachment for light harvesting, and the lower panel depicts decay curves of (i) dye in γ -CD and (ii) a solution of Au nanoparticles attached to γ -CD. The initial part of decay curve i is shown in the inset. Reprinted with permission from ref 378. Copyright 2010 American Chemical Society.

nano-particles. These plasmon-enhanced light-harvesting-based photocatalysts have been well-documented in recent articles by Zhou et al.³⁴⁴ and Wang et al.³⁴⁵ for organic synthesis, clean energy, photovoltaics, and photodynamic therapy.

4.1. Metal-Nanoparticle-Based Energy Transfer

The fundamental understanding of the metal-nanoparticle-based energy transfer process is discussed in this section. Recent findings revealed that the fluorescence quenching of fluorophore in the presence of small metal nanoparticles is due to absorption not scattering, whereas the enhancement of the fluorescence intensity of fluorophore occurs for larger metal nanoparticles due to scattering not absorption.³⁴⁶ The fluorescence enhancement leads to an increase of the radiative decay rate, and this fluorescence enhancement effect diminishes if the distance between fluorophore and metal nanoparticle is too large. Experimental data suggested that the optimum distance between fluorophore molecules and metal nanoparticle would be in the range of 5–10 nm,^{347–350} and the optimum distance and the orientation of molecules have important roles in fluorescence enhancement. Significant attention has been given to understanding the fluorescence quenching of dye molecules in the presence of metal nanoparticles.³⁵¹ Dulkeith et al.³⁹ have showed the drastic quenching of lissamine dye in the presence of Au nanoparticles, and they demonstrated the influence of the size of Au nanoparticles on fluorescence dynamics of the dye and the contribution of radiative and nonradiative decay rate (Figure 22A) on this phenomena. They compared the experimental data with the theoretical data derived from Gersten and Nitzan's model.³⁵²

Recently, Bagchi and co-workers^{353,354} have theoretically calculated the energy transfer from dye to metal nanoparticles (Figure 22B) where the rate of energy transfer (EET) is $1/d^6$ -dependent for large separation between donor and acceptor compared to the radius of the nanoparticle. The general formula of rate of energy transfer is given by $1/d^\sigma$, where the σ value is in between 3 and 4 at $d = a$ and $d = 4a$, where d is the distance between donor and acceptor and a is the radius of the nanoparticle. Another theoretical work predicted that the rate of energy transfer from dye molecule to metal nanoparticle is r^{-6} -dependent at large distances.³⁵⁵ The photoluminescence quenching and the shortening of decay time of Rhodamine 6G dye in the presence of Au nanoparticles confirm the efficient energy transfer from dye to Au nanoparticles.³⁵⁶ Radiative and nonradiative rates are calculated, and it is seen that PL quenching is higher than the change of radiative rate. The change of the nonradiative rate causes the shortening of the decay time. This study confirmed that the energy transfer from dye to Au nanoparticles is not due to a reabsorption process. Furthermore, analysis confirmed that it is $1/d^4$ -distance-dependent, which is called a surface energy transfer (SET) process. As it is a $1/d^4$ -distance-dependent process, this process is able to measure longer distances, which might helpful to measure large-scale biomolecules. Experimentally, Yun et al.³⁵⁷ have shown that the SET process is the most suitable mechanism to explain the quenching of fluorescein dye appended to 1.4 nm Au nanoparticles using dsDNA (Figure 22C,D). Again, recent findings suggest that the rate of energy transfer is controlled by the size and shape of the metal particles.^{358,359} By using the SET process, the molecular surface

coverage on the nanoparticles³⁶⁰ and the thickness of the shell in core–shell nanoparticles³⁶¹ have been measured.

4.2. Energy Transfer between Confined Dye and Metal Nanoparticles

In this section, we will discuss the importance of porous-material-based light-harvesting systems for energy storage. The supramolecular organization of the acceptor molecules are found inside the nanochannels of porous host structures like sol–gel matrix, mesoporous silica, zeolites, and cyclodextrin, which facilitates the unidirectional energy transfer. Zeolite-based light-harvesting systems are promising for the storage of solar energy due to an efficient photoelectron transfer process.³⁶² Recently, considerable attention has been given to understand the energy transfer process between fluorophores inside porous materials.^{362–373} Tolbert and co-workers³⁶⁷ have investigated the energy transfer process of conjugated polymer inside mesoporous silica, and the time-resolved anisotropic study revealed the unidirectional energy transfer. The supramolecular organization of the dyes inside the porous materials leads to a large change in the initial anisotropy, which suggests the unidirectional energy transfer. Using the concept of encapsulation of dye inside the porous materials for light harvesting, a system was designed that encapsulates Rhodamine 6G dye molecules inside the mesoporous silica channels, and Au nanoparticles are attached on the surface of the mesoporous silica to investigate the energy transfer between dye and Au nanoparticle (Figure 23A).³⁷⁴ It is evident that the rotational motion of the dye is restricted due to encapsulation of the dye inside the channels of the porous materials and that will eventually modify the photophysical properties of the dye molecules.³⁷⁴ The advantage of the encapsulation of dye inside the channels is that dye molecules are accommodated without concentration quenching because the molecular size of the dye is less than the radius of channels. Similar to mesoporous silica, another porous host is zeolite, which has a rigid three-dimensional framework with channels and is optically transparent.^{365,366} A zeolite-based light-harvesting system was developed where dye molecules (Coumarin 480) are encapsulated inside the channels of zeolite and the surface of the zeolite is functionalized by Au nanoparticles,³⁷⁵ where the size of the Au nanoparticles is higher than the diameter of the channels to avoid incorporation of Au nanoparticles inside the channels of the zeolite (Figure 23B). Steady-state and time-resolved spectroscopic studies revealed that PL quenching and shortening of the decay time of the dye are observed in the presence of Au nanoparticles, and the calculated energy transfer is 70%, which is found to be promising. Freeman et al.³⁷⁶ have designed a system based on QD attached to cyclodextrin for sensing applications using an energy transfer process. Tang and co-workers³⁷⁷ have studied the energy transfer between fluorescein dye and a Au nanoparticle, by designing a Au NPs– β -CDs–FL assembly where Au nanoparticles are attached to fluorescein–cyclodextrin molecules, and applied the process to cholesterol sensing. Similarly, assemblies of nanotubular γ -CD aggregates with coumarin 480 dye and Au nanoparticle were reported to undergo an efficient surface energy transfer process.³⁷⁸ Cyclodextrins are cyclic oligosaccharide compounds having truncated conical structure, and the interior cavity of cyclodextrins is hydrophobic in nature and a large number of organic molecules can be accommodated inside the cavity.³⁷⁹ Fundamental study of the dynamics of dye molecules inside the nanocavity using time-resolved spectroscopy is an important

area of research.^{380–382} Using cyclodextrin molecule, a system was designed where dye molecules are encapsulated inside the cavity of cyclodextrin and metal nanoparticles are attached to investigate the energy transfer between dye and metal nanoparticle (Figure 23C). Interesting findings revealed that 99% PL quenching of dye molecules is observed in the presence of Au nanoparticle.³⁷⁸ The energy transfer process is confirmed by measuring the decay time of the dye in the presence and absence of Au nanoparticles. Ultrafast spectroscopic study further revealed the electron transfer process between dye and Au nanoparticle (Figure 23C).³⁷⁸ This new finding provides the ability to design new challenging light-harvesting systems.

4.3. Metal Nanoparticle– π -Conjugated Semiconductor Hybrid

Recently, metal– π -conjugated semiconductor composites were found to be very important materials because of their potential applications in optoelectronic, photovoltaic, and light-harvesting devices.^{61,383} Plasmon–exciton interaction is a very important physical phenomenon in metal– π -conjugated semiconductor composites, where π -conjugated semiconductor polymers generate excitons after photoexcitation and these excitons can easily interact with plasmons of metal nanoparticles, which lead to the energy transfer or charge transfer. In metal–organic semiconductor hybrid systems, a strong coupling between plasmon and exciton has been observed by Bellessa et al.³⁸⁴ The photophysical processes of conjugated polymer and the surface plasmon of metal nanoparticles are greatly influenced by exciton–plasmon interaction.³⁸⁵ Heeger and co-workers have shown that Au nanoparticles quench the fluorescence of cationic polyfluorene with a very high Stern–Volmer constant.³⁸⁶ They have shown that this superquenching of the fluorescence occurs mainly due to energy transfer or electron transfer within the conjugated polymer backbone. The quenching is also assisted by a strong electrostatic interaction between conjugated polymer and Au NPs. The conjugation length in the conjugated polymers is modified in the presence of metal nanoparticles, which influences the shifting of the π – π^* absorption band. Masuhara et al. have reported ~20 nm red-shifting of the π – π^* absorption of poly(1,6-di(*N*-carbazolyl)-2,4-hexadiyne) in the presence of Ag NPs.³⁸⁷ This study reveals that different electronic states are generated due to interaction of the plasmon band of metal nanoparticles with excitons of the proximal polymer molecules. Again, Guan et al. have observed the enhancement of the two-photon emission peak of metal nanoparticles in metal NP–conjugated polymer hybrids.³⁸⁸ This enhanced two-photon emission of metal nanoparticles arises due to coupling between metal nanoparticles and conjugated polymers. Blue-shifting and the enhancement of the emission intensity of poly(*p*-phenylene ethynylene) polymer are observed in the presence of silver nanocube arrays.³⁸⁹ The blue-shifting is due to conformational changes in the presence of metal NPs, and the enhancement of the emission band is due to plasmonic effects. Again, the spontaneous emission properties of the π -conjugated semiconductor hybrid system are controlled by localized surface plasmon effects of Au@SiO₂.³⁹⁰ In such a system, light energy is absorbed by Au@SiO₂, which acts as the antenna material and transfers its energy to the π -conjugated semiconductor. The local field effect of the surface plasmon of the metal nanoparticle enhances the PL intensity of poly(2-methoxy-5-(2'-ethylhexyloxy)-*p*-phenylene vinylene) (MEH-PPV) in Au–

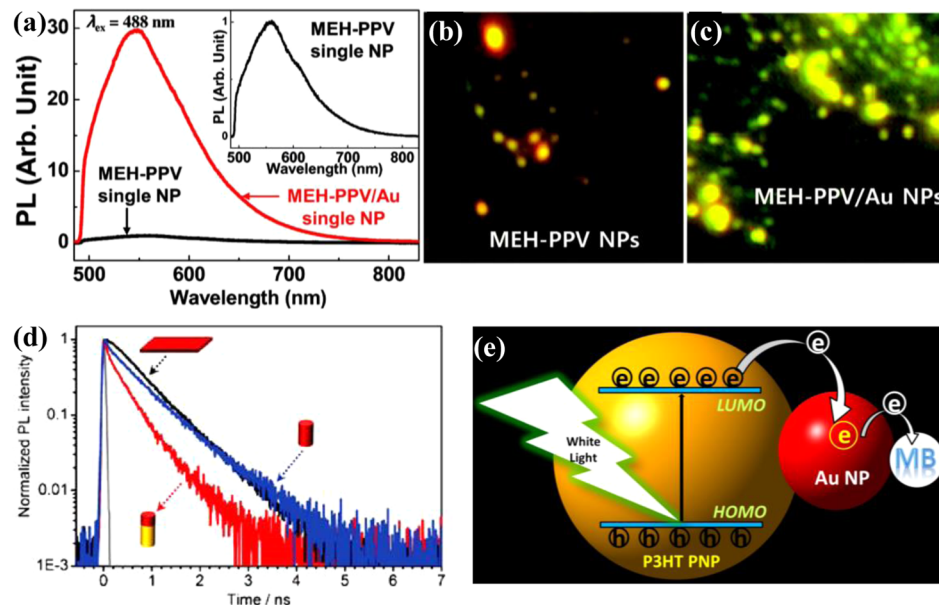


Figure 24. (a) PL spectra of the MEH-PPV single NP (black curve) and MEH-PPV/Au single NP (red curve). Inset: Magnification of the PL spectrum of MEH-PPV single NP for a reference. Color CCD images of the (b) MEH-PPV NPs and (c) MEH-PPV/Au NPs. Reprinted with permission from ref 391. Copyright 2009 American Chemical Society. (d) Decay curves of a P3HT thin film (black), a single P3HT nanowire (blue), and a gold–P3HT nanowire (red) along with the instrument response function (IRF) (gray). Reprinted with permission from ref 392. Copyright 2010 Wiley-VCH Verlag GmbH & Co. KGaA. (e) Schematic representation of electron transfer from P3HT PNP to Au NPs in the P3HT PNP–Au NP composite system that finally degrades MB dye. Reprinted with permission from ref 396. Copyright 2015 Royal Society of Chemistry.

MEH-PPV composite (Figure 24a–c).³⁹¹ It was found for poly(3-hexylthiophene) (P3HT)–Au hybrid systems that the shortening of the decay time of the polymer was due to modification of the radiative decay rate in the presence of metal nanomaterials (Figure 24d).³⁹² The nature of the conjugated polymer hosts, such as poly(*N*-vinylcarbazole) (PVK), 2-(4-biphenyl)-5-(4-*tert*-butylphenyl)-1,3,4-oxadiazole (PBD), and a mixture of PVK and PBD blend polymer, has a strong influence on the energy transfer process. The nonradiative energy transfer process is verified by FRET and SET methods.³⁹³ PL quenching and the shortening of the decay time of the semiconducting polymer in the presence of metal nanoparticles confirm the energy transfer process. Again, the effect of the size of the Au nanoparticle on the energy transfer process was investigated and it is evident that the size of the Au nanoparticle enhances the energy transfer rate.³⁹⁴ Recently, the electronic properties of aggregated structures of conjugated molecules received attention for light-harvesting materials, and it was found that the overall hole mobility is enhanced in the presence of metal.³⁹⁵ A light-harvesting system based on P3HT–Au NP composites was designed to enhance the photocatalytic properties (Figure 24e) under visible light. Analysis suggested that the electron transfer rate increases with an increase in the concentration of Au nanoparticles, which leads to charge separation by suppressing charge recombination.³⁹⁶ Use of this newly developed organic–inorganic hybrid nanostructure of π -conjugated semiconductor nanoparticle and metal NPs can be a strategy for improving photocatalytic properties.

4.4. Metal Nanoparticle–Inorganic Semiconductor Heterostructures

In this section, we discuss heterostructural materials composed of metal nanoparticles and inorganic semiconductor nanoparticles and their important applications in photocatalysis and solar energy conversion and their photovoltaic and nonlinear

properties. The modification of the electronic properties of metal–semiconductor is revealed because the subgap structure emerges near the metal–semiconductor nanocontact.^{397,398} The exciton–plasmon interaction of semiconductor–metal heterostructures modifies the spontaneous emission properties and the radiative relaxation rate of exciton. Upon photoexcitation of such a heterostructure, the charge separation occurs because the Fermi energy level of the metal nanoparticle acts as an electron reservoir that enhances the lifetime of photogenerated carriers of the semiconductor. For solar cell applications, the longer lifetime of photogenerated carriers is required without an exciton recombination process. Weak coupling of exciton and plasmon in heterostructures modifies the radiative rate, whereas strong coupling exhibits an energy level split at the resonance frequency.³⁹⁹ In the case of surface plasmon and quantum well excitons in a hybrid metal–semiconductor nanostructure, a coherent coupling is demonstrated.⁴⁰⁰ Achermann and co-workers have reported the modification of the radiative decay of dipole emitters in the presence of anisotropic metal nanostructures in hybrid metal–semiconductor nanostructures.⁴⁰¹ A number of heterostructures containing metal and metal chalcogenides of different morphologies, like tipped rods, decorated rods, tetrapods, nanoflowers, core–shells, were reported as promising light-harvesting systems.^{402–415} It is demonstrated that metal–semiconductor assembled superstructures are used for a wavelength-based biodetection tool due to plasmon–exciton interaction.⁴¹⁶ Significant photoluminescence quenching and the shortening of the decay rates of CdSe nanorods are observed in Au/CdSe heterostructure after photoexcitation, which is explained by efficient energy transfer from exciton to plasmon.⁴¹⁷ A similar result is observed in close-packed metal and semiconductor nanoparticle monolayer films,⁴¹⁸ where the direct and stepwise energy transfer from semiconductor to metal is evident.

The recently developed pentapod heterostructure of Au/CdSe (Figure 25A) is another potential material to improve the

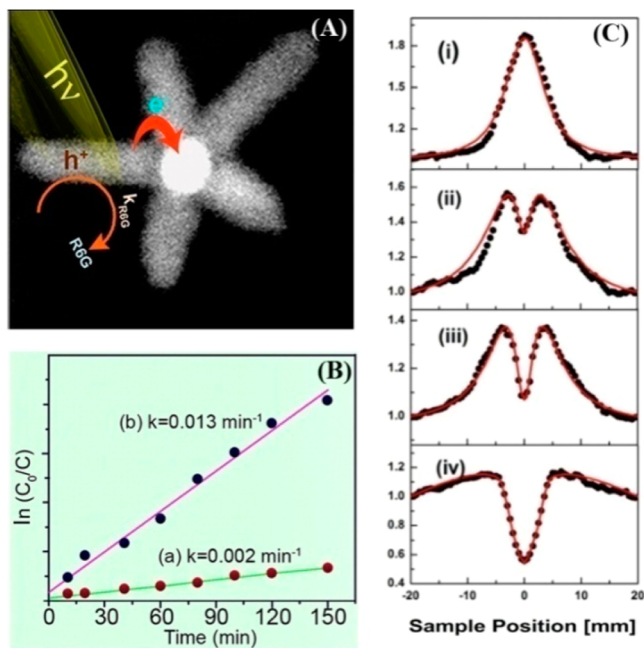


Figure 25. (A) TEM image of Au/CdSe pentapod heterostructures with Au core and CdSe arms and the photoinduced electron transfer from CdSe arm to Au core. (B) Rate of photodegradation of R6G dye in the presence of (a) CdSe QDs and (b) Au/CdSe heterostructures. Reprinted with permission from ref 245. Copyright 2012 American Chemical Society. (C) Intensity-dependent nonlinear absorption curves for Au–CdSe nanoflowers at different laser inputs: (i) 8.75 GW/cm², (ii) 14 GW/cm², (iii) 34 GW/cm², and (iv) 55 GW/cm². Reprinted with permission from ref 425. Copyright 2014 American Chemical Society.

photocatalytic properties, because of the enhancement of the lifetime of photogenerated carriers.⁴¹⁷ Steady-state and time-resolved spectroscopic studies confirmed the electron transfer process from photoexcited CdSe to Au nanoparticle, which leads to an improvement of the charge separation.²⁴⁵ It is interesting to note that Au/CdSe pentapod heterostructure exhibits photocatalytic activity (Figure 25B) with significant dye degradation (88%) under UV radiation. These heterostructural materials, such as Au–CdS, Ag–CdS, core–shell structures, and Au–CdTe nanoparticle structures, also exhibit a nonlinear optical property due to effective plasmon–exciton interaction.^{419–424} The nonlinear optical switching properties and the enhanced nonlinear optical response are obtained in Au–CdSe heterostructures (Figure 25C).⁴²⁵ Analysis revealed that the transformation from saturable absorption (SA) to reverse saturable absorption (RSA), i.e., the switching behavior, is observed with increasing laser intensity. The enhanced effective two-photon absorption cross section (σ_{eff}) and the nonlinear refraction of Au–CdSe hetero-nanostructures are evident at higher intensities because of the charge transfer from CdSe to Au nanoparticles at higher intensities. Again, the positive nonlinearity at low laser intensities is due to electron transfer from the d band to the sp band in Au nanoparticles.⁴²⁵ The nonlinear properties of these heterostructures can open up avenues for developing new challenging devices. In our opinion, emphasis should be given to the design of metal–semiconductor heterostructures and to an understanding of their

charge transfer dynamics for the development of future-generation light-harvesting systems.

5. BASIC ASPECTS OF π -CONJUGATED SEMICONDUCTOR NANOPARTICLES

Here, we discuss the importance of π -conjugated semiconductor nanoparticles, which are now promising light-harvesting materials because of their several advantages, like semiconductor-like properties, high absorption cross-section, and broad emission spectra, which can overlap with a large variety of energy acceptors.⁴²⁶ π -Conjugated polymer is basically a multichromophoric system, and each subunit acts as a chromophore as the extended π -conjugation is broken at intervals by bending or twisting and causes the inhomogeneous broadening of absorption spectrum.⁴²⁷ Using quantum-chemical calculation, Beenken and Pullerits have found that the bending and twisting (static geometric defects) are not only responsible for significant localization of the excited states to a certain segments. The dynamic localization of excitation due to the interaction between the nuclear and electronic degrees of freedom is responsible for the formation of the spectroscopic units.⁴²⁸ In photovoltaic and solar cell applications, the generation of excitons in the photoexcited π -conjugated polymer plays an important role. Two types of excitons, i.e., interchain and intrachain, are identified, where interchain exciton transfer occurs between two chain segments coupled through space, whereas intrachain exciton transfer occurs in the extended π -conjugation along the polymer backbone (Figure 26).⁴²⁷ It is found that the Förster energy transfer from shorter

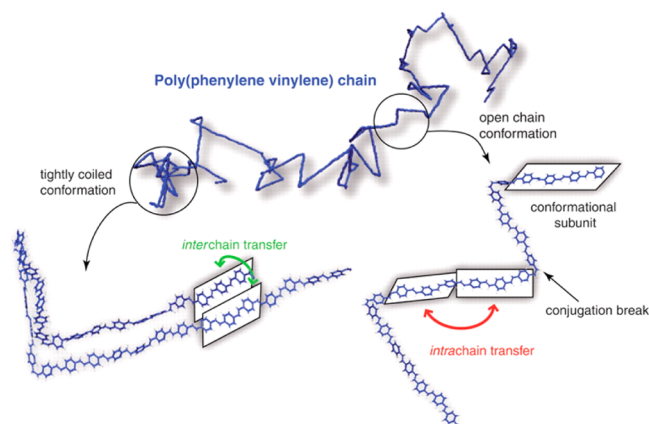


Figure 26. Intra- and interchain energy transfer of a single-chain conformation of a poly(phenylenevinylene) conjugated polymer. Reprinted with permission from ref 427. Copyright 2009 AAAS.

spectroscopic units to the longer ones leads to red-shifting of the emission spectra. It is reported that the delocalization of π -electrons is found in every monomeric unit over a significant part of the chain and the electronic properties of π -conjugated polymers depend on both the chain length and the exciton diffusion length.⁹⁷ Less attention has been given to inter- and intramolecular interactions of π -conjugated semiconducting polymer systems which influence the performance of light-harvesting systems.⁴²⁹ Recently, π -conjugated semiconducting nanoparticles have received considerable attention as potential light-harvesting materials that are prepared from π -conjugated molecules by coiling. It is expected that both inter- and intramolecular interactions are modified due to coiling of the conjugated backbone of semiconducting polymer molecules.

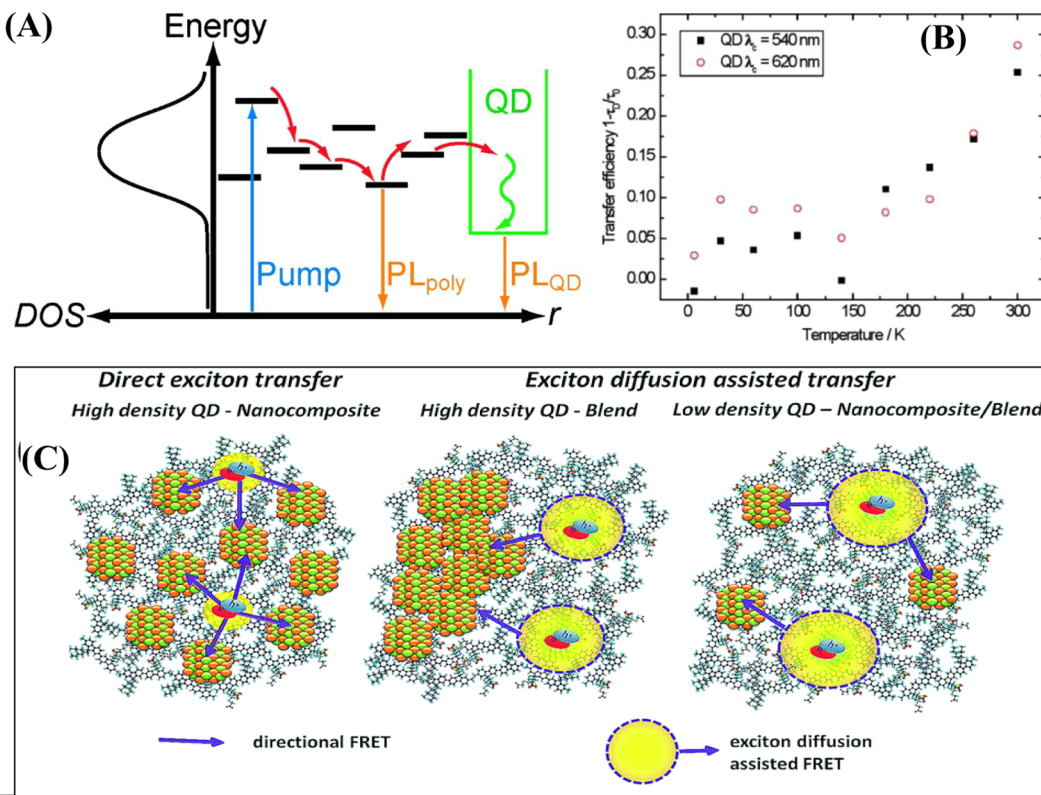


Figure 27. (A) Schematic representation of exciton-diffusion-assisted nonradiative energy transfer from a conjugated polymer (CP) to colloidal QD. (B) Temperature-dependent nonradiative energy transfer efficiencies in the blended CP–QD films. Adapted with permission from ref 441. Copyright 2009 American Chemical Society. (C) Representative schematic for the exciton transfer in the high-density QD-incorporated (left) nanocomposite and (middle) blend and the low-density QD-incorporated (right) nanocomposite/blend. Reprinted with permission from ref 442. Copyright 2014 Royal Society of Chemistry.

For photovoltaics and other optoelectronic applications, the important issues are exciton length, exciton formation, electronic delocalization, inter- and intramolecular interactions, charge transfer, etc.^{430–432} As fluorescence markers, dye-doped conjugated polymer nanoparticles exhibit a number of advantageous properties, such as excellent photostability and extraordinary fluorescence brightness.^{48,433,434}

5.1. Exciton Dynamics of π -Conjugated Semiconductor Nanoparticles

Here, we will discuss the significance of the exciton dynamics of conjugated polymers in the development of potential light-harvesting and optoelectronic applications. It is known that the exciton diffusion length of organic semiconductors is crucial for optoelectronic applications, and the value of exciton diffusion length is typically on the order of 10 nm.^{435,436} Longer exciton diffusion length is desirable for enhanced light-harvesting performance^{437,438} in solar cells, whereas the exciton diffusion is undesirable in the case of a light-emitting diode (LED), because it causes trapping of the excitons at the trap/defect sites, which causes nonradiative recombination. In such an organic semiconductor, the exciton diffusion occurs either via exciton hopping within the delocalized excited-state landscape of the organic semiconductor or via FRET between different chromophoric units of the organic semiconductor. Thus, the fundamental knowledge of the exciton formation and diffusion in conjugated polymers after photoexcitation is very important. Tamai et al.⁴³⁹ have provided in-depth knowledge of singlet exciton diffusion in crystalline conjugated polymers by using transient absorption spectroscopy, and analysis revealed that

singlet exciton decay is faster with increasing excitation intensity because of singlet–singlet annihilation. In the organic–inorganic composite/hybrid systems, a fundamental understanding of exciton formation and the diffusion, transfer, and dissociation of the excitons is crucial. Recently, Guzelturk and Demir⁴⁴⁰ have illustrated the excitonic diffusion and exciton transfer in an organic–inorganic hybrid system for potential applications in light-generation and light-harvesting applications. They showed that the exciton diffusion is drastically decreased in high density QD incorporated hybrid system because a large number of QDs suppress the interchain exciton diffusion. The nonradiative energy transfer is more efficient when an exciton of the organic part is effectively closer to the acceptor QDs and exciton-diffusion-assisted nonradiative energy transfer (Figure 27 A) occurs from conjugated polymer to colloidal QDs.⁴⁴¹ Again, exciton transfer efficiency is found to be suppressed at low temperature (see Figure 27B) due to temperature deactivation of the exciton diffusion in the conjugated polymer. It is reported that the defect emission also suppresses the exciton diffusion in the conjugated polymers.⁴⁴² A schematic representation is given in Figure 27C for the exciton diffusion and the exciton transfer in the blended and the hybrid composites.

5.2. Dye-Encapsulated π -Conjugated Semiconductor Nanoparticles

Here, the fundamental aspects of the photophysical properties of dye-encapsulated polymer nanoparticles and their potential uses are discussed. Considering the importance of these luminescent nanomaterials, attention has been given to

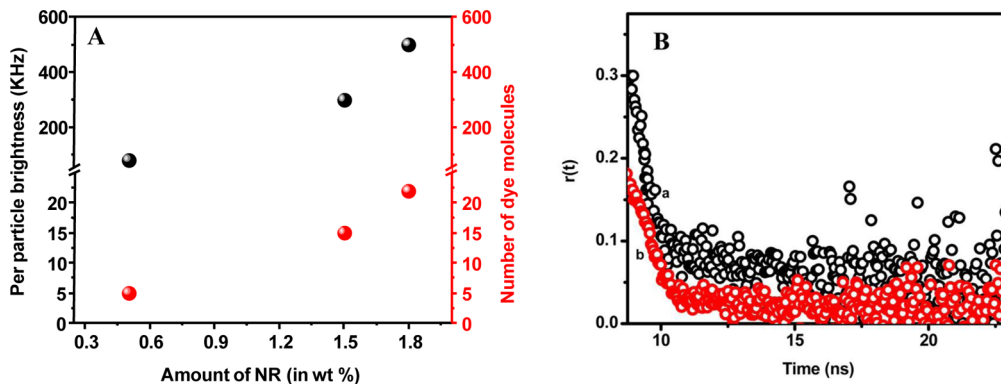


Figure 28. (A) Particle brightness (black balls) and number of dye molecules per particle (red balls) upon changing the concentration of the dye inside the polymer NP. (B) Time-resolved anisotropy decay curves of (a) 0.5 wt % and (b) 1.8 wt % NR-doped PVK polymer nanoparticles. Reprinted with permission from ref 443. Copyright 2013 American Chemical Society.

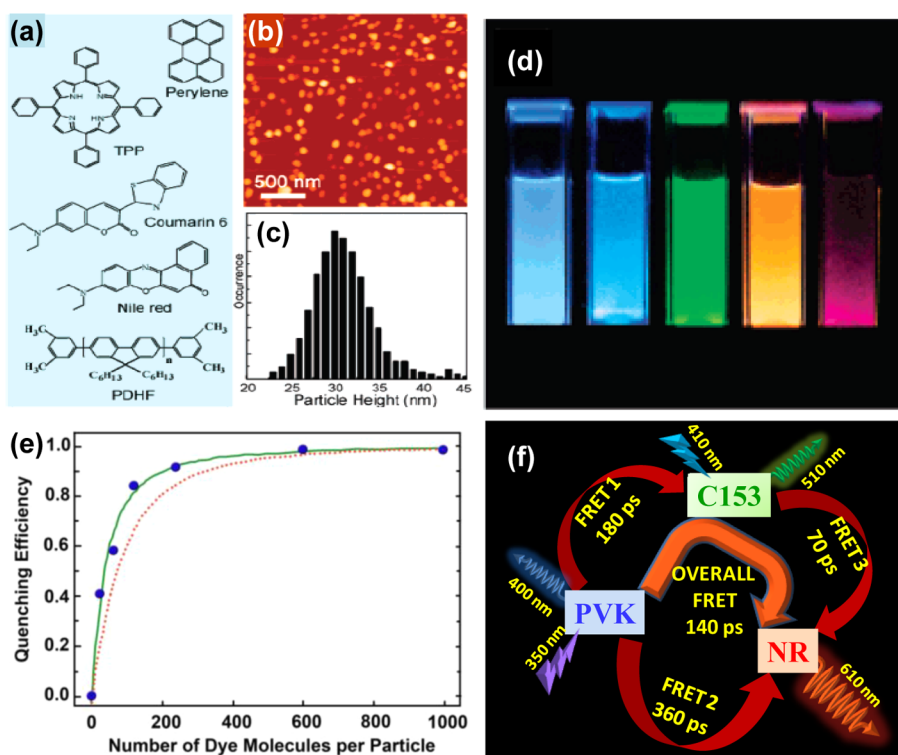


Figure 29. (a) Chemical structures of different fluorescent dye molecules and the conjugated polymer host, PDHF. (b) AFM image of pure Coumarin 6-doped PDHF nanoparticles dispersed on silica substrate. (c) Histogram of the particle size distribution. (d) Photograph of the fluorescence emission from aqueous suspensions of the dye-doped PDHF nanoparticles under UV lamp excitation (365 nm). (e) Quenching efficiency as a function of the number of dye molecules per particle for the PDHF nanoparticles. The blue dots are the experimental results and the dotted curve is from the Förster transfer model; the solid curve represents the results of the combined exciton diffusion and Förster transfer model. Reprinted with permission from ref 48. Copyright 2008 American Chemical Society. (f) Multistep energy transfer processes within semiconducting polymer PVK nanoparticles to C153 and NR dyes. Reprinted with permission from ref 453. Copyright 2014 Royal Society of Chemistry.

fluorophore-doped polymer nanoparticles as an alternative luminescent source because of several advantages, i.e., their easy synthetic procedure, higher photostability, higher brightness, and color tunability. The brightness of the dye-encapsulated polymer nanoparticle is improved by enhancing the radiative decay rate. The reduction of the nonradiative decay rate and the simultaneous enhancement of the radiative decay rate are due to confinement of dye molecules inside the polymer nanoparticle.⁴⁹ The size of the nanoparticles and the concentration of the dye molecules control the rotational motion, wobbling motion, and lateral diffusion of the dye molecules. Thus, the dye concentration, nanoparticle size, and

diffusion kinetics of dye are important parameters in dye-encapsulated fluorescent polymer nanoparticles for developing efficient luminescent nanomaterials. Dye-doped nanoparticles are used for bioimaging and fluorescent probes because of their brightness. Recently, the brightness of a single dye-doped nanoparticle has been measured by using fluorescence correlation spectroscopic (FCS) study. Analysis reveals that the brightness of the nanoparticle increases upon increasing the concentration of dye inside the nanoparticle (Figure 28A).⁴⁴³ Again, the impact of dye concentration is revealed by the time-resolved anisotropic study (Figure 28B),⁴⁴³ and it is reported that the concentration of dye molecules controls the

rotational motion of dye molecules and other photophysical properties. Furthermore, a fundamental study on the influence of polymer nanoparticle size on the diffusion constant, radiative decay rate, and diffusion coefficient for the wobbling motion of dye molecules has been done. The radiative decay rate and lateral diffusion constant are increased with an increase in the size of polymer nanoparticles.⁴⁴³ It is reported that energy transfer between different conformations of dye molecules inside the polymer nanoparticles is possible.⁴⁴⁴

Therefore, emphasis has been given to develop dye-doped polymer nanoparticles to study their energy transfer process.⁴⁴⁵ For efficient energy transfer between semiconductor polymer nanoparticles and dye, spectral overlap between the emission spectrum of host polymer and the absorption spectrum of dye molecules is required. Scherf and co-workers⁴⁴⁶ have attached two cationic dyes, Rhodamine 6G and tetramethyl Rhodamine ethyl ester perchlorate (Rhodamine) electrostatically to the surface of negatively charged polyfluorene nanoparticles and found that the efficient energy transfer is observed from conjugated polymer nanoparticles to fluorescent dye molecules due to a nonradiative transition.^{49,443} McNeill and co-workers⁴⁸ have prepared different fluorescent-dye-doped polyfluorene nanoparticles having an average size of ~30 nm diameter (Figure 29a–c) for enhancing brightness with tunable emission (Figure 29d). It was found that the quenching efficiency or energy transfer efficiency depends on the number of dye molecules inside the polymer nanoparticles (Figure 29e). Multiple-dye-doped polymer nanoparticles have been developed for multicolor emission, and the emission wavelength can be tuned by changing the concentration ratio of different dyes.⁴⁴⁷ Again, solvatochromic and photochromic dye-doped conjugated polymer nanoparticles have been developed for their color tuning and photoswitching properties.^{448–450} It was reported that exciton migration enhances the energy transfer process in dye-doped poly(9,9-diethyl fluorine-*co*-benzothiadiazole) (PFBT) nanoparticles.⁴⁵¹ Light-induced conversion of spiropyran to merocyanine is evident by ultraviolet light irradiation.⁴⁵² Analysis revealed that the brightness and the radiative decay of dye-doped polymer nanoparticles are controlled by the size of nanoparticles. Steady-state and time-resolved spectroscopic studies indicate the efficient energy transfer (82.5%) from PVK semiconducting nanoparticles to dye molecules.⁴⁹ In another study, tuning of the emission wavelength from 350 to 700 nm by changing the relative concentrations of multiple dye molecules [i.e., Nile Red (NR) and Coumarin 153 (C153) dyes] is evident. This tuning of emission wavelength is possible by multistep cascading energy transfer from host to different dyes.⁴⁵³ Bright white light emission with the quantum yield of 14% is achieved in such multicomponent-dye-doped polymer nanoparticles. The mechanism of the energy transfer is as follows: photoexcited PVK organic semiconducting nanoparticles transfer the energy nonradiatively toward red-emitting (NR) dye molecules in the absence of green-emitting (C153) dye. However, the PVK semiconducting nanoparticle (host) preferentially transfers its excited energy to C153 dye because of better spectral overlap between the emission spectrum of the host polymer nanoparticle and the absorption spectrum of the guest (C153) dye than the spectral overlap between the emission spectrum of C153 dye and the absorption spectrum of NR dye. The proposed cascaded energy transfer process (Figure 29f) is from PVK to C153 to NR,⁴⁵³ where the C153 molecule acts as a molecular ladder. An ultrafast spectroscopic study confirmed

that the multistep cascaded energy transfer occurs from the excited polymer nanoparticle to red-emitting dye via green-emitting dye. The energy transfer time constants were calculated, and the values were 180 ps for polymer nanoparticle to green-emitting dye and 360 ps for polymer nanoparticle to red-emitting dye, and the overall energy transfer process is 140 ps (Figure 29f).

Recent findings reveal that the conjugated polymers act as efficient light antenna materials and generate singlet oxygen (${}^1\text{O}_2$) by photosensitizing the photosensitizer (PS) molecules via FRET.^{454–456} Furthermore, McNeill and co-workers have developed a system containing PS-doped polyfluorene nanoparticles for singlet oxygen generation.⁴⁵⁷ Our group developed PS-attached (Rose Bengal dye) C153-doped PVK nanoparticles for singlet oxygen generation, where PVK nanoparticles act as efficient light-absorbing antenna materials.⁴⁵⁸ Using a spectroscopic study, it was confirmed that the cascade energy transfer occurs from polymer host to encapsulated dye (C153) to photosensitizer molecule (Rose Bengal) dye to generate singlet oxygen (${}^1\text{O}_2$). In our opinion, newly developed dye-doped polymer nanoparticles are very promising for developing efficient light-harvesting systems. Thus, research focus should be given to the development of new systems and to the understanding of their photophysical properties.

5.3. Self-Assembled π -Conjugated Semiconductor Nanostructures

Several artificial photodriven systems were fabricated to mimic the photosynthetic system in green plants by using self-assembled and organized multichromophoric conjugated organic moieties where photoinduced energy transfer occurs toward acceptor molecules.^{24,459,460} Here, we highlight the significance of assembly structures in the design of light-harvesting system based on π -conjugated multichromophoric organic molecules and illustrate the relationship between the structure and the electronic properties of self-assembled nanostructures. Recently, a DNA–porphyrin self-assembled complex was designed for artificial light harvesting where arrangement of chromophores is on the nanometer scale to facilitate the light-harvesting efficiency.⁴⁶¹ Again, Dutta et al.⁴⁶² have designed a tunable artificial light-harvesting system where multiple organic dyes are attached to DNA. Again, the ordered structure of small oligothiophene/polythiophene molecules is being used for photodriven devices because of their efficient charge/energy transfer properties.^{463–468} Exciton migration in such an assembled structure is important to understand because that will provide knowledge for device fabrication. In the crystalline domain of the polythiophene assembled structure, one-dimensional singlet exciton energy migration is evident, but three-dimensional exciton diffusion is observed in the amorphous domain.⁴³⁹ Recently, the importance of molecular aggregation in light-harvesting systems was addressed. A system was designed by using self-assembled H-aggregation of quaterthiophene (QTH) with PMMA polymer nanoparticles doped with Nile Red dye.⁴⁶⁹ The antenna effect and the enhanced effective molar extinction coefficient for Nile Red dye molecules suggest that the system is promising for light-harvesting applications. Here, the overall energy transfer process from H-aggregation of QTH to Nile Red dye depends on the concentration of QTH and dye. Considering the energy transfer process from internally ordered QTH to randomly distributed NR dye molecules inside polymer nanoparticles, the blue to white light emission can be tuned by controlling the

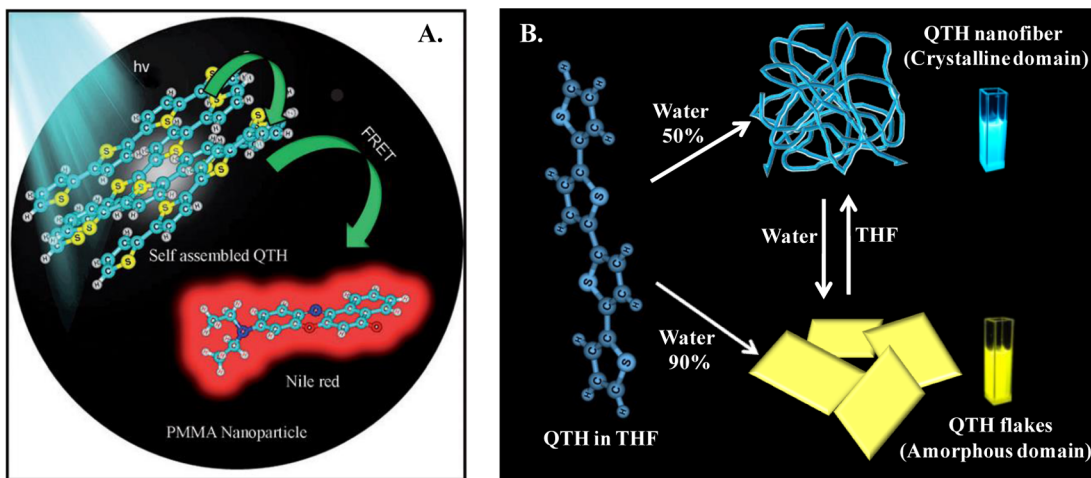


Figure 30. (A) Schematic representation of the energy-transfer process from self-assembled quaterthiophene (QTH) to Nile Red dye doped PMMA nanoparticle. Reprinted with permission from ref 469. Copyright 2015 Wiley-VCH Verlag GmbH & Co. KGaA. (B) Schematic representation of the reversible transformation of the morphology of quaterthiophene from a crystalline fiber to an amorphous flake under UV-light. Reprinted with permission from ref 470. Copyright 2015 Wiley-VCH Verlag GmbH & Co. KGaA.

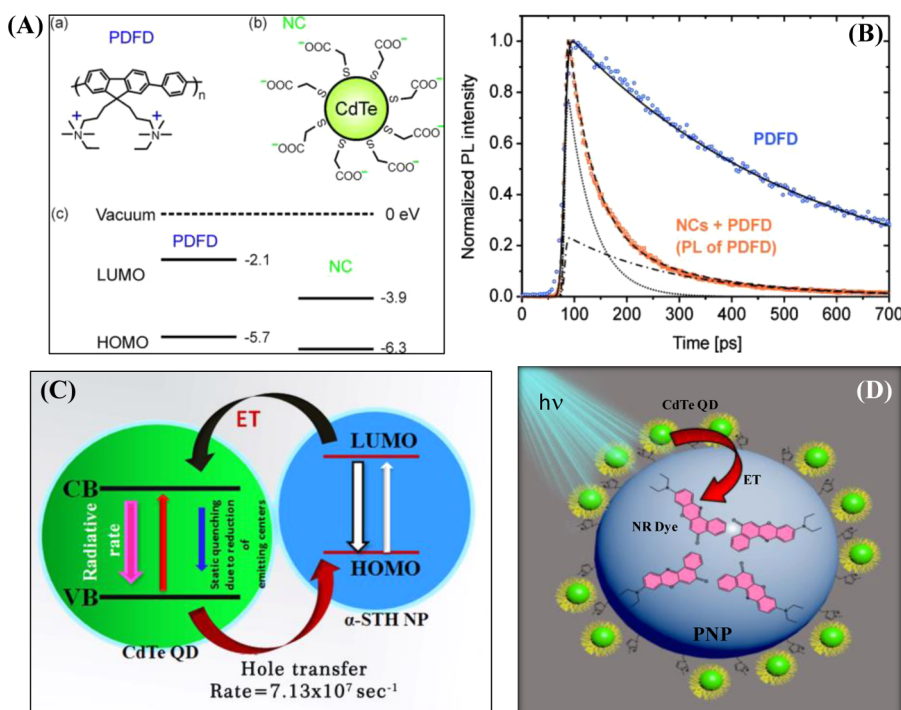


Figure 31. (A) Structure of PDFD and thioglycolic acid capped CdTe NC and a diagram of the HOMO–LUMO levels (eV) of PDFD and the CdTe NCs. (B) Time-resolved decay curves of PDFD in the presence and absence of CdTe nanocrystals. Reprinted with permission from ref 475. Copyright 2009 American Chemical Society. (C) Schematic representation of the energy transfer and hole transfer processes in the CdTe QD and α -sexithiophene (α -STH) NP system. Reprinted with permission from ref 488. Copyright 2012 Wiley-VCH Verlag GmbH & Co. KGaA. (D) Schematic representation of the energy transfer from QDs to Nile Red dye molecules inside polymer nanoparticles. Reprinted with permission from ref 489. Copyright 2015 Royal Society of Chemistry.

ratio of QTH and Nile Red dye (Figure 30A).⁴⁶⁹ This study definitely encourages us to develop new light-harvesting systems based on aggregated molecules encapsulated in polymer nanomaterials. A recent study highlighted the relationship between the structure of QTH molecules and its photoswitching and thermoresponsive properties.⁴⁷⁰ Tuning of the photoluminescence property from yellow to blue or reversible emission is revealed by changing the molecular arrangement of QTH from flake to fiber nanostructures (Figure 30B). Interestingly, the crystalline nature is found to vary by

changing the morphology, which eventually influences the photoswitching and thermoresponsive photoluminescence properties. Further, the relaxation dynamics and restricted chromophoric properties of self-assembled nano/microstructured morphologies suggest the hindered rotation of the chromophore units due to interchromophore coupling.⁴⁷⁰ Attention should be given to understanding the structure and electronic properties of self-assembled nanostructures to develop challenging systems.

5.4. π -Conjugated Semiconductor Nanoparticle–QD Hybrid Systems

New findings open avenues for light harvesting using triplet exciton energy transfer in π -conjugated semiconductor nanoparticle–QD hybrid systems. Recently, emphasis has been given to the resonance energy transfer of singlet excitons from organic molecules to inorganic nanocrystals because triplet exciton through resonance energy transfer is spin-forbidden.⁴⁵⁵ Rao and co-workers⁴⁷¹ have shown that 1.9 triplets transfer from pentacene to PbSe nanoparticles for every photon absorption in pentacene. This result opens a new avenue to generate white light emission, without using phosphorescent molecules, in which triplets could be harvested through transfer to QDs, where electron–hole pair could recombine radiatively. Baldo et al.⁴⁷² have recently demonstrated that the triplet excitons transfer to PbS QDs in the tetracene–PbS QD system avoids an undesirable energy sink, which is important for light-harvesting systems. It well-established that important parameters are the electronic energy level alignments and the size and shape of QDs for optoelectronic, photovoltaic, and light-harvesting devices based on QDs.^{473,474} Feldmann et al.⁴⁷⁵ have designed the type II organic–inorganic hybrid structure poly[9,9-bis(3'-(*N,N*-dimethyl)-*N*-ethylammonium)propyl]-2,7-fluorene-*alt*-1,4-phenylene] dibromide (PDFD)–CdTe QD, where positively charged PDFD molecules are electrostatically attached to anionic CdTe QDs to align the electronic energy level. The efficient energy transfer from conjugated polymer to QDs (Figure 31 A,B) has been confirmed by steady-state and time-resolved spectroscopic studies.⁴⁷⁵ Mahrt et al.⁴⁴¹ have highlighted that the energy transfer efficiency is influenced by the exciton diffusion process in the case of polyfluorene-based conjugated polymer–CdSe/ZnS core–shell QD hybrid system. Again, the energy transfer is controlled by the intra/intermolecular interactions and the extent of molecular packing in conjugated polymer–QD hybrid systems.^{476–478} The very fast energy transfer rate from conjugated PPV molecules to PbS QDs is evident.⁴⁷⁹ Morphology is another factor that can influence the energy transfer from a π -conjugated polyfluorene nanoparticle to an InGaN/GaN quantum well (QW).⁴⁸⁰ Excitonic diffusion and photoinduced charge transfer phenomena are other important parameters to control the energy transfer process in the nanohybrid systems.^{185,481} Prasad et al. have reported that the hole mobility plays an important role in the PVK–QD nanocomposite system and the size of the QD particle controls the hole mobility.⁴⁸² The charge carrier dynamics in type II heterojunction of GaAs nanowires–semiconducting polymer has been studied by ultrafast spectroscopy. Analysis revealed that the ionization potential of semiconducting polymer controls the charge carrier lifetime.⁴⁸³

In inorganic–organic hybrid systems, the organic–inorganic interface is another important parameter that controls the performance of light-harvesting devices. Thus, a fundamental knowledge of the charge transfer at the interface of organic and inorganic materials is required to develop efficient devices. Interfacial energy transfer and electron transfer processes in conjugated polymer–CdSe QD hybrid systems have been studied by using ultrafast spectroscopy and it is found that interfacial energy transfer occurs on the sub-picosecond time scale and the rate of electron transfer is \sim 800 fs.⁴⁸⁴ Thus, the electron transfer process is the predominant process, rather than the interfacial energy transfer process, in this hybrid system. Similarly, the hole transfer process between conjugated polymer nanoparticle and QDs was investigated and it was

revealed that the hole transfer from QD to conjugated polymer is very slow (\sim 1 ns) compared to the electron/energy transfer process. In the hole transfer process from QD to conjugated polymer, the impact of the polaron in conjugated polymer at high pump photon energy is evident.^{485,486} It is reported that the charge separation and charge migration enhance the carrier lifetime in nanowire hybrid heterojunction devices.^{185,487} The hole transfer from CdTe QDs to α -sexithiophene (α -STH) nanoparticles (Figure 31C) of hybrid α -STH nanoparticle–CdTe QD nanocomposites is confirmed by photoluminescence quenching of CdTe QDs with an increase of the concentration of α -STH nanomaterials.⁴⁸⁸ The interfacial charge carrier generation and the charge dissociation between polymer nanoparticle and inorganic nanocrystals are found to be the fundamental processes for organic–inorganic hybrid devices. In a recent work, an inorganic–organic hybrid light-harvesting system has been designed where inorganic QDs are anchored on the surface of a dye-encapsulating polymer nanoparticle.⁴⁸⁹ In such hybrid systems, QDs act as an antenna material that absorbs the visible light, followed by funneling of the exciton energy from QDs to Nile Red dye encapsulated in polymer nanoparticles to enhance the energy transfer efficiency (Figure 31D).⁴⁸⁹ The surface of the polymer nanoparticles is negatively charged due to surface defects. Thus, surface functionalization of polymer nanoparticles is essential to develop polymer–inorganic hybrids.⁴⁹⁰ After photoexcitation of QDs, the emission intensity of the CdTe QDs is decreased and the PL intensity of the Nile Red dye is enhanced, indicating the energy transfer process from QDs to the dye.⁴⁸⁹ The depolarization of Nile Red dye emission inside the PMMA nanoparticles was investigated by a time-resolved anisotropic study. Considerable attention should be paid to the influence of the size and shape of QDs on the interfacial charge carrier generation, and the charge dissociation between polymer nanoparticle and inorganic nanocrystals should be the focus of future research. In our opinion, research emphasis may be directed toward the development of hybrid materials for new-generation light-harvesting systems.

6. PORPHYRIN-BASED FUNCTIONAL NANOSYSTEMS FOR LIGHT HARVESTING

Another potential strategy is to design artificial light-harvesting system based on porphyrins and their aggregates.^{491,492} The main light-harvesting pigment in the natural light-harvesting system is prophyrin (Figure 32A) because porphyrin molecules are represented by heme proteins, chlorophylls, pheophytins, and many other forms. Mainly, hydrogen bonding, π – π stacking, electrostatic interactions, van der Waals forces, etc. are involved for the formation of porphyrin aggregates.^{493–495} Two well-defined absorption bands, high-energy B-bands (also known as Soret bands) and low-energy Q-bands, are observed in porphyrins and metalloporphyrins, where B- and Q-bands arise from π – π^* electronic transitions. The Soret absorption band is due to $S_0 \rightarrow S_2$ electronic transitions, and the Q-band is due to $S_0 \rightarrow S_1$ electronic transitions.⁴⁹⁶ In porphyrin monomer, the internal conversion, i.e., $S_2 \rightarrow S_1$, is very fast (about sub-picosecond). Commonly, J- and H-type aggregations are formed by self-assembly of porphyrin, where J-type occurs due to edge-to-edge arrangement of molecules and H-type occurs due to face-to-face arrangement of molecules, which eventually changes the transition dipoles. The red- and blue-shifting of the absorption band are observed for J- and H-type aggregation, respectively.⁴⁹⁷ In case of H-aggregation,

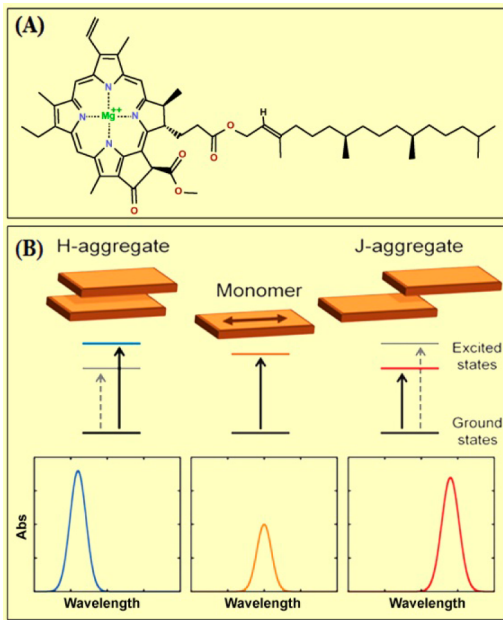


Figure 32. (A) Structure of the π -conjugated porphyrin ring in chlorophyll molecule. (B) Typical arrangements of H- and J-aggregates (exemplified for a dimer) for a π -conjugated molecule (monomer) and the corresponding effects in the absorption UV–vis spectra. Full arrows depict allowed (strong) transitions and dashed arrows forbidden (or weak) ones. The double arrow represents the transition dipole for the monomer. Reprinted with permission from ref 499. Copyright 2014 Royal Society of Chemistry.

higher excited states are transitionally allowed and S_2 exciton state decays faster whereas lower excited states are allowed for J-aggregation.⁴⁹⁸ Thus, it is clear that the packing of the porphyrin molecules change the electronic properties which will influence the exciton dynamics. In J-aggregation of porphyrin molecules, Soret and Q-bands are bathochromic shifted (Figure 32B) and the shortening of the decay time is evident.⁴⁹⁹ J-Aggregates are considered to be an efficient model to mimic the chlorophyll-based light-harvesting system.

In this section, the influences of porphyrin aggregation on photoinduced energy transfer and the photocatalytic properties of porphyrin-based functional nanomaterials are discussed. It was already reported that porphyrin-based systems are promising for different light-driven processes.⁵⁰⁰ Recent advances in supramolecular structures of porphyrins and the photophysical interactions between porphyrin and carbon nanotubes/graphene for solar energy conversion are given in detail.⁵⁰¹ Nazeeruddin et al. have designed dye-sensitized solar cell using porphyrin nanocrystals for light energy conversion to electrical energy.⁵⁰² Furthermore, the enhanced catalytic properties of porphyrin nanoparticle have been highlighted by Drain and co-workers.⁵⁰³ Considerable attention has been given to porphyrin nanoparticle formation to find out potential applications. It is reported that porphyrin nanoparticles are formed by the inter-bis-porphyrin π – π stacking from bis(zinc octaethylporphyrin) $[(\text{ZnOEP})_2]$.⁵⁰⁴ A new light-harvesting system has been designed where porphyrin molecule is encapsulated into semiconducting polymer nanoparticles for efficient energy transfer from polymer host to porphyrin molecule.⁵⁰⁵ The energy transfer from conjugated polymer nanoparticles to porphyrin is confirmed by steady-state and time-resolved spectroscopy. An interesting finding recently

reported that porphyrin nanoaggregates generate photoinduced singlet oxygen by fluorescence resonance energy transfer. Singlet oxygen generation by efficient energy transfer from poly[9,9-dibromoethylfluorene-2,7-ylenethylene-*alt*-1,4-(2,5-dimethoxy)phenylene] (PFEMO) to tetraphenylporphyrin (TPP) by two-photon excitation is also reported.⁵⁰⁶ McNeill and his co-worker have reported another system for singlet oxygen generation from platinum(II) octaethylporphine (PtOEP)-doped polyfluorene nanoparticles.⁵⁰⁷ We have designed a conjugate of porphyrin nanoaggregate with phthalocyanine molecule to generate singlet oxygen. Analysis revealed that the nanoaggregate of porphyrin is formed by H-aggregation of porphyrin molecules. After photoexcitation of porphyrin nanoaggregates, the excited singlet (S_1) state of the Q-band is promoted to the second excited singlet (S_2) state of the B-band. De-excitation from the S_2 state to the S_1 state occurs by internal conversion and then the system undergoes intersystem crossing from the S_1 state to the triplet (T_1) state (Figure 33).^{508,509} Finally, the triplet state energy transfers to

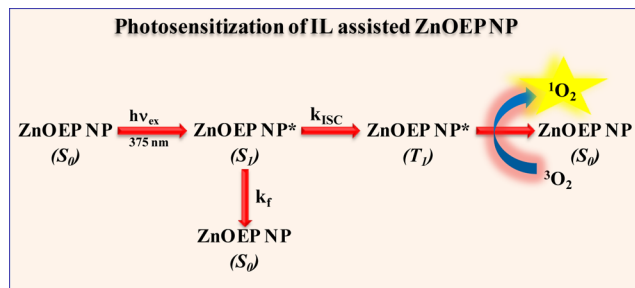


Figure 33. A schematic representation of singlet oxygen generation from ZnOEP nanoparticles. Reprinted with permission from ref 509. Copyright 2014 Royal Society of Chemistry.

the triplet oxygen and it converts to singlet oxygen. Recent findings reveal that the porphyrin nanoaggregates are potential materials for light-harvesting applications.

6.1. Self-Assembled Porphyrin Nanostructures

Porphyrin nanostructures are suitable for photocatalysis and solar energy applications because of the semiconducting properties of J-aggregated porphyrin, which plays an important role in the strong excitonic interaction.⁵¹⁰ The hierachal structures of self-assembled porphyrin aggregates are found to be similar to the light-harvesting aggregates of photosynthetic bacteria.^{511–515} The structure of porphyrin, concentration of porphyrin in solution, pH of the solution, and counterions of inorganic salts in the medium control the porphyrin aggregation.⁵¹² In the case of nonaggregated monomers, a very weak intermolecular π – π interaction is evident, because the π -conjugated electrons are locally delocalized over their macrocyclic plane. However, in the case of J-aggregation of π -conjugated organic molecules, a strong intermolecular π -electronic coupling is evident between the coherently aligned chromophores and that enhances the coherent electronic delocalization.^{516,517} Using transient absorption spectroscopy, Ghosh et al. have investigated the fundamental photophysical processes, like exciton energy and charge transfer of porphyrin aggregates, and found that the enhanced photoinduced charge separation occurs in the J-aggregate structure (Figure 34*i*) at porphyrin/TiO₂ interface.⁵¹⁸ In zirconium/hafnium porphyrin–phthalocyanine complexes, porphyrin has strong blue absorption for the B-band and phthalocyanine has strong

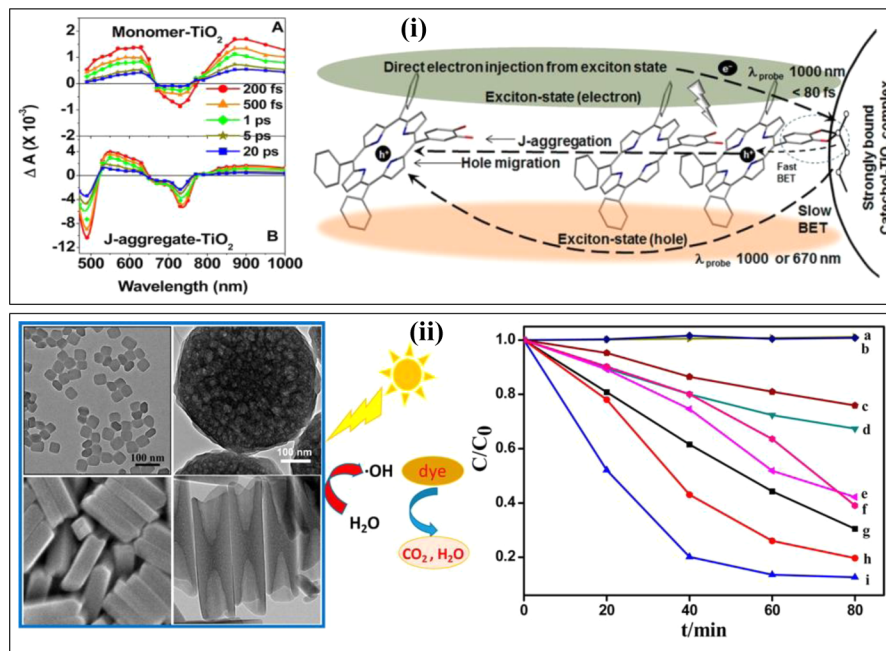


Figure 34. (i) Transient absorption spectrum of (A) monomer porphyrin–TiO₂ NP and (B) J-aggregated porphyrin–TiO₂ NP in aqueous solution at 200 and 500 fs and 1, 5, and 20 ps delay time. Schematic representation of the interfacial electron transfer in the J-aggregate–TiO₂ composite. Reprinted with permission from ref 518. Copyright 2011 Wiley-VCH Verlag GmbH & Co. KGaA. (ii) SEM images (first column) of zinc porphyrin (ZnTPP) nanocrystals with different morphologies and their shape-dependent photocatalytic activities in the photodegradation of methyl orange pollutants. Reprinted with permission from ref 520. Copyright 2014 American Chemical Society.

absorption in the red region for the Q-band, which is useful for solar light collection.⁵¹⁹ Another strategy to improve the photocatalytic activity is to consider the shape of the nanoaggregates, and spheres, rods, flakes, and flower-shaped porphyrin nanostructures have found potential as photocatalysts under visible light (Figure 34ii).⁵²⁰ It is reported that rod-shaped assemblies exhibit 81% photocatalytic activity because of coherent electronic delocalization due to a stronger intermolecular $\pi-\pi$ interaction that facilitates the electron transfer process.^{521,522} Guo et al. have developed spherical nanoaggregates and nanofibers of porphyrin for photocatalysis applications and revealed that the photocatalysis properties of nanofibers are superior to those of spherical nanoaggregates of ZnTPyP.⁵²¹ Recently, Bera et al. have demonstrated that a composite one-dimensional (1D) nanostructure of 5,10,15,20-tetrakis(4-carboxyphenyl)porphyrin (TCPP) and reduced graphene oxide (RGO) enhanced photoinduced charge separation. They have observed a very fast decay of TCPP nanorods (NRs) in the TCPP NR–RGO composite due to the electron transfer process and an enhancement of photocurrent under visible-light illumination. This study opens up new possibilities for the application of this type of hybrid for solar energy conversion.⁵²³ The aggregation of porphyrin modifies the electronic properties, which may influence on the charge separation and the energy transfer between π -conjugated polymer–porphyrin composites upon photoexcitation. The design of porphyrin-based hybrid materials and a fundamental understanding of their charge carrier generation and transportation are essential for developing efficient light-harvesting systems.

6.2. Porphyrin Composite Systems

Use of carbon-nanotube- and graphene-based composites with porphyrins is another strategy for light energy conversion, because the carbon network promotes the charge transfer with

porphyrin molecules.⁵⁰¹ The utilization of porphyrin–semiconducting QD hybrid systems for light harvesting and other potential photonic applications is not well-addressed.^{524,525} Recently, it was reported that semiconducting QDs are used to sensitize porphyrin molecules effectively by photoinduced energy transfer in QD–porphyrin composite systems. Using this hybrid strategy, Xing et al. have reported the porphyrin–CdTe QD composite system for photosensitizer detection.⁵²⁶ Using a kinetic model, the energy transfer from alloy QDs to porphyrin molecule was investigated and the analysis revealed that the average number of porphyrin molecule participating during the energy transfer process changes upon changing the concentration of porphyrin.⁵²⁷ The average number of porphyrin molecules interacts with one QD to control the energy transfer efficiency. A fundamental understanding is very important to make nanoassemblies of QD–porphyrin for efficient light-harvesting systems because it is seen that PE545 antenna protein binds eight chromophores in photosynthetic light-harvesting complexes.⁵²⁸ It is interesting to note that the restoration of luminescence of QD is possible by preventing the energy transfer from QD to porphyrin by using cucurbit[7]uril (CB[7]) (acts as a receptor).⁵²⁷ This off/on fluorescence of luminescent QD can be used for sensing applications. Borczyskowski and co-workers have reported the quenching of the fluorescence of CdSe and CdSe/ZnS QDs after assembly formation with free-base porphyrin molecules via FRET along with nonradiative relaxation via surface states.^{529,530} Again, the energy transfer from CdSe QDs to the porphyrins has been reported.⁵³¹ Energy-transfer-based sensitization in QD–porphyrin and QD–phthalocyanine nanocomposites is found to be more efficient compared to the use of pure porphyrin or pure phthalocyanine moieties for photosensitization because singlet oxygen is generated by photoexcitation of QD–porphyrin assemblies.^{46,529,530,532–536} Using the photoinduced electron

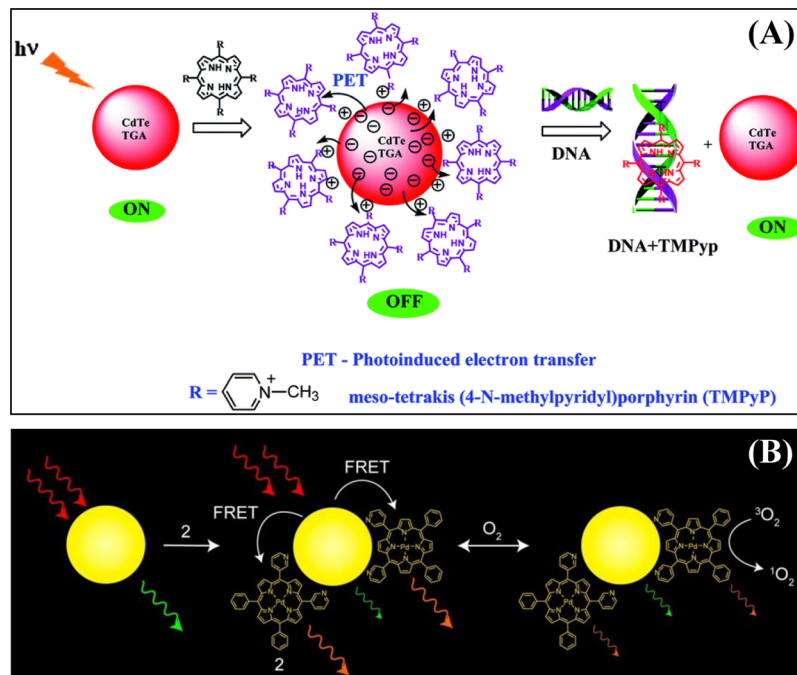


Figure 35. (A) Sensing of DNA by using a QD–cationic porphyrin probe. Reprinted with permission from ref 537. Copyright 2014 Royal Society of Chemistry. (B) Schematic representation of singlet oxygen generation from self-assembled Pd porphyrin (2)–QD assemblies. Reprinted with permission from ref 538. Copyright 2013 American Chemical Society.

transfer process, Renganathan and co-workers have detected DNA by regenerating the fluorescence of QD by inhibiting the electron transfer from QD to porphyrin (Figure 35A).⁵³⁷ A multistep energy transfer from QDs to porphyrin molecules is evident (Figure 35B) in the promotion first to the excited singlet (S_1) state for Q-band, second to the excited singlet (S_2) state for B-band, and finally to the S_1 state via internal conversion, which converts to the singlet oxygen.⁵³⁸ Recently, Nemykin and co-workers have designed porphyrin–QD assembled structures by noncovalently attaching tetraazaporphyrins to CdSe QDs, and the energy transfer efficiency is controlled by a competing trap-assisted ultrafast quenching mechanism.⁵³⁹ From the analysis, it is assumed that QD–porphyrin hybrid structures are promising for development of efficient light-harvesting systems. Further study in this field is required for fundamental knowledge of interfacial charge transfer, energy transfer, and electron transfer during the interactions of porphyrin with inorganic nanocrystals.

7. CONCLUSIONS AND OUTLOOK

Here, we discussed the current status and strategies of potential light-harvesting systems based on nanoparticles, where we highlighted the interaction of light with antenna materials such as semiconductor quantum dots (QDs), metal nanoparticles, organic semiconductor nanoparticles, and porphyrin-based nanoparticles. The size-, shape-, and composition-dependent exciton generation, exciton decay dynamics, and photoinduced energy transfer of QDs are addressed. The fundamental knowledge of these photophysical processes is important for development of efficient light-harvesting systems. The manipulation of energy and electron transfer processes between QDs and graphene in graphene–QDs composites will give new opportunities for developing potential devices for light harvesting. Future works on nano-biohybrid systems utilizing natural light-harvesting proteins are promising. The use of

nanomaterial-based unidirectional energy transfer is a promising strategy in the design of potential energy storage systems. Utilization of photosynthetic light-harvesting complexes or proteins coupled with metal nanoparticles is a design strategy for light-harvesting and solar cell devices. Emphasis should be given to understand the exciton–plasmon interaction of metal–semiconductor heterostructures, because this interaction modifies the spontaneous emission properties and enhances the device performance. Metal–semiconductor heterostructures are promising for solar cell and nonlinear applications because of their charge separation and enhancement of radiative rate. Thus, the development of heterostructure–graphene composites for new challenging light-harvesting systems is another unexplored strategy. Considerable attention should be paid to a fundamental knowledge of exciton diffusion, interfacial charge transfer (hole/electron), energy transfer, and electron transfer in π -conjugated polymer–inorganic nanoparticle hybrid systems to develop potential photocatalysts, solar cells, and other applications. Another interesting area of research is metal nanoparticle– π -conjugated polymer hybrid systems, where plasmon–exciton interaction modifies the performance of the devices. In addition, the knowledge of the exciton diffusion and exciton transfer in organic semiconductor–inorganic nanocrystal composites is important to develop light-harvesting systems. Furthermore, a new concept based on triplet exciton energy transfer from organic semiconductor to inorganic semiconductor nanocrystals could open up new light-harvesting systems. Thus, the design of nanosystems for light-emitting diodes and solar cells that optimizes device performance will be an emerging area of research. On the basis of the interesting findings with regard to porphyrin-based functional nanomaterials, there are several issues that need to be explored in the future to reveal the practical usability of these materials in the field of photonics, optoelectronics, and sensor chemistry. Porphyrin-encapsulated organic semiconducting nanomaterials

can be used in artificial light-harvesting systems with proper modification to enhance the unidirectional energy transfer from organic semiconductor to porphyrin molecules. For light-energy conversion, graphene/carbon nanotubes–porphyrin composite is a promising system for photocatalysis and solar cell devices, because they enhance charge transfer and electron transport to the surface of graphene or carbon nanotube surface. Porphyrin–quantum dot composite systems may be used in photodynamic therapy and biological sensing. Therefore, ultrafast spectroscopic investigation is required to study the fundamental spectroscopic properties of these composite systems in detail. The employment of composite or hybrid materials of carbon dots or polymer dots and Au clusters is another potential strategy in the design of light-harvesting system. In our opinion, many issues need to be addressed to develop potential light-harvesting system based on nanomaterials, and this field of research promises to grow in the coming years, as applications are still in the embryonic stage.

AUTHOR INFORMATION

Corresponding Author

*E-mail: msap@iacs.res.in. Phone: (91)-33-2473-4971. Fax: (91)-33-2473-2805.

Notes

The authors declare no competing financial interest.

Biographies

Simanta Kundu, born in 1987, obtained his B.Sc (Hons) in chemistry from Ramakrishna Mission Residential College Narendrapur, University of Calcutta (Kolkata, India) in 2007 and his M.Sc in chemistry with a specialization in inorganic chemistry from the University of Calcutta in 2009. He obtained his Ph.D. from Jadavpur University (Kolkata, India) in 2015, under the supervision of Prof. Amitava Patra. Currently, he is a visiting fellow in the Department of Chemical Sciences, Tata Institute of Fundamental Research (Mumbai, India). His research interests include synthesis and characterization of different colloidal semiconducting QDs and hybrid materials for light-harvesting applications.

Amitava Patra, born in 1965, received his Ph.D. in 1993 from Jadavpur University (Kolkata, India). He is now a senior professor in the Department of Materials Science at the Indian Association for the Cultivation of Science (Kolkata, India). He is a fellow of the Indian Academy of Sciences (FASc), the National Academy of Sciences (FNASc), India, and the Royal Society of Chemistry (FRSC). He is a recipient of the C. N. R. Rao National Prize for Chemical Research, the DAE-SRC Outstanding Investigator Award, the A.V. Rama Rao Foundation Prize in Chemistry, the AsiaNANO 2010 Award, a CRSI Bronze Medal, a Ramanujan Fellowship, and the MRSI Medal. He is or was an advisory board member of *Nanoscale*, *Journal of Physical Chemistry*, and other journals. He is author or coauthor of more than 178 scientific papers, 3 book chapters, and 2 Indian patents. His research interests include decay dynamics, energy transfer, and electron transfer of QD, Au nanoparticles, polymer- and porphyrin-based luminescent nanoparticles, and doped materials for photonic applications.

ACKNOWLEDGMENTS

“DAE-SRC Outstanding Investigator Award” is gratefully acknowledged for financial support. S.K. also thanks IACS for awarding a fellowship. Special thanks to Mr. Gopal Krishna Manna, IACS, for graphic design.

REFERENCES

- (1) Cheng, Y.-C.; Fleming, G. R. Dynamics of Light Harvesting in Photosynthesis. *Annu. Rev. Phys. Chem.* **2009**, *60*, 241–262.
- (2) Scholes, G. D.; Fleming, G. R.; Olaya-Castro, A.; van Grondelle, R. Lessons from Nature About Solar Light Harvesting. *Nat. Chem.* **2011**, *3*, 763–774.
- (3) Ritz, T.; Damjanović, A.; Schulter, K. The Quantum Physics of Photosynthesis. *ChemPhysChem* **2002**, *3*, 243–248.
- (4) Thilagam, A. Natural Light Harvesting Systems: Unraveling the Quantum Puzzles. *J. Math. Chem.* **2015**, *53*, 466–494.
- (5) Croce, R.; van Amerongen, H. Natural Strategies for Photosynthetic Light Harvesting. *Nat. Chem. Biol.* **2014**, *10*, 492–501.
- (6) Glazer, A. N.; Chan, C.; Williams, R. C.; Yeh, S. W.; Clark, J. H. Kinetics of Energy Flow in the Phycobilisome Core. *Science* **1985**, *230*, 1051–1053.
- (7) Fleming, G. R.; Schlau-Cohen, G. S.; Amarnath, K.; Zaks, J. Design Principles of Photosynthetic Light-Harvesting. *Faraday Discuss.* **2012**, *155*, 27–41.
- (8) Barber, J. Photosynthetic Energy Conversion: Natural and Artificial. *Chem. Soc. Rev.* **2009**, *38*, 185–196.
- (9) Pullerits, T.; Sundström, V. Photosynthetic Light-Harvesting Pigment–Protein Complexes: Toward Understanding How and Why. *Acc. Chem. Res.* **1996**, *29*, 381–389.
- (10) Zeng, Y.; Li, Y.-Y.; Chen, J.; Yang, G.; Li, Y. Dendrimers: A Mimic Natural Light-Harvesting System. *Chem. - Asian J.* **2010**, *5*, 992–1005.
- (11) Song, Y.; Yang, Y.; Medforth, C. J.; Pereira, E.; Singh, A. K.; Xu, H.; Jiang, Y.; Brinker, C. J.; van Swol, F.; Shelnutt, J. A. Controlled Synthesis of 2-D and 3-D Dendritic Platinum Nanostructures. *J. Am. Chem. Soc.* **2004**, *126*, 635–645.
- (12) Adronov, A.; Gilat, S. L.; Fréchet, J. M. J.; Ohta, K.; Neuwahl, F. V. R.; Fleming, G. R. Light Harvesting and Energy Transfer in Laser-Dye-Labeled Poly(Aryl Ether) Dendrimers. *J. Am. Chem. Soc.* **2000**, *122*, 1175–1185.
- (13) Kodis, G.; Terazono, Y.; Liddell, P. A.; Andreasson, J.; Garg, V.; Hambourger, M.; Moore, T. A.; Moore, A. L.; Gust, D. Energy and Photoinduced Electron Transfer in a Wheel-Shaped Artificial Photosynthetic Antenna-Reaction Center Complex. *J. Am. Chem. Soc.* **2006**, *128*, 1818–1827.
- (14) Wang, J.-L.; Yan, J.; Tang, Z.-M.; Xiao, Q.; Ma, Y.; Pei, J. Gradient Shape-Persistent Π -Conjugated Dendrimers for Light-Harvesting: Synthesis, Photophysical Properties, and Energy Funneling. *J. Am. Chem. Soc.* **2008**, *130*, 9952–9962.
- (15) Jeong, Y.-H.; Son, M.; Yoon, H.; Kim, P.; Lee, D.-H.; Kim, D.; Jang, W.-D. Inside Back Cover: Guest-Induced Photophysical Property Switching of Artificial Light-Harvesting Dendrimers. *Angew. Chem., Int. Ed.* **2014**, *53*, 7089–7089.
- (16) Zhang, X.; Zeng, Y.; Yu, T.; Chen, J.; Yang, G.; Li, Y. Advances in Photofunctional Dendrimers for Solar Energy Conversion. *J. Phys. Chem. Lett.* **2014**, *5*, 2340–2350.
- (17) Ajayaghosh, A.; Praveen, V. K.; Vijayakumar, C.; George, S. J. Molecular Wire Encapsulated into Π Organogels: Efficient Supramolecular Light-Harvesting Antennae with Color-Tunable Emission. *Angew. Chem., Int. Ed.* **2007**, *46*, 6260–6265.
- (18) Ajayaghosh, A.; Praveen, V. K.; Vijayakumar, C. Organogels as Scaffolds for Excitation Energy Transfer and Light Harvesting. *Chem. Soc. Rev.* **2008**, *37*, 109–122.
- (19) Duan, P.; Yanai, N.; Nagatomi, H.; Kimizuka, N. Photon Upconversion in Supramolecular Gel Matrixes: Spontaneous Accumulation of Light-Harvesting Donor–Acceptor Arrays in Nanofibers and Acquired Air Stability. *J. Am. Chem. Soc.* **2015**, *137*, 1887–1894.
- (20) Choi, M.-S.; Aida, T.; Yamazaki, T.; Yamazaki, I. A Large Dendritic Multiporphyrin Array as a Mimic of the Bacterial Light-Harvesting Antenna Complex: Molecular Design of an Efficient Energy Funnel for Visible Photons. *Angew. Chem., Int. Ed.* **2001**, *40*, 3194–3198.
- (21) Aratani, N.; Kim, D.; Osuka, A. Discrete Cyclic Porphyrin Arrays as Artificial Light-Harvesting Antenna. *Acc. Chem. Res.* **2009**, *42*, 1922–1934.

- (22) Balaban, T. S. Tailoring Porphyrins and Chlorins for Self-Assembly in Biomimetic Artificial Antenna Systems. *Acc. Chem. Res.* **2005**, *38*, 612–623.
- (23) Ishida, Y.; Shimada, T.; Masui, D.; Tachibana, H.; Inoue, H.; Takagi, S. Efficient Excited Energy Transfer Reaction in Clay/Porphyrin Complex toward an Artificial Light-Harvesting System. *J. Am. Chem. Soc.* **2011**, *133*, 14280–14286.
- (24) Wasielewski, M. R. Self-Assembly Strategies for Integrating Light Harvesting and Charge Separation in Artificial Photosynthetic Systems. *Acc. Chem. Res.* **2009**, *42*, 1910–1921.
- (25) Frischmann, P. D.; Mahata, K.; Wurthner, F. Powering the Future of Molecular Artificial Photosynthesis with Light-Harvesting Metallosupramolecular Dye Assemblies. *Chem. Soc. Rev.* **2013**, *42*, 1847–1870.
- (26) Miller, R. A.; Presley, A. D.; Francis, M. B. Self-Assembling Light-Harvesting Systems from Synthetically Modified Tobacco Mosaic Virus Coat Proteins. *J. Am. Chem. Soc.* **2007**, *129*, 3104–3109.
- (27) Kumar, C. V.; Duff, M. R. DNA-Based Supramolecular Artificial Light Harvesting Complexes. *J. Am. Chem. Soc.* **2009**, *131*, 16024–16026.
- (28) Nam, Y. S.; Shin, T.; Park, H.; Magyar, A. P.; Choi, K.; Fantner, G.; Nelson, K. A.; Belcher, A. M. Virus-Templated Assembly of Porphyrins into Light-Harvesting Nanoantennae. *J. Am. Chem. Soc.* **2010**, *132*, 1462–1463.
- (29) Miller, R. A.; Stephanopoulos, N.; McFarland, J. M.; Rosko, A. S.; Geissler, P. L.; Francis, M. B. Impact of Assembly State on the Defect Tolerance of TMV-Based Light Harvesting Arrays. *J. Am. Chem. Soc.* **2010**, *132*, 6068–6074.
- (30) Channon, K. J.; Devlin, G. L.; MacPhee, C. E. Efficient Energy Transfer within Self-Assembling Peptide Fibers: A Route to Light-Harvesting Nanomaterials. *J. Am. Chem. Soc.* **2009**, *131*, 12520–12521.
- (31) Zou, Q.; Liu, K.; Abbas, M.; Yan, X. Peptide-Modulated Self-Assembly of Chromophores toward Biomimetic Light-Harvesting Nanoarchitectonics. *Adv. Mater.* **2016**, *28*, 1031–1043.
- (32) Takeda, H.; Goto, Y.; Maegawa, Y.; Ohsuna, T.; Tani, T.; Matsumoto, K.; Shimada, T.; Inagaki, S. Visible-Light-Harvesting Periodic Mesoporous Organosilica. *Chem. Commun.* **2009**, 6032–6034.
- (33) Nabiev, I.; Rakovich, A.; Sukhanova, A.; Lukashev, E.; Zagidullin, V.; Pachenko, V.; Rakovich, Y. P.; Donegan, J. F.; Rubin, A. B.; Govorov, A. O. Fluorescent Quantum Dots as Artificial Antennas for Enhanced Light Harvesting and Energy Transfer to Photosynthetic Reaction Centers. *Angew. Chem., Int. Ed.* **2010**, *49*, 7217–7221.
- (34) Inagaki, S.; Ohtani, O.; Goto, Y.; Okamoto, K.; Ikai, M.; Yamanaka, K.-i.; Tani, T.; Okada, T. Light Harvesting by a Periodic Mesoporous Organosilica Chromophore. *Angew. Chem., Int. Ed.* **2009**, *48*, 4042–4046.
- (35) Rao, K. V.; Datta, K. K. R.; Eswaramoorthy, M.; George, S. J. Light-Harvesting Hybrid Hydrogels: Energy-Transfer-Induced Amplified Fluorescence in Noncovalently Assembled Chromophore–Organoclay Composites. *Angew. Chem., Int. Ed.* **2011**, *50*, 1179–1184.
- (36) Govorov, A. O. Enhanced Optical Properties of a Photosynthetic System Conjugated with Semiconductor Nanoparticles: The Role of Förster Transfer. *Adv. Mater.* **2008**, *20*, 4330–4335.
- (37) Robel, I.; Subramanian, V.; Kuno, M.; Kamat, P. V. Quantum Dot Solar Cells. Harvesting Light Energy with CdSe Nanocrystals Molecularly Linked to Mesoscopic TiO₂ Films. *J. Am. Chem. Soc.* **2006**, *128*, 2385–2393.
- (38) Alivisatos, A. P. Perspectives on the Physical Chemistry of Semiconductor Nanocrystals. *J. Phys. Chem.* **1996**, *100*, 13226–13239.
- (39) Michalet, X.; Pinaud, F. F.; Bentolila, L. A.; Tsay, J. M.; Doose, S.; Li, J. J.; Sundaresan, G.; Wu, A. M.; Gambhir, S. S.; Weiss, S. Quantum Dots for Live Cells, in Vivo Imaging, and Diagnostics. *Science* **2005**, *307*, 538–544.
- (40) Resch-Genger, U.; Grabolle, M.; Cavaliere-Jaricot, S.; Nitschke, R.; Nann, T. Quantum Dots Versus Organic Dyes as Fluorescent Labels. *Nat. Methods* **2008**, *5*, 763–775.
- (41) Mansur, H. S. Quantum Dots and Nanocomposites. *Wiley Interdiscip. Rev.: Nanomed. Nanobiotechnol.* **2010**, *2*, 113–129.
- (42) Medintz, I. L.; Mattoussi, H. Quantum Dot-Based Resonance Energy Transfer and Its Growing Application in Biology. *Phys. Chem. Chem. Phys.* **2009**, *11*, 17–45.
- (43) Wargnier, R.; Baranov, A. V.; Maslov, V. G.; Stsiapura, V.; Artemyev, M.; Pluot, M.; Sukhanova, A.; Nabiev, I. Energy Transfer in Aqueous Solutions of Oppositely Charged CdSe/ZnS Core/Shell Quantum Dots and in Quantum Dot–Nanogold Assemblies. *Nano Lett.* **2004**, *4*, 451–457.
- (44) Sadhu, S.; Haldar, K. K.; Patra, A. Size Dependent Resonance Energy Transfer between Semiconductor Quantum Dots and Dye Using FRET and Kinetic Model. *J. Phys. Chem. C* **2010**, *114*, 3891–3897.
- (45) Ji, J.; He, L.; Shen, Y.; Hu, P.; Li, X.; Jiang, L.-P.; Zhang, J.-R.; Li, L.; Zhu, J.-J. High-Efficient Energy Funneling Based on Electro-chemiluminescence Resonance Energy Transfer in Graded-Gap Quantum Dots Bilayers for Immunoassay. *Anal. Chem.* **2014**, *86*, 3284–3290.
- (46) Samia, A. C. S.; Dayal, S.; Burda, C. Quantum Dot-Based Energy Transfer: Perspectives and Potential for Applications in Photodynamic Therapy. *Photochem. Photobiol.* **2006**, *82*, 617–625.
- (47) Goldman, E. R.; Medintz, I. L.; Whitley, J. L.; Hayhurst, A.; Clapp, A. R.; Uyeda, H. T.; Deschamps, J. R.; Lassman, M. E.; Mattoussi, H. A Hybrid Quantum Dot–Antibody Fragment Fluorescence Resonance Energy Transfer-Based TNT Sensor. *J. Am. Chem. Soc.* **2005**, *127*, 6744–6751.
- (48) Wu, C.; Zheng, Y.; Szymanski, C.; McNeill, J. Energy Transfer in a Nanoscale Multichromophoric System: Fluorescent Dye-Doped Conjugated Polymer Nanoparticles. *J. Phys. Chem. C* **2008**, *112*, 1772–1781.
- (49) Bhattacharyya, S.; Paramanik, B.; Patra, A. Energy Transfer and Confined Motion of Dyes Trapped in Semiconducting Conjugated Polymer Nanoparticles. *J. Phys. Chem. C* **2011**, *115*, 20832–20839.
- (50) Scholes, G. D.; Fleming, G. R. On the Mechanism of Light Harvesting in Photosynthetic Purple Bacteria: B800 to B850 Energy Transfer. *J. Phys. Chem. B* **2000**, *104*, 1854–1868.
- (51) van Grondelle, R.; Novoderezhkin, V. I. Energy Transfer in Photosynthesis: Experimental Insights and Quantitative Models. *Phys. Chem. Chem. Phys.* **2006**, *8*, 793–807.
- (52) Novoderezhkin, V. I.; van Grondelle, R. Physical Origins and Models of Energy Transfer in Photosynthetic Light-Harvesting. *Phys. Chem. Chem. Phys.* **2010**, *12*, 7352–7365.
- (53) Beenken, W. J. D.; Pullerits, T. Excitonic Coupling in Polythiophenes: Comparison of Different Calculation Methods. *J. Chem. Phys.* **2004**, *120*, 2490–2495.
- (54) Lakowicz, J. R. *Principles of Fluorescence Spectroscopy*, 3rd ed.; Springer, 2006; Vol. XXVI, 954 pp.
- (55) Förster, T. Zwischenmolekulare Energiewanderung und Fluoreszenz. *Ann. Phys.* **1948**, *437*, 55–75.
- (56) Zheng, K.; Žídek, K.; Abdellah, M.; Zhu, N.; Chábera, P.; Lenngren, N.; Chi, Q.; Pullerits, T. Directed Energy Transfer in Films of CdSe Quantum Dots: Beyond the Point Dipole Approximation. *J. Am. Chem. Soc.* **2014**, *136*, 6259–6268.
- (57) Chance, R. R.; Prock, A.; Silbey, R. In *Advances in Chemical Physics*; John Wiley & Sons, Inc., 2007.
- (58) Persson, B. N. J.; Lang, N. D. Electron-Hole-Pair Quenching of Excited States near a Metal. *Phys. Rev. B: Condens. Matter Mater. Phys.* **1982**, *26*, 5409–5415.
- (59) Dulkeith, E.; Morteani, A. C.; Niedereichholz, T.; Klar, T. A.; Feldmann, J.; Levi, S. A.; van Veggel, F. C. J. M.; Reinhoudt, D. N.; Möller, M.; Gittins, D. I. Fluorescence Quenching of Dye Molecules Near Gold Nanoparticles: Radiative and Nonradiative Effects. *Phys. Rev. Lett.* **2002**, *89*, 203002.
- (60) Dulkeith, E.; Ringler, M.; Klar, T. A.; Feldmann, J.; Muñoz Javier, A.; Parak, W. J. Gold Nanoparticles Quench Fluorescence by Phase Induced Radiative Rate Suppression. *Nano Lett.* **2005**, *5*, 585–589.

- (61) Gonorov, A. O.; Bryant, G. W.; Zhang, W.; Skeini, T.; Lee, J.; Kotov, N. A.; Slocik, J. M.; Naik, R. R. Exciton–Plasmon Interaction and Hybrid Excitons in Semiconductor–Metal Nanoparticle Assemblies. *Nano Lett.* **2006**, *6*, 984–994.
- (62) Liu, G. L.; Yin, Y.; Kunchakarra, S.; Mukherjee, B.; Gerion, D.; Jett, S. D.; Bear, D. G.; Gray, J. W.; Alivisatos, A. P.; Lee, L. P.; et al. A Nanoplasmonic Molecular Ruler for Measuring Nuclease Activity and DNA Footprinting. *Nat. Nanotechnol.* **2006**, *1*, 47–52.
- (63) Saraswat, S.; Desiréddy, A.; Zheng, D.; Guo, L.; Lu, H. P.; Bigioni, T. P.; Isailovic, D. Energy Transfer from Fluorescent Proteins to Metal Nanoparticles. *J. Phys. Chem. C* **2011**, *115*, 17587–17593.
- (64) Jones, M.; Lo, S. S.; Scholes, G. D. Signatures of Exciton Dynamics and Carrier Trapping in the Time-Resolved Photoluminescence of Colloidal CdSe Nanocrystals. *J. Phys. Chem. C* **2009**, *113*, 18632–18642.
- (65) de Mello Donegá, C.; Bode, M.; Meijerink, A. Size- and Temperature-Dependence of Exciton Lifetimes in CdSe Quantum Dots. *Phys. Rev. B: Condens. Matter Mater. Phys.* **2006**, *74*, 085320.
- (66) Bawendi, M. G.; Wilson, W. L.; Rothberg, L.; Carroll, P. J.; Jedju, T. M.; Steigerwald, M. L.; Brus, L. E. Electronic Structure and Photoexcited-Carrier Dynamics in Nanometer-Size CdSe Clusters. *Phys. Rev. Lett.* **1990**, *65*, 1623–1626.
- (67) Rossetti, R.; Ellison, J. L.; Gibson, J. M.; Brus, L. E. Size Effects in the Excited Electronic States of Small Colloidal CdS Crystallites. *J. Chem. Phys.* **1984**, *80*, 4464–4469.
- (68) Rossetti, R.; Hull, R.; Gibson, J. M.; Brus, L. E. Excited Electronic States and Optical Spectra of ZnS and CdS Crystallites in the \approx 15 to 50 Å Size Range: Evolution from Molecular to Bulk Semiconducting Properties. *J. Chem. Phys.* **1985**, *82*, 552–559.
- (69) Brus, L. E. Electron–Electron and Electron-Hole Interactions in Small Semiconductor Crystallites: The Size Dependence of the Lowest Excited Electronic State. *J. Chem. Phys.* **1984**, *80*, 4403–4409.
- (70) Jones, M.; Scholes, G. D. On the Use of Time-Resolved Photoluminescence as a Probe of Nanocrystal Photoexcitation Dynamics. *J. Mater. Chem.* **2010**, *20*, 3533–3538.
- (71) Mews, A.; Kadavanich, A. V.; Banin, U.; Alivisatos, A. P. Structural and Spectroscopic Investigations of CdS/HgS/CdS Quantum-Dot Quantum Wells. *Phys. Rev. B: Condens. Matter Mater. Phys.* **1996**, *53*, R13242–R13245.
- (72) Burda, C.; Green, T. C.; Link, S.; El-Sayed, M. A. Electron Shuttling across the Interface of CdSe Nanoparticles Monitored by Femtosecond Laser Spectroscopy. *J. Phys. Chem. B* **1999**, *103*, 1783–1788.
- (73) Klimov, V. I.; McBranch, D. W. Femtosecond 1P-to-1S Electron Relaxation in Strongly Confined Semiconductor Nanocrystals. *Phys. Rev. Lett.* **1998**, *80*, 4028–4031.
- (74) Javier, A.; Magana, D.; Jennings, T.; Strouse, G. F. Nanosecond Exciton Recombination Dynamics in Colloidal CdSe Quantum Dots under Ambient Conditions. *Appl. Phys. Lett.* **2003**, *83*, 1423–1425.
- (75) Zhang, J.; Zhang, X.; Zhang, J. Y. Size-Dependent Time-Resolved Photoluminescence of Colloidal CdSe Nanocrystals. *J. Phys. Chem. C* **2009**, *113*, 9512–9515.
- (76) Wu, W.; Yu, D.; Ye, H.-a.; Gao, Y.; Chang, Q. Temperature and Composition Dependent Excitonic Luminescence and Exciton–Phonon Coupling in CdSeS Nanocrystals. *Nanoscale Res. Lett.* **2012**, *7*, 301.
- (77) Kim, M. R.; Park, S.-Y.; Jang, D.-J. Composition Variation and Thermal Treatment of $Zn_xCd_{1-x}S$ Alloy Nanoparticles to Exhibit Controlled and Efficient Luminescence. *J. Phys. Chem. C* **2010**, *114*, 6452–6457.
- (78) Zhang, B. P.; Li, Y. Q.; Yasuda, T.; Segawa, Y.; Edamatsu, K.; Itoh, T. Time-Resolved Photoluminescence of ZnCdSe Single Quantum Dots. *J. Cryst. Growth* **2000**, *214–215*, 765–769.
- (79) Morello, G.; Anni, M.; Cozzoli, P. D.; Manna, L.; Cingolani, R.; De Giorgi, M. Picosecond Photoluminescence Decay Time in Colloidal Nanocrystals: The Role of Intrinsic and Surface States. *J. Phys. Chem. C* **2007**, *111*, 10541–10545.
- (80) Wang, X.; Qu, L.; Zhang, J.; Peng, X.; Xiao, M. Surface-Related Emission in Highly Luminescent CdSe Quantum Dots. *Nano Lett.* **2003**, *3*, 1103–1106.
- (81) Wu, F.; Zhang, J. Z.; Kho, R.; Mehra, R. K. Radiative and Nonradiative Lifetimes of Band Edge States and Deep Trap States of CdS Nanoparticles Determined by Time-Correlated Single Photon Counting. *Chem. Phys. Lett.* **2000**, *330*, 237–242.
- (82) Sadhu, S.; Saha Chowdhury, P.; Patra, A. Synthesis and Time-Resolved Photoluminescence Spectroscopy of Capped CdS Nanocrystals. *J. Lumin.* **2008**, *128*, 1235–1240.
- (83) Chowdhury, P. S.; Ghosh, P.; Patra, A. Study of Photophysical Properties of Capped CdS Nanocrystals. *J. Lumin.* **2007**, *124*, 327–332.
- (84) Xu, S.; Mikhailovsky, A. A.; Hollingsworth, J. A.; Klimov, V. I. Hole Intraband Relaxation in Strongly Confined Quantum Dots: Revisiting the “Phonon Bottleneck” Problem. *Phys. Rev. B: Condens. Matter Mater. Phys.* **2002**, *65*, 045319.
- (85) Sewall, S. L.; Cooney, R. R.; Anderson, K. E. H.; Dias, E. A.; Kambhampati, P. State-to-State Exciton Dynamics in Semiconductor Quantum Dots. *Phys. Rev. B: Condens. Matter Mater. Phys.* **2006**, *74*, 235328.
- (86) Jones, M.; Lo, S. S.; Scholes, G. D. Quantitative Modeling of the Role of Surface Traps in CdSe/CdS/ZnS Nanocrystal Photoluminescence Decay Dynamics. *Proc. Natl. Acad. Sci. U. S. A.* **2009**, *106*, 3011–3016.
- (87) Sewall, S. L.; Cooney, R. R.; Anderson, K. E. H.; Dias, E. A.; Sagar, D. M.; Kambhampati, P. State-Resolved Studies of Biexcitons and Surface Trapping Dynamics in Semiconductor Quantum Dots. *J. Chem. Phys.* **2008**, *129*, 084701.
- (88) Kilina, S.; Ivanov, S.; Tretiak, S. Effect of Surface Ligands on Optical and Electronic Spectra of Semiconductor Nanoclusters. *J. Am. Chem. Soc.* **2009**, *131*, 7717–7726.
- (89) Kambhampati, P. Hot Exciton Relaxation Dynamics in Semiconductor Quantum Dots: Radiationless Transitions on the Nanoscale. *J. Phys. Chem. C* **2011**, *115*, 22089–22109.
- (90) Rogach, A. L.; Klar, T. A.; Lupton, J. M.; Meijerink, A.; Feldmann, J. Energy Transfer with Semiconductor Nanocrystals. *J. Mater. Chem.* **2009**, *19*, 1208–1221.
- (91) Wuister, S. F.; van Houselt, A.; de Mello Donegá, C.; Vanmaekelbergh, D.; Meijerink, A. Temperature Antiquenching of the Luminescence from Capped CdSe Quantum Dots. *Angew. Chem.* **2004**, *116*, 3091–3095.
- (92) Fomenko, V.; Nesbitt, D. J. Solution Control of Radiative and Nonradiative Lifetimes: A Novel Contribution to Quantum Dot Blinking Suppression. *Nano Lett.* **2008**, *8*, 287–293.
- (93) Little, R. B.; Burda, C.; Link, S.; Logunov, S.; El-Sayed, M. A. Charge Separation Effects on the Rate of Nonradiative Relaxation Processes in Quantum Dots–Quantum Well Heteronanostructures. *J. Phys. Chem. A* **1998**, *102*, 6581–6584.
- (94) Burda, C.; Link, S.; Green, T. C.; El-Sayed, M. A. New Transient Absorption Observed in the Spectrum of Colloidal CdSe Nanoparticles Pumped with High-Power Femtosecond Pulses. *J. Phys. Chem. B* **1999**, *103*, 10775–10780.
- (95) Burda, C.; El-Sayed, M. A. High-density Femtosecond Transient Absorption Spectroscopy of Semiconductor Nanoparticles. A Tool to Investigate Surface Quality. *Pure Appl. Chem.* **2000**, *72*, 165.
- (96) Mohamed, M. B.; Burda, C.; El-Sayed, M. A. Shape Dependent Ultrafast Relaxation Dynamics of CdSe Nanocrystals: Nanorods vs Nanodots. *Nano Lett.* **2001**, *1*, 589–593.
- (97) Scholes, G. D.; Rumbles, G. Excitons in Nanoscale Systems. *Nat. Mater.* **2006**, *5*, 683–696.
- (98) Kambhampati, P. Unraveling the Structure and Dynamics of Excitons in Semiconductor Quantum Dots. *Acc. Chem. Res.* **2011**, *44*, 1–13.
- (99) Klimov, V. I. Mechanisms for Photogeneration and Recombination of Multiexcitons in Semiconductor Nanocrystals: Implications for Lasing and Solar Energy Conversion. *J. Phys. Chem. B* **2006**, *110*, 16827–16845.

- (100) Klimov, V. I. Optical Nonlinearities and Ultrafast Carrier Dynamics in Semiconductor Nanocrystals. *J. Phys. Chem. B* **2000**, *104*, 6112–6123.
- (101) Stewart, J. T.; Padilha, L. A.; Bae, W. K.; Koh, W.-K.; Pietryga, J. M.; Klimov, V. I. Carrier Multiplication in Quantum Dots within the Framework of Two Competing Energy Relaxation Mechanisms. *J. Phys. Chem. Lett.* **2013**, *4*, 2061–2068.
- (102) Bischof, T. S.; Correa, R. E.; Rosenberg, D.; Dauler, E. A.; Bawendi, M. G. Measurement of Emission Lifetime Dynamics and Biexciton Emission Quantum Yield of Individual InAs Colloidal Nanocrystals. *Nano Lett.* **2014**, *14*, 6787–6791.
- (103) Chuang, C.-H.; Burda, C. Contribution of Femtosecond Laser Spectroscopy to the Development of Advanced Optoelectronic Nanomaterials. *J. Phys. Chem. Lett.* **2012**, *3*, 1921–1927.
- (104) Zhang, J. Z.; O’Neil, R. H.; Roberti, T. W. Femtosecond Studies of Photoinduced Electron Dynamics at the Liquid-Solid Interface of Aqueous CdS Colloids. *J. Phys. Chem.* **1994**, *98*, 3859–3864.
- (105) Zhang, J. Z. Ultrafast Studies of Electron Dynamics in Semiconductor and Metal Colloidal Nanoparticles: Effects of Size and Surface. *Acc. Chem. Res.* **1997**, *30*, 423–429.
- (106) Zhang, J. Z. Interfacial Charge Carrier Dynamics of Colloidal Semiconductor Nanoparticles. *J. Phys. Chem. B* **2000**, *104*, 7239–7253.
- (107) Roberti, T. W.; Cherepy, N. J.; Zhang, J. Z. Nature of the Power-Dependent Ultrafast Relaxation Process of Photoexcited Charge Carriers in II-VI Semiconductor Quantum Dots: Effects of Particle Size, Surface, and Electronic Structure. *J. Chem. Phys.* **1998**, *108*, 2143–2151.
- (108) Asbury, J. B.; Anderson, N. A.; Hao, E.; Ai, X.; Lian, T. Parameters Affecting Electron Injection Dynamics from Ruthenium Dyes to Titanium Dioxide Nanocrystalline Thin Film. *J. Phys. Chem. B* **2003**, *107*, 7376–7386.
- (109) Anderson, N. A.; Lian, T. Ultrafast Electron Transfer at the Molecule-Semiconductor Nanoparticle Interface. *Annu. Rev. Phys. Chem.* **2005**, *56*, 491–519.
- (110) Al Salman, A.; Tortschanoff, A.; van der Zwan, G.; van Mourik, F.; Chergui, M. A Model for the Multi-Exponential Excited-State Decay of CdSe Nanocrystals. *Chem. Phys.* **2009**, *357*, 96–101.
- (111) Bawendi, M. G.; Steigerwald, M. L.; Brus, L. E. The Quantum Mechanics of Larger Semiconductor Clusters (“Quantum Dots”). *Annu. Rev. Phys. Chem.* **1990**, *41*, 477–496.
- (112) Nirmal, M.; Brus, L. Luminescence Photophysics in Semiconductor Nanocrystals. *Acc. Chem. Res.* **1999**, *32*, 407–414.
- (113) Kaschke, M.; Ernsting, N. P.; Müller, U.; Weller, H. Ultrafast Electron Ejection and Trapping in Semiconductor Colloids after Multiple Photon Absorption. *Chem. Phys. Lett.* **1990**, *168*, 543–550.
- (114) Hilczer, M.; Tachiya, M. Stochastic Approach to Charge Separation in Multiexcited Quantum Dots. *J. Phys. Chem. C* **2009**, *113*, 18451–18454.
- (115) Sadhu, S.; Patra, A. Relaxation Dynamics of Anisotropic Shaped CdS Nanoparticles. *J. Phys. Chem. C* **2011**, *115*, 16867–16872.
- (116) Sadhu, S.; Patra, A. Lattice Strain Controls the Carrier Relaxation Dynamics in $\text{Cd}_x\text{Zn}_{1-x}\text{S}$ Alloy Quantum Dots. *J. Phys. Chem. C* **2012**, *116*, 15167–15173.
- (117) Hartmann, L.; Kumar, A.; Welker, M.; Fiore, A.; Julien-Rabat, C.; Gromova, M.; Bardet, M.; Reiss, P.; Baxter, P. N. W.; Chandezon, F.; Pansu, R. B. Quenching Dynamics in CdSe Nanoparticles: Surface-Induced Defects Upon Dilution. *ACS Nano* **2012**, *6*, 9033–9041.
- (118) Tachiya, M. Application of a Generating Function to Reaction Kinetics in Micelles. Kinetics of Quenching of Luminescent Probes in Micelles. *Chem. Phys. Lett.* **1975**, *33*, 289–292.
- (119) Zheng, K.; Karki, K.; Žídek, K.; Pullerits, T. Ultrafast Photoinduced Dynamics in Quantum Dot-Based Systems for Light Harvesting. *Nano Res.* **2015**, *8*, 2125–2142.
- (120) Žídek, K.; Zheng, K.; Abdellah, M.; Chábera, P.; Pullerits, T.; Tachiya, M. Simultaneous Creation and Recovery of Trap States on Quantum Dots in a Photoirradiated CdSe–ZnO System. *J. Phys. Chem. C* **2014**, *118*, 27567–27573.
- (121) Abdellah, M.; Marschan, R.; Žídek, K.; Messing, M. E.; Abdelwahab, A.; Chábera, P.; Zheng, K.; Pullerits, T. Hole Trapping: The Critical Factor for Quantum Dot Sensitized Solar Cell Performance. *J. Phys. Chem. C* **2014**, *118*, 25802–25808.
- (122) Garrett, M. D.; Dukes, A. D., III; McBride, J. R.; Smith, N. J.; Pennycook, S. J.; Rosenthal, S. J. Band Edge Recombination in CdSe, CdS and $\text{CdS}_x\text{Se}_{1-x}$ Alloy Nanocrystals Observed by Ultrafast Fluorescence Upconversion: The Effect of Surface Trap States. *J. Phys. Chem. C* **2008**, *112*, 12736–12746.
- (123) Ma, H.; Ma, G.-H.; Wang, W.-J.; Gao, X.-X.; Ma, H.-L. Size-Dependent Optical Properties and Carriers Dynamics in CdSe/ZnS Quantum Dots. *Chin. Phys. B* **2008**, *17*, 1280–1285.
- (124) Nirmal, M.; Murray, C. B.; Bawendi, M. G. Fluorescence-Line Narrowing in CdSe Quantum Dots: Surface Localization of the Photogenerated Exciton. *Phys. Rev. B: Condens. Matter Mater. Phys.* **1994**, *50*, 2293–2300.
- (125) Yagi, I.; Mikami, K.; Ebina, K.; Okamura, M.; Uosaki, K. Size-Dependent Carrier Dynamics in CdS Nanoparticles by Femtosecond Visible-Pump/IR-Probe Measurements. *J. Phys. Chem. B* **2006**, *110*, 14192–14197.
- (126) Krishnamurthy, S.; Kamat, P. V. Cdse—Graphene Oxide Light-Harvesting Assembly: Size-Dependent Electron Transfer and Light Energy Conversion Aspects. *ChemPhysChem* **2014**, *15*, 2129–2135.
- (127) Zhu, N.; Zheng, K.; Karki, K. J.; Abdellah, M.; Zhu, Q.; Carlson, S.; Haase, D.; Žídek, K.; Ulstrup, J.; Canton, S. E.; Pullerits, T.; Chi, Q. Sandwiched Confinement of Quantum Dots in Graphene Matrix for Efficient Electron Transfer and Photocurrent Production. *Sci. Rep.* **2015**, *5*, 9860.
- (128) Kundu, S.; Sadhu, S.; Bera, R.; Paramanik, B.; Patra, A. Fluorescence Dynamics and Stochastic Model for Electronic Interaction of Graphene Oxide with CdTe QD in Graphene Oxide-CdTe QD Composite. *J. Phys. Chem. C* **2013**, *117*, 23987–23995.
- (129) Debgupta, J.; Mandal, S.; Kalita, H.; Aslam, M.; Patra, A.; Pillai, V. Photophysical and Photoconductivity Properties of Thiol-Functionalized Graphene-CdSe QD Composites. *RSC Adv.* **2014**, *4*, 13788–13795.
- (130) Kim, J.; Nair, P. S.; Wong, C. Y.; Scholes, G. D. Sizing up the Exciton in Complex-Shaped Semiconductor Nanocrystals. *Nano Lett.* **2007**, *7*, 3884–3890.
- (131) Shabaev, A.; Efros, A. L. 1D Exciton Spectroscopy of Semiconductor Nanorods. *Nano Lett.* **2004**, *4*, 1821–1825.
- (132) Chae, W.-S.; Shin, H.-W.; Lee, E.-S.; Shin, E.-J.; Jung, J.-S.; Kim, Y.-R. Excitation Dynamics in Anisotropic Nanostructures of Star-Shaped CdS. *J. Phys. Chem. B* **2005**, *109*, 6204–6209.
- (133) Schlegel, G.; Bohnenberger, J.; Potapova, I.; Mews, A. Fluorescence Decay Time of Single Semiconductor Nanocrystals. *Phys. Rev. Lett.* **2002**, *88*, 137401.
- (134) van Driel, A. F.; Nikolaev, I. S.; Vergeer, P.; Lodahl, P.; Vanmaekelbergh, D.; Vos, W. L. Statistical Analysis of Time-Resolved Emission from Ensembles of Semiconductor Quantum Dots: Interpretation of Exponential Decay Models. *Phys. Rev. B: Condens. Matter Mater. Phys.* **2007**, *75*, 035329.
- (135) Ouyang, J.; Ripmeester, J. A.; Wu, X.; Kingston, D.; Yu, K.; Joly, A. G.; Chen, W. Upconversion Luminescence of Colloidal CdS and ZnCdS Semiconductor Quantum Dots. *J. Phys. Chem. C* **2007**, *111*, 16261–16266.
- (136) Zhang, F. J.; Zhang, L. M.; Claus, R. O. Nonlinear Differential Ultrafast Laser Absorption Spectroscopy Observation of Charge Carrier Dynamics of $\text{CdS}_x\text{Se}_{1-x}$ Nanocrystal Doped Glasses. *Smart Mater. Struct.* **2007**, *16*, 243.
- (137) Shen, Q.; Toyoda, T.; Hirose, Y.; Katayama, K.; Yui, H.; Fujinami, M.; Sawada, T.; Harata, A. Ultrafast Dynamics of $\text{CdS}_x\text{Se}_{1-x}$ Nanocrystals Doped in Glasses Studied by Ultrafast Transient Lensing Effect. *Anal. Sci./Suppl.* **2002**, *17*, s241–s244.
- (138) Smith, A. M.; Mohs, A. M.; Nie, S. Tuning the Optical and Electronic Properties of Colloidal Nanocrystals by Lattice Strain. *Nat. Nanotechnol.* **2009**, *4*, 56–63.

- (139) Zhong, X.; Feng, Y.; Knoll, W.; Han, M. Alloyed $Zn_xCd_{1-x}S$ Nanocrystals with Highly Narrow Luminescence Spectral Width. *J. Am. Chem. Soc.* **2003**, *125*, 13559–13563.
- (140) Yeh, J.-W.; Chang, S.-Y.; Hong, Y.-D.; Chen, S.-K.; Lin, S.-J. Anomalous Decrease in X-Ray Diffraction Intensities of Cu–Ni–Al–Co–Cr–Fe–Si Alloy Systems with Multi-Principal Elements. *Mater. Chem. Phys.* **2007**, *103*, 41–46.
- (141) Nahory, R. E.; Pollack, M. A.; Johnston, W. D.; Barns, R. L. Band Gap Versus Composition and Demonstration of Vegard's Law for $In_{1-x}Ga_xAs_yP_{1-y}$ Lattice Matched to InP. *Appl. Phys. Lett.* **1978**, *33*, 659–661.
- (142) Nakamura, Y.; Oguro, K.; Uehara, I.; Akiba, E. X-Ray Diffraction Peak Broadening and Lattice Strain in $LaNi_5$ -Based Alloys. *J. Alloys Compd.* **2000**, *298*, 138–145.
- (143) Fancey, S. J.; Buller, G. S.; Massa, J. S.; Walker, A. C.; Perrin, S. D.; Dann, A. J.; Robertson, M. J. Time Resolved Photoluminescence Study of Strained-Layer InGaAsP/InP Heterostructures. *J. Cryst. Growth* **1998**, *183*, 269–273.
- (144) Masadeh, A. S.; Božin, E. S.; Farrow, C. L.; Paglia, G.; Juhas, P.; Billinge, S. J. L.; Karkamkar, A.; Kanatzidis, M. G. Quantitative Size-Dependent Structure and Strain Determination of CdSe Nanoparticles Using Atomic Pair Distribution Function Analysis. *Phys. Rev. B: Condens. Matter Mater. Phys.* **2007**, *76*, 115413.
- (145) Gilbert, B.; Huang, F.; Zhang, H.; Waychunas, G. A.; Banfield, J. F. Nanoparticles: Strained and Stiff. *Science* **2004**, *305*, 651–654.
- (146) Veilleux, V.; Lachance-Quirion, D.; Doré, K.; Landry, D. B.; Charette, P. G.; Allen, C. N. Strain-Induced Effects in Colloidal Quantum Dots: Lifetime Measurements and Blinking Statistics. *Nanotechnology* **2010**, *21*, 134024.
- (147) Abdellah, M.; Žídek, K.; Zheng, K.; Chábera, P.; Messing, M. E.; Pullerits, T. Balancing Electron Transfer and Surface Passivation in Gradient CdSe/ZnS Core–Shell Quantum Dots Attached to ZnO. *J. Phys. Chem. Lett.* **2013**, *4*, 1760–1765.
- (148) Barceló, I.; Guillén, E.; Lana-Villarreal, T.; Gómez, R. Preparation and Characterization of Nickel Oxide Photocathodes Sensitized with Colloidal Cadmium Selenide Quantum Dots. *J. Phys. Chem. C* **2013**, *117*, 22509–22517.
- (149) Zheng, K.; Žídek, K.; Abdellah, M.; Zhang, W.; Chábera, P.; Lenngren, N.; Yartsev, A.; Pullerits, T. Ultrafast Charge Transfer from CdSe Quantum Dots to P-Type NiO: Hole Injection vs Hole Trapping. *J. Phys. Chem. C* **2014**, *118*, 18462–18471.
- (150) Kilina, S. V.; Kilin, D. S.; Prezhdo, O. V. Breaking the Phonon Bottleneck in PbSe and CdSe Quantum Dots: Time-Domain Density Functional Theory of Charge Carrier Relaxation. *ACS Nano* **2009**, *3*, 93–99.
- (151) Beard, M. C.; Midgett, A. G.; Law, M.; Semonin, O. E.; Ellingson, R. J.; Nozik, A. J. Variations in the Quantum Efficiency of Multiple Exciton Generation for a Series of Chemically Treated PbSe Nanocrystal Films. *Nano Lett.* **2009**, *9*, 836–845.
- (152) Omogo, B.; Aldana, J. F.; Heyes, C. D. Radiative and Nonradiative Lifetime Engineering of Quantum Dots in Multiple Solvents by Surface Atom Stoichiometry and Ligands. *J. Phys. Chem. C* **2013**, *117*, 2317–2327.
- (153) Williams, E. S.; Major, K. J.; Tobias, A.; Woodall, D.; Morales, V.; Lippincott, C.; Moyer, P. J.; Jones, M. Characterizing the Influence of TOPO on Exciton Recombination Dynamics in Colloidal CdSe Quantum Dots. *J. Phys. Chem. C* **2013**, *117*, 4227–4237.
- (154) Koole, R.; Schapotschnikow, P.; de Mello Donegá, C.; Vlugt, T. J. H.; Meijerink, A. Time-Dependent Photoluminescence Spectroscopy as a Tool To Measure the Ligand Exchange Kinetics on a Quantum Dot Surface. *ACS Nano* **2008**, *2*, 1703–1714.
- (155) Morris-Cohen, A. J.; Vasilenko, V.; Amin, V. A.; Reuter, M. G.; Weiss, E. A. Model for Adsorption of Ligands to Colloidal Quantum Dots with Concentration-Dependent Surface Structure. *ACS Nano* **2012**, *6*, 557–565.
- (156) Tagliazucchi, M.; Tice, D. B.; Sweeney, C. M.; Morris-Cohen, A. J.; Weiss, E. A. Ligand-Controlled Rates of Photoinduced Electron Transfer in Hybrid CdSe Nanocrystal/Poly(Viologen) Films. *ACS Nano* **2011**, *5*, 9907–9917.
- (157) Clapp, A. R.; Medintz, I. L.; Mattoussi, H. Förster Resonance Energy Transfer Investigations Using Quantum-Dot Fluorophores. *ChemPhysChem* **2006**, *7*, 47–57.
- (158) Sadhu, S.; Patra, A. A Brief Overview of Some Physical Studies on the Relaxation Dynamics and Förster Resonance Energy Transfer of Semiconductor Quantum Dots. *ChemPhysChem* **2013**, *14*, 2641–2653.
- (159) Medintz, I. L.; Clapp, A. R.; Mattoussi, H.; Goldman, E. R.; Fisher, B.; Mauro, J. M. Self-Assembled Nanoscale Biosensors Based on Quantum Dot FRET Donors. *Nat. Mater.* **2003**, *2*, 630–638.
- (160) Curutchet, C.; Franceschetti, A.; Zunger, A.; Scholes, G. D. Examining Förster Energy Transfer for Semiconductor Nanocrystalline Quantum Dot Donors and Acceptors. *J. Phys. Chem. C* **2008**, *112*, 13336–13341.
- (161) Mutluğün, E.; Nizamoğlu, S.; Demir, H. V. Highly Efficient Nonradiative Energy Transfer Using Charged CdSe/ZnS Nanocrystals for Light-Harvesting in Solution. *Appl. Phys. Lett.* **2009**, *95*, 033106.
- (162) Boulesbaa, A.; Huang, Z.; Wu, D.; Lian, T. Competition between Energy and Electron Transfer from CdSe QDs to Adsorbed Rhodamine B. *J. Phys. Chem. C* **2010**, *114*, 962–969.
- (163) Ensslen, P.; Wagenknecht, H.-A. One-Dimensional Multichromophore Arrays Based on DNA: From Self-Assembly to Light-Harvesting. *Acc. Chem. Res.* **2015**, *48*, 2724–2733.
- (164) Spillmann, C. M.; Medintz, I. L. Use of Biomolecular Scaffolds for Assembling Multistep Light Harvesting and Energy Transfer Devices. *J. Photochem. Photobiol., C* **2015**, *23*, 1–24.
- (165) Medintz, I. L.; Pons, T.; Susumu, K.; Boeneman, K.; Dennis, A. M.; Farrell, D.; Deschamps, J. R.; Melinger, J. S.; Bao, G.; Mattoussi, H. Resonance Energy Transfer between Luminescent Quantum Dots and Diverse Fluorescent Protein Acceptors. *J. Phys. Chem. C* **2009**, *113*, 18552–18561.
- (166) Algar, W. R.; Ancona, M. G.; Malanoski, A. P.; Susumu, K.; Medintz, I. L. Assembly of a Concentric Förster Resonance Energy Transfer Relay on a Quantum Dot Scaffold: Characterization and Application to Multiplexed Protease Sensing. *ACS Nano* **2012**, *6*, 11044–11058.
- (167) Lu, H.; Schöps, O.; Woggon, U.; Niemeyer, C. M. Self-Assembled Donor Comprising Quantum Dots and Fluorescent Proteins for Long-Range Fluorescence Resonance Energy Transfer. *J. Am. Chem. Soc.* **2008**, *130*, 4815–4827.
- (168) Spillmann, C. M.; Ancona, M. G.; Buckhout-White, S.; Algar, W. R.; Stewart, M. H.; Susumu, K.; Huston, A. L.; Goldman, E. R.; Medintz, I. L. Achieving Effective Terminal Exciton Delivery in Quantum Dot Antenna-Sensitized Multistep DNA Photonic Wires. *ACS Nano* **2013**, *7*, 7101–7118.
- (169) Dennis, A. M.; Bao, G. Quantum Dot–Fluorescent Protein Pairs as Novel Fluorescence Resonance Energy Transfer Probes. *Nano Lett.* **2008**, *8*, 1439–1445.
- (170) Sadhu, S.; Tachiya, M.; Patra, A. A Stochastic Model for Energy Transfer from CdS Quantum Dots/Rods (Donors) to Nile Red Dye (Acceptors). *J. Phys. Chem. C* **2009**, *113*, 19488–19492.
- (171) Tachiya, M. Kinetics of Quenching of Luminescent Probes in Micellar Systems. II. *J. Chem. Phys.* **1982**, *76*, 340–348.
- (172) Haldar, K. K.; Sen, T.; Mandal, S.; Patra, A. Photophysical Properties of Au–CdTe Hybrid Nanostructures of Varying Sizes and Shapes. *ChemPhysChem* **2012**, *13*, 3989–3996.
- (173) Halivni, S.; Sitt, A.; Hadar, I.; Banin, U. Effect of Nanoparticle Dimensionality on Fluorescence Resonance Energy Transfer in Nanoparticle–Dye Conjugated Systems. *ACS Nano* **2012**, *6*, 2758–2765.
- (174) Artemyev, M.; Ustinovich, E.; Nabiev, I. Efficiency of Energy Transfer from Organic Dye Molecules to CdSe–ZnS Nanocrystals: Nanorods Versus Nanodots. *J. Am. Chem. Soc.* **2009**, *131*, 8061–8065.
- (175) Hardzei, M.; Artemyev, M.; Molinari, M.; Troyon, M.; Sukhanova, A.; Nabiev, I. Comparative Efficiency of Energy Transfer from CdSe–ZnS Quantum Dots or Nanorods to Organic Dye Molecules. *ChemPhysChem* **2012**, *13*, 330–335.

- (176) Sadhu, S.; Patra, A. Donor-Acceptor Systems: Energy Transfer from CdS Quantum Dots/Rods to Nile Red Dye. *ChemPhysChem* **2008**, *9*, 2052–2058.
- (177) Chowdhury, P. S.; Sen, P.; Patra, A. Optical Properties of CdS Nanoparticles and the Energy Transfer from CdS Nanoparticles to Rhodamine 6G. *Chem. Phys. Lett.* **2005**, *413*, 311–314.
- (178) Dayal, S.; Burda, C. Surface Effects on Quantum Dot-Based Energy Transfer. *J. Am. Chem. Soc.* **2007**, *129*, 7977–7981.
- (179) Hoffman, J. B.; Choi, H.; Kamat, P. V. Size-Dependent Energy Transfer Pathways in CdSe Quantum Dot–Squaraine Light-Harvesting Assemblies: Förster Versus Dexter. *J. Phys. Chem. C* **2014**, *118*, 18453–18461.
- (180) Sadhu, S.; Patra, A. Composition Effects on Quantum Dot-Based Resonance Energy Transfer. *Appl. Phys. Lett.* **2008**, *93*, 183104.
- (181) Lightcap, I. V.; Kamat, P. V. Fortification of CdSe Quantum Dots with Graphene Oxide. Excited State Interactions and Light Energy Conversion. *J. Am. Chem. Soc.* **2012**, *134*, 7109–7116.
- (182) Haldar, K. K.; Sen, T.; Patra, A. Metal Conjugated Semiconductor Hybrid Nanoparticle-Based Fluorescence Resonance Energy Transfer. *J. Phys. Chem. C* **2010**, *114*, 4869–4874.
- (183) Lewis, N. S.; Nocera, D. G. Powering the Planet: Chemical Challenges in Solar Energy Utilization. *Proc. Natl. Acad. Sci. U. S. A.* **2006**, *103*, 15729–15735.
- (184) Kamat, P. V. Quantum Dot Solar Cells. Semiconductor Nanocrystals as Light Harvesters. *J. Phys. Chem. C* **2008**, *112*, 18737–18753.
- (185) Chen, G.; Seo, J.; Yang, C.; Prasad, P. N. Nanochemistry and Nanomaterials for Photovoltaics. *Chem. Soc. Rev.* **2013**, *42*, 8304–8338.
- (186) Etgar, L. Semiconductor Nanocrystals as Light Harvesters in Solar Cells. *Materials* **2013**, *6*, 445.
- (187) Kim, M. R.; Ma, D. Quantum-Dot-Based Solar Cells: Recent Advances, Strategies, and Challenges. *J. Phys. Chem. Lett.* **2015**, *6*, 85–99.
- (188) Nozik, A. J. Quantum Dot Solar Cells. *Phys. E* **2002**, *14*, 115–120.
- (189) Carey, G. H.; Abdelhady, A. L.; Ning, Z.; Thon, S. M.; Bakr, O. M.; Sargent, E. H. Colloidal Quantum Dot Solar Cells. *Chem. Rev.* **2015**, *115*, 12732–12763.
- (190) Kramer, I. J.; Sargent, E. H. The Architecture of Colloidal Quantum Dot Solar Cells: Materials to Devices. *Chem. Rev.* **2014**, *114*, 863–882.
- (191) Wang, X. Recent Progress in Colloidal Quantum Dot Photovoltaics. *Front. Optoelectron.* **2015**, *8*, 241–251.
- (192) Liu, Y.; Gibbs, M.; Puthussery, J.; Gaik, S.; Ihly, R.; Hillhouse, H. W.; Law, M. Dependence of Carrier Mobility on Nanocrystal Size and Ligand Length in PbSe Nanocrystal Solids. *Nano Lett.* **2010**, *10*, 1960–1969.
- (193) Kongkanand, A.; Tvrdy, K.; Takechi, K.; Kuno, M.; Kamat, P. V. Quantum Dot Solar Cells. Tuning Photoresponse through Size and Shape Control of CdSe–TiO₂ Architecture. *J. Am. Chem. Soc.* **2008**, *130*, 4007–4015.
- (194) Kang, M. S.; Sahu, A.; Norris, D. J.; Frisbie, C. D. Size-Dependent Electrical Transport in CdSe Nanocrystal Thin Films. *Nano Lett.* **2010**, *10*, 3727–3732.
- (195) Henry, C. H. Limiting Efficiencies of Ideal Single and Multiple Energy Gap Terrestrial Solar Cells. *J. Appl. Phys.* **1980**, *51*, 4494–4500.
- (196) Kramer, I. J.; Levina, L.; Debnath, R.; Zhitomirsky, D.; Sargent, E. H. Solar Cells Using Quantum Funnels. *Nano Lett.* **2011**, *11*, 3701–3706.
- (197) Wang, X.; Koleilat, G. I.; Tang, J.; Liu, H.; Kramer, I. J.; Debnath, R.; Brzozowski, L.; Barkhouse, D. A. R.; Levina, L.; Hoogland, S.; et al. Tandem Colloidal Quantum Dot Solar Cells Employing a Graded Recombination Layer. *Nat. Photonics* **2011**, *5*, 480–484.
- (198) Robel, I.; Kuno, M.; Kamat, P. V. Size-Dependent Electron Injection from Excited CdSe Quantum Dots into TiO₂ Nanoparticles. *J. Am. Chem. Soc.* **2007**, *129*, 4136–4137.
- (199) Smith, A. M.; Nie, S. Semiconductor Nanocrystals: Structure, Properties, and Band Gap Engineering. *Acc. Chem. Res.* **2010**, *43*, 190–200.
- (200) Peng, X. Band Gap and Composition Engineering on a Nanocrystal (BCEN) in Solution. *Acc. Chem. Res.* **2010**, *43*, 1387–1395.
- (201) Santra, P. K.; Kamat, P. V. Tandem-Layered Quantum Dot Solar Cells: Tuning the Photovoltaic Response with Luminescent Ternary Cadmium Chalcogenides. *J. Am. Chem. Soc.* **2013**, *135*, 877–885.
- (202) Bernard, J. E.; Zunger, A. Electronic Structure of ZnS, ZnSe, ZnTe, and Their Pseudobinary Alloys. *Phys. Rev. B: Condens. Matter Mater. Phys.* **1987**, *36*, 3199–3228.
- (203) Feng, Z. C.; Becla, P.; Kim, L. S.; Perkowitz, S.; Feng, Y. P.; Poon, H. C.; Williams, K. P.; Pitt, G. D. Raman, Infrared, Photoluminescence and Theoretical Studies of the II-VI-VI Ternary CdSeTe. *J. Cryst. Growth* **1994**, *138*, 239–243.
- (204) Shu, T.; Zhou, Z.; Wang, H.; Liu, G.; Xiang, P.; Rong, Y.; Han, H.; Zhao, Y. Efficient Quantum Dot-Sensitized Solar Cell with Tunable Energy Band CdSe_xS_(1-x) Quantum Dots. *J. Mater. Chem.* **2012**, *22*, 10525–10529.
- (205) Pan, Z.; Zhao, K.; Wang, J.; Zhang, H.; Feng, Y.; Zhong, X. Near Infrared Absorption of CdSe_xTe_{1-x} Alloyed Quantum Dot Sensitized Solar Cells with More Than 6% Efficiency and High Stability. *ACS Nano* **2013**, *7*, 5215–5222.
- (206) MacDonald, B. I.; Martucci, A.; Rubanov, S.; Watkins, S. E.; Mulvaney, P.; Jasieniak, J. J. Layer-by-Layer Assembly of Sintered CdSe_xTe_{1-x} Nanocrystal Solar Cells. *ACS Nano* **2012**, *6*, 5995–6004.
- (207) Zhao, H.; Fan, Z.; Liang, H.; Selopal, G. S.; Gonfa, B. A.; Jin, L.; Soudi, A.; Cui, D.; Enrichi, F.; Natile, M. M.; et al. Controlling Photoinduced Electron Transfer from PbS@CdS Core@Shell Quantum Dots to Metal Oxide Nanostructured Thin Films. *Nanoscale* **2014**, *6*, 7004–7011.
- (208) Han, S.; Pu, Y.-C.; Zheng, L.; Zhang, J. Z.; Fang, X. Shell-Thickness Dependent Electron Transfer and Relaxation in Type-II Core-Shell CdS/TiO₂ Structures with Optimized Photoelectrochemical Performance. *J. Mater. Chem. A* **2015**, *3*, 22627–22635.
- (209) Ning, Z.; Tian, H.; Yuan, C.; Fu, Y.; Qin, H.; Sun, L.; Agren, H. Solar Cells Sensitized with Type-II ZnSe-CdS Core/Shell Colloidal Quantum Dots. *Chem. Commun.* **2011**, *47*, 1536–1538.
- (210) Ning, Z.; Yuan, C.; Tian, H.; Fu, Y.; Li, L.; Sun, L.; Agren, H. Type-II Colloidal Quantum Dot Sensitized Solar Cells with a Thiourea Based Organic Redox Couple. *J. Mater. Chem.* **2012**, *22*, 6032–6037.
- (211) Zhang, Q.; Chen, G.; Yang, Y.; Shen, X.; Zhang, Y.; Li, C.; Yu, R.; Luo, Y.; Li, D.; Meng, Q. Toward Highly Efficient CdS/CdSe Quantum Dots-Sensitized Solar Cells Incorporating Ordered Photoanodes on Transparent Conductive Substrates. *Phys. Chem. Chem. Phys.* **2012**, *14*, 6479–6486.
- (212) Tian, J.; Zhang, Q.; Zhang, L.; Gao, R.; Shen, L.; Zhang, S.; Qu, X.; Cao, G. ZnO/TiO₂ Nanocable Structured Photoelectrodes for CdS/CdSe Quantum Dot Co-Sensitized Solar Cells. *Nanoscale* **2013**, *5*, 936–943.
- (213) Pan, Z.; Zhang, H.; Cheng, K.; Hou, Y.; Hua, J.; Zhong, X. Highly Efficient Inverted Type-I CdS/CdSe Core/Shell Structure QD-Sensitized Solar Cells. *ACS Nano* **2012**, *6*, 3982–3991.
- (214) Santra, P. K.; Kamat, P. V. Mn-Doped Quantum Dot Sensitized Solar Cells: A Strategy to Boost Efficiency over 5%. *J. Am. Chem. Soc.* **2012**, *134*, 2508–2511.
- (215) Sheng, P.; Li, W.; Cai, J.; Wang, X.; Tong, X.; Cai, Q.; Grimes, C. A. A Novel Method for the Preparation of a Photocorrosion Stable Core/Shell CdTe/CdS Quantum Dot TiO₂ Nanotube Array Photoelectrode Demonstrating an AM 1.5G Photoconversion Efficiency of 6.12%. *J. Mater. Chem. A* **2013**, *1*, 7806–7815.
- (216) Wang, J.; Mora-Seró, I.; Pan, Z.; Zhao, K.; Zhang, H.; Feng, Y.; Yang, G.; Zhong, X.; Bisquert, J. Core/Shell Colloidal Quantum Dot Exciplex States for the Development of Highly Efficient Quantum-Dot-Sensitized Solar Cells. *J. Am. Chem. Soc.* **2013**, *135*, 15913–15922.
- (217) McElroy, N.; Page, R. C.; Espinbarro-Valazquez, D.; Lewis, E.; Haigh, S.; O'Brien, P.; Binks, D. J. Comparison of Solar Cells

- Sensitised by CdTe/CdSe and CdSe/CdTe Core/Shell Colloidal Quantum Dots with and without a CdS Outer Layer. *Thin Solid Films* **2014**, *560*, 65–70.
- (218) Chuang, C.-H. M.; Brown, P. R.; Bulović, V.; Bawendi, M. G. Improved Performance and Stability in Quantum Dot Solar Cells through Band Alignment engineering. *Nat. Mater.* **2014**, *13*, 796–801.
- (219) Pan, Z.; Mora-Seró, I.; Shen, Q.; Zhang, H.; Li, Y.; Zhao, K.; Wang, J.; Zhong, X.; Bisquert, J. High-Efficiency “Green” Quantum Dot Solar Cells. *J. Am. Chem. Soc.* **2014**, *136*, 9203–9210.
- (220) Luo, J.; Wei, H.; Huang, Q.; Hu, X.; Zhao, H.; Yu, R.; Li, D.; Luo, Y.; Meng, Q. Highly Efficient Core-Shell CuInS₂-Mn Doped CdS Quantum Dot Sensitized Solar Cells. *Chem. Commun.* **2013**, *49*, 3881–3883.
- (221) Zhitomirsky, D.; Voznyy, O.; Levina, L.; Hoogland, S.; Kemp, K. W.; Ip, A. H.; Thon, S. M.; Sargent, E. H. Engineering Colloidal Quantum Dot Solids within and Beyond the Mobility-Invariant Regime. *Nat. Commun.* **2014**, *5*, 3803.
- (222) Akselrod, G. M.; Prins, F.; Poulikakos, L. V.; Lee, E. M. Y.; Weidman, M. C.; Mork, A. J.; Willard, A. P.; Bulović, V.; Tisdale, W. A. Subdiffusive Exciton Transport in Quantum Dot Solids. *Nano Lett.* **2014**, *14*, 3556–3562.
- (223) Chuang, C.-H. M.; Maurano, A.; Brandt, R. E.; Hwang, G. W.; Jean, J.; Buonassisi, T.; Bulović, V.; Bawendi, M. G. Open-Circuit Voltage Deficit, Radiative Sub-Bandgap States, and Prospects in Quantum Dot Solar Cells. *Nano Lett.* **2015**, *15*, 3286–3294.
- (224) Straus, D. B.; Goodwin, E. D.; Gaulding, E. A.; Muramoto, S.; Murray, C. B.; Kagan, C. R. Increased Carrier Mobility and Lifetime in CdSe Quantum Dot Thin Films through Surface Trap Passivation and Doping. *J. Phys. Chem. Lett.* **2015**, *6*, 4605–4609.
- (225) Ip, A. H.; Thon, S. M.; Hoogland, S.; Voznyy, O.; Zhitomirsky, D.; Debnath, R.; Levina, L.; Rollny, L. R.; Carey, G. H.; Fischer, A.; et al. Hybrid Passivated Colloidal Quantum Dot Solids. *Nat. Nanotechnol.* **2012**, *7*, 577–582.
- (226) Talapin, D. V.; Lee, J.-S.; Kovalenko, M. V.; Shevchenko, E. V. Prospects of Colloidal Nanocrystals for Electronic and Optoelectronic Applications. *Chem. Rev.* **2010**, *110*, 389–458.
- (227) Sambur, J. B.; Riha, S. C.; Choi, D.; Parkinson, B. A. Influence of Surface Chemistry on the Binding and Electronic Coupling of CdSe Quantum Dots to Single Crystal TiO₂ Surfaces. *Langmuir* **2010**, *26*, 4839–4847.
- (228) King, L. A.; Riley, D. J. Importance of QD Purification Procedure on Surface Adsorbance of QDs and Performance of QD Sensitized Photoanodes. *J. Phys. Chem. C* **2012**, *116*, 3349–3355.
- (229) Barkhouse, D. A. R.; Pattantyus-Abraham, A. G.; Levina, L.; Sargent, E. H. Thiols Passivate Recombination Centers in Colloidal Quantum Dots Leading to Enhanced Photovoltaic Device Efficiency. *ACS Nano* **2008**, *2*, 2356–2362.
- (230) Wuister, S. F.; de Mello Donegá, C.; Meijerink, A. Influence of Thiol Capping on the Exciton Luminescence and Decay Kinetics of CdTe and CdSe Quantum Dots. *J. Phys. Chem. B* **2004**, *108*, 17393–17397.
- (231) Jang, J.; Liu, W.; Son, J. S.; Talapin, D. V. Temperature-Dependent Hall and Field-Effect Mobility in Strongly Coupled All-Inorganic Nanocrystal Arrays. *Nano Lett.* **2014**, *14*, 653–662.
- (232) Lee, J.-S.; Kovalenko, M. V.; Huang, J.; Chung, D. S.; Talapin, D. V. Band-Like Transport, High Electron Mobility and High Photoconductivity in All-Inorganic Nanocrystal Arrays. *Nat. Nanotechnol.* **2011**, *6*, 348–352.
- (233) Liu, W.; Lee, J.-S.; Talapin, D. V. III–V Nanocrystals Capped with Molecular Metal Chalcogenide Ligands: High Electron Mobility and Ambipolar Photoresponse. *J. Am. Chem. Soc.* **2013**, *135*, 1349–1357.
- (234) Kovalenko, M. V.; Schaller, R. D.; Jarzab, D.; Loi, M. A.; Talapin, D. V. Inorganically Functionalized PbS–CdS Colloidal Nanocrystals: Integration into Amorphous Chalcogenide Glass and Luminescent Properties. *J. Am. Chem. Soc.* **2012**, *134*, 2457–2460.
- (235) Jiang, C.; Lee, J.-S.; Talapin, D. V. Soluble Precursors for CuInSe₂, CuIn_{1-x}Ga_xSe₂, and Cu₂ZnSn(S,Se)₄ Based on Colloidal Nanocrystals and Molecular Metal Chalcogenide Surface Ligands. *J. Am. Chem. Soc.* **2012**, *134*, 5010–5013.
- (236) Kovalenko, M. V.; Scheele, M.; Talapin, D. V. Colloidal Nanocrystals with Molecular Metal Chalcogenide Surface Ligands. *Science* **2009**, *324*, 1417–1420.
- (237) Tang, J.; Kemp, K. W.; Hoogland, S.; Jeong, K. S.; Liu, H.; Levina, L.; Furukawa, M.; Wang, X.; Debnath, R.; Cha, D.; et al. Colloidal-Quantum-Dot Photovoltaics Using Atomic-Ligand Passivation. *Nat. Mater.* **2011**, *10*, 765–771.
- (238) Žídek, K.; Abdellah, M.; Zheng, K.; Pullerits, T. Electron Relaxation in the CdSe Quantum Dot-ZnO Composite: Prospects for Photovoltaic Applications. *Sci. Rep.* **2014**, *4*, 7244.
- (239) Kholmicheva, N.; Moroz, P.; Rijal, U.; Bastola, E.; Uprety, P.; Liyanage, G.; Razgoniaev, A.; Ostrowski, A. D.; Zamkov, M. Plasmonic Nanocrystal Solar Cells Utilizing Strongly Confined Radiation. *ACS Nano* **2014**, *8*, 12549–12559.
- (240) Fujishima, A.; Honda, K. Electrochemical Photolysis of Water at a Semiconductor Electrode. *Nature* **1972**, *238*, 37–38.
- (241) Tong, H.; Ouyang, S.; Bi, Y.; Umezawa, N.; Oshikiri, M.; Ye, J. Nano-Photocatalytic Materials: Possibilities and Challenges. *Adv. Mater.* **2012**, *24*, 229–251.
- (242) Djurisic, A. B.; Leung, Y. H.; Ching Ng, A. M. Strategies for Improving the Efficiency of Semiconductor Metal Oxide Photocatalysis. *Mater. Horiz.* **2014**, *1*, 400–410.
- (243) Fresno, F.; Portela, R.; Suarez, S.; Coronado, J. M. Photocatalytic Materials: Recent Achievements and near Future Trends. *J. Mater. Chem. A* **2014**, *2*, 2863–2884.
- (244) Vaneski, A.; Schneider, J.; Susha, A. S.; Rogach, A. L. Colloidal Hybrid Heterostructures Based on II–VI Semiconductor Nanocrystals for Photocatalytic Hydrogen Generation. *J. Photochem. Photobiol., C* **2014**, *19*, 52–61.
- (245) Haldar, K. K.; Sinha, G.; Lahtinen, J.; Patra, A. Hybrid Colloidal Au-CdSe Pentapod Heterostructures Synthesis and Their Photocatalytic Properties. *ACS Appl. Mater. Interfaces* **2012**, *4*, 6266–6272.
- (246) Khanchandani, S.; Kundu, S.; Patra, A.; Ganguli, A. K. Band Gap Tuning of ZnO/In₂S₃ Core/Shell Nanorod Arrays for Enhanced Visible-Light-Driven Photocatalysis. *J. Phys. Chem. C* **2013**, *117*, 5558–5567.
- (247) Khanchandani, S.; Kundu, S.; Patra, A.; Ganguli, A. K. Shell Thickness Dependent Photocatalytic Properties of ZnO/CdS Core–Shell Nanorods. *J. Phys. Chem. C* **2012**, *116*, 23653–23662.
- (248) Xu, Y.-S.; Zhang, W.-D. Ag/AgBr-Grafted Graphite-Like Carbon Nitride with Enhanced Plasmonic Photocatalytic Activity under Visible Light. *ChemCatChem* **2013**, *5*, 2343–2351.
- (249) Hou, W.; Cronin, S. B. A Review of Surface Plasmon Resonance-Enhanced Photocatalysis. *Adv. Funct. Mater.* **2013**, *23*, 1612–1619.
- (250) Abe, R. Recent Progress on Photocatalytic and Photoelectrochemical Water Splitting under Visible Light Irradiation. *J. Photochem. Photobiol., C* **2010**, *11*, 179–209.
- (251) Zhou, H.; Qu, Y.; Zeid, T.; Duan, X. Towards Highly Efficient Photocatalysts Using Semiconductor Nanoarchitectures. *Energy Environ. Sci.* **2012**, *5*, 6732–6743.
- (252) Tang, J.; Durrant, J. R.; Klug, D. R. Mechanism of Photocatalytic Water Splitting in TiO₂: Reaction of Water with Photoholes, Importance of Charge Carrier Dynamics, and Evidence for Four-Hole Chemistry. *J. Am. Chem. Soc.* **2008**, *130*, 13885–13891.
- (253) Hashimoto, K.; Irie, H.; Fujishima, A. TiO₂ Photocatalysis: A Historical Overview and Future Prospects. *Jpn. J. Appl. Phys.* **2005**, *44*, 8269.
- (254) Kudo, A.; Miseki, Y. Heterogeneous Photocatalyst Materials for Water Splitting. *Chem. Soc. Rev.* **2009**, *38*, 253–278.
- (255) Maitra, U.; Lingampalli, S.; Rao, C. Artificial Photosynthesis and the Splitting of Water To Generate Hydrogen. *Curr. Sci.* **2014**, *106*, 518–527.
- (256) Girginer, B.; Galli, G.; Chiellini, E.; Bicak, N. Preparation of Stable CdS Nanoparticles in Aqueous Medium and Their Hydrogen

- Generation Efficiencies in Photolysis of Water. *Int. J. Hydrogen Energy* **2009**, *34*, 1176–1184.
- (257) Andrew Frame, F.; Carroll, E. C.; Larsen, D. S.; Sarahan, M.; Browning, N. D.; Osterloh, F. E. First Demonstration of CdSe as a Photocatalyst for Hydrogen Evolution from Water under UV and Visible Light. *Chem. Commun.* **2008**, 2206–2208.
- (258) Holmes, M. A.; Townsend, T. K.; Osterloh, F. E. Quantum Confinement Controlled Photocatalytic Water Splitting by Suspended CdSe Nanocrystals. *Chem. Commun.* **2012**, *48*, 371–373.
- (259) Wang, X.; Liu, G.; Lu, G. Q.; Cheng, H.-M. Stable Photocatalytic Hydrogen Evolution from Water over ZnO–CdS Core–Shell Nanorods. *Int. J. Hydrogen Energy* **2010**, *35*, 8199–8205.
- (260) Shemesh, Y.; Macdonald, J. E.; Menagen, G.; Banin, U. Synthesis and Photocatalytic Properties of a Family of CdS–PdX Hybrid Nanoparticles. *Angew. Chem., Int. Ed.* **2011**, *50*, 1185–1189.
- (261) Frame, F. A.; Osterloh, F. E. CdSe–MoS₂: A Quantum Size-Confined Photocatalyst for Hydrogen Evolution from Water under Visible Light. *J. Phys. Chem. C* **2010**, *114*, 10628–10633.
- (262) Lingampalli, S. R.; Gautam, U. K.; Rao, C. N. R. Highly Efficient Photocatalytic Hydrogen Generation by Solution-Processed ZnO/Pt/CdS, ZnO/Pt/Cd_{1-x}Zn_xS and ZnO/Pt/Cd_{1-x}Se_x Hybrid Nanostructures. *Energy Environ. Sci.* **2013**, *6*, 3589–3594.
- (263) Gupta, U.; Rao, B. G.; Maitra, U.; Prasad, B. E.; Rao, C. N. R. Visible-Light-Induced Generation of H₂ by Nanocomposites of Few-Layer TiS₂ and TaS₂ with CdS Nanoparticles. *Chem. - Asian J.* **2014**, *9*, 1311–1315.
- (264) Lingampalli, S. R.; Roy, A.; Ikram, M.; Rao, C. N. R. Visible-Light Induced Hydrogen Generation with ZnO/NiO/Cd_{1-x}Zn_xS (X = 0, 0.2) Heterostructures. *Chem. Phys. Lett.* **2014**, *610–611*, 316–320.
- (265) Jagadeeswararao, M.; Dey, S.; Nag, A.; Rao, C. N. R. Visible Light-Induced Hydrogen Generation Using Colloidal (ZnS)_{0.4}(AgInS₂)_{0.6} Nanocrystals Capped by S²⁻ Ions. *J. Mater. Chem. A* **2015**, *3*, 8276–8279.
- (266) Mangrulkar, P. A.; Polshettiwar, V.; Labhsetwar, N. K.; Varma, R. S.; Rayalu, S. S. Nano-Ferrites for Water Splitting: Unprecedented High Photocatalytic Hydrogen Production under Visible Light. *Nanoscale* **2012**, *4*, 5202–5209.
- (267) Mangrulkar, P. A.; Joshi, M. M.; Tijare, S. N.; Polshettiwar, V.; Labhsetwar, N. K.; Rayalu, S. S. Nano Cobalt Oxides for Photocatalytic Hydrogen Production. *Int. J. Hydrogen Energy* **2012**, *37*, 10462–10466.
- (268) Zong, X.; Na, Y.; Wen, F.; Ma, G.; Yang, J.; Wang, D.; Ma, Y.; Wang, M.; Sun, L.; Li, C. Visible Light Driven H₂ Production in Molecular Systems Employing Colloidal MoS₂ Nanoparticles as Catalyst. *Chem. Commun.* **2009**, 4536–4538.
- (269) Xiang, Q.; Yu, J.; Jaroniec, M. Synergetic Effect of MoS₂ and Graphene as Cocatalysts for Enhanced Photocatalytic H₂ Production Activity of TiO₂ Nanoparticles. *J. Am. Chem. Soc.* **2012**, *134*, 6575–6578.
- (270) Zong, X.; Yan, H.; Wu, G.; Ma, G.; Wen, F.; Wang, L.; Li, C. Enhancement of Photocatalytic H₂ Evolution on CdS by Loading MoS₂ as Cocatalyst under Visible Light Irradiation. *J. Am. Chem. Soc.* **2008**, *130*, 7176–7177.
- (271) Yang, J.; Shin, H. S. Recent Advances in Layered Transition Metal Dichalcogenides for Hydrogen Evolution Reaction. *J. Mater. Chem. A* **2014**, *2*, 5979–5985.
- (272) Jiang, H. Electronic Band Structures of Molybdenum and Tungsten Dichalcogenides by the GW Approach. *J. Phys. Chem. C* **2012**, *116*, 7664–7671.
- (273) Kang, J.; Tongay, S.; Zhou, J.; Li, J.; Wu, J. Band Offsets and Heterostructures of Two-Dimensional Semiconductors. *Appl. Phys. Lett.* **2013**, *102*, 012111.
- (274) Lukowski, M. A.; Daniel, A. S.; English, C. R.; Meng, F.; Forticaux, A.; Hamers, R. J.; Jin, S. Highly Active Hydrogen Evolution Catalysis from Metallic WS₂ Nanosheets. *Energy Environ. Sci.* **2014**, *7*, 2608–2613.
- (275) Kibsgaard, J.; Chen, Z.; Reinecke, B. N.; Jaramillo, T. F. Engineering the Surface Structure of MoS₂ To preferentially Expose Active Edge Sites For electrocatalysis. *Nat. Mater.* **2012**, *11*, 963–969.
- (276) Ataca, C.; Ciraci, S. Dissociation of H₂O at the Vacancies of Single-Layer MoS₂. *Phys. Rev. B: Condens. Matter Mater. Phys.* **2012**, *85*, 195410.
- (277) Maitra, U.; Gupta, U.; De, M.; Datta, R.; Govindaraj, A.; Rao, C. N. R. Highly Effective Visible-Light-Induced H₂ Generation by Single-Layer 1T-MoS₂ and a Nanocomposite of Few-Layer 2H-MoS₂ with Heavily Nitrogenated Graphene. *Angew. Chem., Int. Ed.* **2013**, *52*, 13057–13061.
- (278) Gupta, U.; Naidu, B. S.; Maitra, U.; Singh, A.; Shirodkar, S. N.; Waghmare, U. V.; Rao, C. N. R. Characterization of Few-Layer 1T-MoSe₂ and Its Superior Performance in the Visible-Light Induced Hydrogen Evolution Reaction. *APL Mater.* **2014**, *2*, 092802.
- (279) Zong, X.; Wu, G.; Yan, H.; Ma, G.; Shi, J.; Wen, F.; Wang, L.; Li, C. Photocatalytic H₂ Evolution on MoS₂/CdS Catalysts under Visible Light Irradiation. *J. Phys. Chem. C* **2010**, *114*, 1963–1968.
- (280) Zhou, W.; Yin, Z.; Du, Y.; Huang, X.; Zeng, Z.; Fan, Z.; Liu, H.; Wang, J.; Zhang, H. Synthesis of Few-Layer MoS₂ Nanosheet-Coated TiO₂ Nanobelt Heterostructures for Enhanced Photocatalytic Activities. *Small* **2013**, *9*, 140–147.
- (281) Min, S.; Lu, G. Sites for High Efficient Photocatalytic Hydrogen Evolution on a Limited-Layered MoS₂ Cocatalyst Confined on Graphene Sheets—the Role of Graphene. *J. Phys. Chem. C* **2012**, *116*, 25415–25424.
- (282) Fan, W.; Lai, Q.; Zhang, Q.; Wang, Y. Nanocomposites of TiO₂ and Reduced Graphene Oxide as Efficient Photocatalysts for Hydrogen Evolution. *J. Phys. Chem. C* **2011**, *115*, 10694–10701.
- (283) Zhang, X.-Y.; Li, H.-P.; Cui, X.-L.; Lin, Y. Graphene/TiO₂ Nanocomposites: Synthesis, Characterization and Application in Hydrogen Evolution from Water Photocatalytic Splitting. *J. Mater. Chem.* **2010**, *20*, 2801–2806.
- (284) Kim, H.-i.; Moon, G.-h.; Monllor-Satoca, D.; Park, Y.; Choi, W. Solar Photoconversion Using Graphene/TiO₂ Composites: Nanographene Shell on TiO₂ Core Versus TiO₂ Nanoparticles on Graphene Sheet. *J. Phys. Chem. C* **2012**, *116*, 1535–1543.
- (285) Xiang, Q.; Yu, J.; Jaroniec, M. Enhanced Photocatalytic H₂-Production Activity of Graphene-Modified Titania Nanosheets. *Nanoscale* **2011**, *3*, 3670–3678.
- (286) Li, Q.; Guo, B.; Yu, J.; Ran, J.; Zhang, B.; Yan, H.; Gong, J. R. Highly Efficient Visible-Light-Driven Photocatalytic Hydrogen Production of CdS-Cluster-Decorated Graphene Nanosheets. *J. Am. Chem. Soc.* **2011**, *133*, 10878–10884.
- (287) Peng, T.; Li, K.; Zeng, P.; Zhang, Q.; Zhang, X. Enhanced Photocatalytic Hydrogen Production over Graphene Oxide–Cadmium Sulfide Nanocomposite under Visible Light Irradiation. *J. Phys. Chem. C* **2012**, *116*, 22720–22726.
- (288) Lv, X.-J.; Fu, W.-F.; Chang, H.-X.; Zhang, H.; Cheng, J.-S.; Zhang, G.-J.; Song, Y.; Hu, C.-Y.; Li, J.-H. Hydrogen Evolution from Water Using Semiconductor Nanoparticle/Graphene Composite Photocatalysts without Noble Metals. *J. Mater. Chem.* **2012**, *22*, 1539–1546.
- (289) Bera, R.; Kundu, S.; Patra, A. 2D Hybrid Nanostructure of Reduced Graphene Oxide–CdS Nanosheet for Enhanced Photocatalysis. *ACS Appl. Mater. Interfaces* **2015**, *7*, 13251–13259.
- (290) Xie, G.; Zhang, K.; Guo, B.; Liu, Q.; Fang, L.; Gong, J. R. Graphene-Based Materials for Hydrogen Generation from Light-Driven Water Splitting. *Adv. Mater.* **2013**, *25*, 3820–3839.
- (291) Yeh, T.-F.; Cihlář, J.; Chang, C.-Y.; Cheng, C.; Teng, H. Roles of Graphene Oxide in Photocatalytic Water Splitting. *Mater. Today* **2013**, *16*, 78–84.
- (292) Bao, N.; Shen, L.; Takata, T.; Domen, K. Self-Templated Synthesis of Nanoporous CdS Nanostructures for Highly Efficient Photocatalytic Hydrogen Production under Visible Light. *Chem. Mater.* **2008**, *20*, 110–117.
- (293) Wu, K.; Zhu, H.; Lian, T. Ultrafast Exciton Dynamics and Light-Driven H₂ Evolution in Colloidal Semiconductor Nanorods and Pt-Tipped Nanorods. *Acc. Chem. Res.* **2015**, *48*, 851–859.
- (294) Amirav, L.; Alivisatos, A. P. Photocatalytic Hydrogen Production with Tunable Nanorod Heterostructures. *J. Phys. Chem. Lett.* **2010**, *1*, 1051–1054.

- (295) Amirav, L.; Alivisatos, A. P. Luminescence Studies of Individual Quantum Dot Photocatalysts. *J. Am. Chem. Soc.* **2013**, *135*, 13049–13053.
- (296) Nakibli, Y.; Kalisman, P.; Amirav, L. Less Is More: The Case of Metal Cocatalysts. *J. Phys. Chem. Lett.* **2015**, *6*, 2265–2268.
- (297) Aronovitch, E.; Kalisman, P.; Mangel, S.; Houben, L.; Amirav, L.; Bar-Sadan, M. Designing Bimetallic Co-Catalysts: A Party of Two. *J. Phys. Chem. Lett.* **2015**, *6*, 3760–3764.
- (298) Kalisman, P.; Nakibli, Y.; Amirav, L. Perfect Photon-to-Hydrogen Conversion Efficiency. *Nano Lett.* **2016**, *16*, 1776–1781.
- (299) Brown, K. A.; Dayal, S.; Ai, X.; Rumbles, G.; King, P. W. Controlled Assembly of Hydrogenase-CdTe Nanocrystal Hybrids for Solar Hydrogen Production. *J. Am. Chem. Soc.* **2010**, *132*, 9672–9680.
- (300) Wang, F.; Wang, W.-G.; Wang, X.-J.; Wang, H.-Y.; Tung, C.-H.; Wu, L.-Z. A Highly Efficient Photocatalytic System for Hydrogen Production by a Robust Hydrogenase Mimic in an Aqueous Solution. *Angew. Chem., Int. Ed.* **2011**, *50*, 3193–3197.
- (301) Greene, B. L.; Joseph, C. A.; Maroney, M. J.; Dyer, R. B. Direct Evidence of Active-Site Reduction and Photodriven Catalysis in Sensitized Hydrogenase Assemblies. *J. Am. Chem. Soc.* **2012**, *134*, 11108–11111.
- (302) Brown, K. A.; Wilker, M. B.; Boehm, M.; Dukovic, G.; King, P. W. Characterization of Photochemical Processes for H₂ Production by CdS Nanorod-[FeFe] Hydrogenase Complexes. *J. Am. Chem. Soc.* **2012**, *134*, 5627–5636.
- (303) Najafpour, M. M.; Govindjee. Govindjee Oxygen Evolving Complex in Photosystem II: Better Than Excellent. *Dalton Trans.* **2011**, *40*, 9076–9084.
- (304) Najafpour, M. M.; Ghobadi, M. Z.; Haghghi, B.; Eaton-Rye, J. J.; Tomo, T.; Shen, J. R.; Allakhverdiev, S. I. Nano-Sized Manganese-Calcium Cluster in Photosystem II. *Biochemistry* **2014**, *79*, 324–336.
- (305) Maitra, U.; Naidu, B. S.; Govindaraj, A.; Rao, C. N. R. Importance of Trivalency and the eg¹ Configuration in the Photocatalytic Oxidation of Water by Mn and Co Oxides. *Proc. Natl. Acad. Sci. U. S. A.* **2013**, *110*, 11704–11707.
- (306) Robinson, D. M.; Go, Y. B.; Mui, M.; Gardner, G.; Zhang, Z.; Mastrogiovanni, D.; Garfunkel, E.; Li, J.; Greenblatt, M.; Dismukes, G. C. Photochemical Water Oxidation by Crystalline Polymorphs of Manganese Oxides: Structural Requirements for Catalysis. *J. Am. Chem. Soc.* **2013**, *135*, 3494–3501.
- (307) Haberreutinger, S. N.; Schmidt-Mende, L.; Stolarsky, J. K. Photocatalytic Reduction of CO₂ on TiO₂ and other Semiconductors. *Angew. Chem., Int. Ed.* **2013**, *52*, 7372–7408.
- (308) Li, K.; An, X.; Park, K. H.; Khraisheh, M.; Tang, J. A Critical Review of CO₂ Photoconversion: Catalysts and Reactors. *Catal. Today* **2014**, *224*, 3–12.
- (309) Handoko, A. D.; Li, K.; Tang, J. Recent Progress in Artificial Photosynthesis: CO₂ Photoreduction to Valuable Chemicals in a Heterogeneous System. *Curr. Opin. Chem. Eng.* **2013**, *2*, 200–206.
- (310) Wang, C.; Thompson, R. L.; Baltrus, J.; Matranga, C. Visible Light Photoreduction of CO₂ Using CdSe/Pt/TiO₂ Heterostructured Catalysts. *J. Phys. Chem. Lett.* **2010**, *1*, 48–53.
- (311) Wang, C.; Thompson, R. L.; Ohodnicki, P.; Baltrus, J.; Matranga, C. Size-Dependent Photocatalytic Reduction of CO₂ with PbS Quantum Dot Sensitized TiO₂ Heterostructured Photocatalysts. *J. Mater. Chem.* **2011**, *21*, 13452–13457.
- (312) Li, X.; Liu, H.; Luo, D.; Li, J.; Huang, Y.; Li, H.; Fang, Y.; Xu, Y.; Zhu, L. Adsorption of CO₂ on Heterostructure CdS(Bi₂S₃)/TiO₂ Nanotube Photocatalysts and Their Photocatalytic Activities in the Reduction of CO₂ to Methanol under Visible Light Irradiation. *Chem. Eng. J.* **2012**, *180*, 151–158.
- (313) Hou, W.; Hung, W. H.; Pavaskar, P.; Goeppert, A.; Aykol, M.; Cronin, S. B. Photocatalytic Conversion of CO₂ to Hydrocarbon Fuels Via Plasmon-Enhanced Absorption and Metallic Interband Transitions. *ACS Catal.* **2011**, *1*, 929–936.
- (314) Fujiwara, H.; Hosokawa, H.; Murakoshi, K.; Wada, Y.; Yanagida, S.; Okada, T.; Kobayashi, H. Effect of Surface Structures on Photocatalytic CO₂ Reduction Using Quantized Cds Nanocrystallites. *J. Phys. Chem. B* **1997**, *101*, 8270–8278.
- (315) Yan, J.; Wu, G.; Dai, W.; Guan, N.; Li, L. Synthetic Design of Gold Nanoparticles on Anatase TiO₂ {001} for Enhanced Visible Light Harvesting. *ACS Sustainable Chem. Eng.* **2014**, *2*, 1940–1946.
- (316) Alvaro, M.; Aprile, C.; Ferrer, B.; Sastre, F.; Garcia, H. Photochemistry of Gold Nanoparticles Functionalized with an Iron(II) Terpyridine Complex. An Integrated Visible Light Photocatalyst for Hydrogen Generation. *Dalton Trans.* **2009**, 7437–7444.
- (317) Sheikh, A.; Yengantiwar, A.; Deo, M.; Kelkar, S.; Ogale, S. Near-Field Plasmonic Functionalization of Light Harvesting Oxide–Oxide Heterojunctions for Efficient Solar Photoelectrochemical Water Splitting: The AuNP/ZnFe₂O₄/ZnO System. *Small* **2013**, *9*, 2091–2096.
- (318) Andreussi, O.; Caprasecca, S.; Cupellini, L.; Guarnetti-Prandi, I.; Guido, C. A.; Jurinovich, S.; Viani, L.; Mennucci, B. Plasmon Enhanced Light Harvesting: Multiscale Modeling of the Fmo Protein Coupled with Gold Nanoparticles. *J. Phys. Chem. A* **2015**, *119*, 5197–5206.
- (319) Beyer, S. R.; Ullrich, S.; Kudera, S.; Gardiner, A. T.; Cogdell, R. J.; Köhler, J. Hybrid Nanostructures for Enhanced Light-Harvesting: Plasmon Induced Increase in Fluorescence from Individual Photosynthetic Pigment–Protein Complexes. *Nano Lett.* **2011**, *11*, 4897–4901.
- (320) Bujak, Ł.; Czechowski, N.; Piatkowski, D.; Litvin, R.; Mackowski, S.; Brotosudarmo, T. H. P.; Cogdell, R. J.; Pichler, S.; Heiss, W. Fluorescence Enhancement of Light-Harvesting Complex 2 from Purple Bacteria Coupled to Spherical Gold Nanoparticles. *Appl. Phys. Lett.* **2011**, *99*, 173701.
- (321) Bujak, Ł.; Brotosudarmo, T.; Czechowski, N.; Olejnik, M.; Ciszak, K.; Litvin, R.; Cogdell, R.; Heiss, W.; Mackowski, S. Spectral Dependence of Fluorescence Enhancement in LH2-Au Nanoparticle Hybrid Nanostructures. *Acta Phys. Pol. A* **2012**, *122*, 252.
- (322) Olejnik, M.; Krajnik, B.; Kowalska, D.; Lin, G.; Mackowski, S. Spectroscopic Studies of Plasmon Coupling between Photosynthetic Complexes and Metallic Quantum Dots. *J. Phys.: Condens. Matter* **2013**, *25*, 194103.
- (323) Kim, I.; Bender, S. L.; Hranisavljevic, J.; Utschig, L. M.; Huang, L.; Wiederrecht, G. P.; Tiede, D. M. Metal Nanoparticle Plasmon-Enhanced Light-Harvesting in a Photosystem I Thin Film. *Nano Lett.* **2011**, *11*, 3091–3098.
- (324) Kim, S.-S.; Na, S.-I.; Jo, J.; Kim, D.-Y.; Nah, Y.-C. Plasmon Enhanced Performance of Organic Solar Cells Using Electrodeposited Ag Nanoparticles. *Appl. Phys. Lett.* **2008**, *93*, 073307.
- (325) Hyun, J. K.; Lauhon, L. J. Spatially Resolved Plasmonically Enhanced Photocurrent from Au Nanoparticles on a Si Nanowire. *Nano Lett.* **2011**, *11*, 2731–2734.
- (326) Zhang, W.; Saliba, M.; Stranks, S. D.; Sun, Y.; Shi, X.; Wiesner, U.; Snaith, H. J. Enhancement of Perovskite-Based Solar Cells Employing Core–Shell Metal Nanoparticles. *Nano Lett.* **2013**, *13*, 4505–4510.
- (327) Gangishetty, M. K.; Lee, K. E.; Scott, R. W. J.; Kelly, T. L. Plasmonic Enhancement of Dye Sensitized Solar Cells in the Red-to-near-Infrared Region Using Triangular Core–Shell Ag@SiO₂ Nanoparticles. *ACS Appl. Mater. Interfaces* **2013**, *5*, 11044–11051.
- (328) Brown, M. D.; Suteewong, T.; Kumar, R. S. S.; D’Innocenzo, V.; Petrozza, A.; Lee, M. M.; Wiesner, U.; Snaith, H. J. Plasmonic Dye-Sensitized Solar Cells Using Core–Shell Metal–Insulator Nanoparticles. *Nano Lett.* **2011**, *11*, 438–445.
- (329) Qi, J.; Dang, X.; Hammond, P. T.; Belcher, A. M. Highly Efficient Plasmon-Enhanced Dye-Sensitized Solar Cells through Metal@Oxide Core–Shell Nanostructure. *ACS Nano* **2011**, *5*, 7108–7116.
- (330) Yen, Y.-C.; Chen, P.-H.; Chen, J.-Z.; Chen, J.-A.; Lin, K.-J. Plasmon-Induced Efficiency Enhancement on Dye-Sensitized Solar Cell by a 3D TNW-AuNP Layer. *ACS Appl. Mater. Interfaces* **2015**, *7*, 1892–1898.
- (331) Standridge, S. D.; Schatz, G. C.; Hupp, J. T. Distance Dependence of Plasmon-Enhanced Photocurrent in Dye-Sensitized Solar Cells. *J. Am. Chem. Soc.* **2009**, *131*, 8407–8409.

- (332) Chang, S.; Li, Q.; Xiao, X.; Wong, K. Y.; Chen, T. Enhancement of Low Energy Sunlight Harvesting in Dye-Sensitized Solar Cells Using Plasmonic Gold Nanorods. *Energy Environ. Sci.* **2012**, *S*, 9444–9448.
- (333) Jeong, N. C.; Prasittichai, C.; Hupp, J. T. Photocurrent Enhancement by Surface Plasmon Resonance of Silver Nanoparticles in Highly Porous Dye-Sensitized Solar Cells. *Langmuir* **2011**, *27*, 14609–14614.
- (334) Ding, I. K.; Zhu, J.; Cai, W.; Moon, S.-J.; Cai, N.; Wang, P.; Zakeeruddin, S. M.; Grätzel, M.; Brongersma, M. L.; Cui, Y.; et al. Plasmonic Dye-Sensitized Solar Cells. *Adv. Energy Mater.* **2011**, *1*, 52–57.
- (335) Li, H.; Hu, X.; Hong, W.; Cai, F.; Tang, Q.; Zhao, B.; Zhang, D.; Cheng, P. Photonic Crystal Coupled Plasmonic Nanoparticle Array for Resonant Enhancement of Light Harvesting and Power Conversion. *Phys. Chem. Chem. Phys.* **2012**, *14*, 14334–14339.
- (336) Naphade, R. A.; Tathavadekar, M.; Jog, J. P.; Agarkar, S.; Ogale, S. Plasmonic Light Harvesting of Dye Sensitized Solar Cells by Au-Nanoparticle Loaded TiO₂ Nanofibers. *J. Mater. Chem. A* **2014**, *2*, 975–984.
- (337) Dong, H.; Wu, Z.; El-Shafei, A.; Xia, B.; Xi, J.; Ning, S.; Jiao, B.; Hou, X. Ag-Encapsulated Au Plasmonic Nanorods for Enhanced Dye-Sensitized Solar Cell Performance. *J. Mater. Chem. A* **2015**, *3*, 4659–4668.
- (338) Bai, Y.; Butburee, T.; Yu, H.; Li, Z.; Amal, R.; Lu, G. Q. M.; Wang, L. Controllable Synthesis of Concave Cubic Gold Core–Shell Nanoparticles for Plasmon-Enhanced Photon Harvesting. *J. Colloid Interface Sci.* **2015**, *449*, 246–251.
- (339) Yun, J.; Hwang, S. H.; Jang, J. Fabrication of Au@Ag Core/Shell Nanoparticles Decorated TiO₂ Hollow Structure for Efficient Light-Harvesting in Dye-Sensitized Solar Cells. *ACS Appl. Mater. Interfaces* **2015**, *7*, 2055–2063.
- (340) Wang, F.; Li, C.; Chen, H.; Jiang, R.; Sun, L.-D.; Li, Q.; Wang, J.; Yu, J. C.; Yan, C.-H. Plasmonic Harvesting of Light Energy for Suzuki Coupling Reactions. *J. Am. Chem. Soc.* **2013**, *135*, 5588–5601.
- (341) Yang, T.-H.; Huang, L.-D.; Pan, M.-Y.; Harn, Y.-W.; Chen, M.-C.; Lin, C.-C.; Wei, P.-K.; Wu, J.-M. Ultrahigh-Density Plasmonic-Nanoparticle-Sensitized Semiconductor Photocatalysts Profit from Cooperative Light Harvesting and Charge Separation Processes: Experiments, Simulations, and Multifunctional Plasmonics. *Part. Part. Syst. Char.* **2014**, *31*, 895–907.
- (342) Zhang, X.; Ke, X.; Du, A.; Zhu, H. Plasmonic Nanostructures to Enhance Catalytic Performance of Zeolites under Visible Light. *Sci. Rep.* **2014**, *4*, 3805.
- (343) Shakir, I.; Ali, Z.; Kang, D. J. Layer by Layer Assembly of Gold Nanoparticles and Graphene Via Langmuir Blodgett Method for Efficient Light-Harvesting in Photocatalytic Applications. *J. Alloys Compd.* **2014**, *617*, 707–712.
- (344) Zhou, N.; Lopez-Puente, V.; Wang, Q.; Polavarapu, L.; Pastoriza-Santos, I.; Xu, Q.-H. Plasmon-Enhanced Light Harvesting: Applications in Enhanced Photocatalysis, Photodynamic Therapy and Photovoltaics. *RSC Adv.* **2015**, *5*, 29076–29097.
- (345) Wang, C.; Astruc, D. Nanogold Plasmonic Photocatalysis for Organic Synthesis and Clean Energy Conversion. *Chem. Soc. Rev.* **2014**, *43*, 7188–7216.
- (346) Lakowicz, J. R. Radiative Decay Engineering 5: Metal-Enhanced Fluorescence and Plasmon Emission. *Anal. Biochem.* **2005**, *337*, 171–194.
- (347) Demchenko, A. P. Nanoparticles and Nanocomposites for Fluorescence Sensing and Imaging. *Methods Appl. Fluoresc.* **2013**, *1*, 022001.
- (348) Malicka, J.; Gryczynski, I.; Gryczynski, Z.; Lakowicz, J. R. Effects of Fluorophore-to-Silver Distance on the Emission of Cyanine–Dye-Labeled Oligonucleotides. *Anal. Biochem.* **2003**, *315*, 57–66.
- (349) Tovmachenko, O. G.; Graf, C.; van den Heuvel, D. J.; van Blaaderen, A.; Gerritsen, H. C. Fluorescence Enhancement by Metal-Core/Silica-Shell Nanoparticles. *Adv. Mater.* **2006**, *18*, 91–95.
- (350) Lee, S. Y.; Nakaya, K.; Hayashi, T.; Hara, M. Quantitative Study of the Gold-Enhanced Fluorescence of CdSe/ZnS Nanocrystals as a Function of Distance Using an AFM Probe. *Phys. Chem. Chem. Phys.* **2009**, *11*, 4403–4409.
- (351) Jennings, T. L.; Singh, M. P.; Strouse, G. F. Fluorescent Lifetime Quenching near D = 1.5 nm Gold Nanoparticles: Probing NSET Validity. *J. Am. Chem. Soc.* **2006**, *128*, 5462–5467.
- (352) Gersten, J.; Nitzan, A. Spectroscopic Properties of Molecules Interacting with Small Dielectric Particles. *J. Chem. Phys.* **1981**, *75*, 1139–1152.
- (353) Bhowmick, S.; Saini, S.; Shenoy, V. B.; Bagchi, B. Resonance Energy Transfer from a Fluorescent Dye to a Metal Nanoparticle. *J. Chem. Phys.* **2006**, *125*, 181102.
- (354) Saini, S.; Srinivas, G.; Bagchi, B. Distance and Orientation Dependence of Excitation Energy Transfer: From Molecular Systems to Metal Nanoparticles. *J. Phys. Chem. B* **2009**, *113*, 1817–1832.
- (355) Swathi, R. S.; Sebastian, K. L. Resonance Energy Transfer from a Fluorescent Dye Molecule to Plasmon and Electron-Hole Excitations of a Metal Nanoparticle. *J. Chem. Phys.* **2007**, *126*, 234701.
- (356) Sen, T.; Sadhu, S.; Patra, A. Surface Energy Transfer from Rhodamine 6G to Gold Nanoparticles: A Spectroscopic Ruler. *Appl. Phys. Lett.* **2007**, *91*, 043104.
- (357) Yun, C. S.; Javier, A.; Jennings, T.; Fisher, M.; Hira, S.; Peterson, S.; Hopkins, B.; Reich, N. O.; Strouse, G. F. Nanometal Surface Energy Transfer in Optical Rulers, Breaking the FRET Barrier. *J. Am. Chem. Soc.* **2005**, *127*, 3115–3119.
- (358) Sen, T.; Patra, A. Resonance Energy Transfer from Rhodamine 6G to Gold Nanoparticles by Steady-State and Time-Resolved Spectroscopy. *J. Phys. Chem. C* **2008**, *112*, 3216–3222.
- (359) Sen, T.; Patra, A. Recent Advances in Energy Transfer Processes in Gold-Nanoparticle-Based Assemblies. *J. Phys. Chem. C* **2012**, *116*, 17307–17317.
- (360) Sen, T.; Patra, A. Formation of Self-Assembled Au Nanoparticles and the Study of Their Optical Properties by Steady-State and Time-Resolved Spectroscopies. *J. Phys. Chem. C* **2009**, *113*, 13125–13132.
- (361) Haldar, K. K.; Sen, T.; Patra, A. Au@ZnO Core-Shell Nanoparticles Are Efficient Energy Acceptors with Organic Dye Donors. *J. Phys. Chem. C* **2008**, *112*, 11650–11656.
- (362) Borja, M.; Dutta, P. K. Storage of Light Energy by Photoelectron Transfer across a Sensitized Zeolite-Solution Interface. *Nature* **1993**, *362*, 43–45.
- (363) Calzaferri, G.; Huber, S.; Maas, H.; Minkowski, C. Host–Guest Antenna Materials. *Angew. Chem., Int. Ed.* **2003**, *42*, 3732–3758.
- (364) Zabala Ruiz, A.; Li, H.; Calzaferri, G. Organizing Supramolecular Functional Dye–Zeolite Crystals. *Angew. Chem., Int. Ed.* **2006**, *45*, 5282–5287.
- (365) Scaiano, J. C.; García, H. Intrazeolite Photochemistry: Toward Supramolecular Control of Molecular Photochemistry. *Acc. Chem. Res.* **1999**, *32*, 783–793.
- (366) Guerrero-Martínez, A.; Fibikar, S.; Pastoriza-Santos, I.; Liz-Marzán, L. M.; De Cola, L. Microcontainers with Fluorescent Anisotropic Zeolite L Cores and Isotropic Silica Shells. *Angew. Chem., Int. Ed.* **2009**, *48*, 1266–1270.
- (367) Nguyen, T.-Q.; Wu, J.; Doan, V.; Schwartz, B. J.; Tolbert, S. H. Control of Energy Transfer in Oriented Conjugated Polymer-Mesoporous Silica Composites. *Science* **2000**, *288*, 652–656.
- (368) Chang, Z.; Kevan, L. Photoionization of Tetraphenylporphyrin in Mesoporous SiMCM-48, AlMCM-48, and TiMCM-48 Molecular Sieves. *Langmuir* **2002**, *18*, 911–916.
- (369) Lee, K. J.; Oh, J. H.; Kim, Y.; Jang, J. Fabrication of Photoluminescent-Dye Embedded Poly(Methyl Methacrylate) Nanofibers and Their Fluorescence Resonance Energy Transfer Properties. *Adv. Mater.* **2006**, *18*, 2216–2219.
- (370) Hernandez, R.; Fransville, A.-C.; Minoofar, P.; Dunn, B.; Zink, J. I. Controlled Placement of Luminescent Molecules and Polymers in Mesostructured Sol–Gel Thin Films. *J. Am. Chem. Soc.* **2001**, *123*, 1248–1249.

- (371) Burt, M. C.; Dave, B. C. Externally Tunable Dynamic Confinement Effect in Organosilica Sol–Gels. *J. Am. Chem. Soc.* **2006**, *128*, 11750–11751.
- (372) Wirnsberger, G.; Yang, P.; Huang, H. C.; Scott, B.; Deng, T.; Whitesides, G. M.; Chmelka, B. F.; Stucky, G. D. Patterned Block-Copolymer-Silica Mesostructures as Host Media for the Laser Dye Rhodamine 6G. *J. Phys. Chem. B* **2001**, *105*, 6307–6313.
- (373) Scott, B. J.; Bartl, M. H.; Wirnsberger, G.; Stucky, G. D. Energy Transfer in Dye-Doped Mesostructured Composites. *J. Phys. Chem. A* **2003**, *107*, 5499–5502.
- (374) Sen, T.; Jana, S.; Koner, S.; Patra, A. Energy Transfer between Confined Dye and Surface Attached Au Nanoparticles of Mesoporous Silica. *J. Phys. Chem. C* **2010**, *114*, 707–714.
- (375) Sen, T.; Jana, S.; Koner, S.; Patra, A. Efficient Energy Transfer between Confined Dye and Y-Zeolite Functionalized Au Nanoparticles. *J. Phys. Chem. C* **2010**, *114*, 19667–19672.
- (376) Freeman, R.; Finder, T.; Bahshi, L.; Willner, I. β -Cyclodextrin-Modified CdSe/ZnS Quantum Dots for Sensing and Chiroselective Analysis. *Nano Lett.* **2009**, *9*, 2073–2076.
- (377) Zhang, N.; Liu, Y.; Tong, L.; Xu, K.; Zhuo, L.; Tang, B. A Novel Assembly of Au NPs- β -CDs-FL for the Fluorescent Probing of Cholesterol and its Application in Blood Serum. *Analyst* **2008**, *133*, 1176–1181.
- (378) Sen, T.; Haldar, K. K.; Patra, A. Quenching of Confined C480 Dye in the Presence of Metal-Conjugated γ -Cyclodextrin. *J. Phys. Chem. C* **2010**, *114*, 11409–11413.
- (379) D’Souza, V. T.; Bender, M. L. Miniature Organic Models of Enzymes. *Acc. Chem. Res.* **1987**, *20*, 146–152.
- (380) Vajda, S.; Jimenez, R.; Rosenthal, S. J.; Fidler, V.; Fleming, G. R.; Castner, E. W. Femtosecond to Nanosecond Solvation Dynamics in Pure Water and inside the γ -Cyclodextrin Cavity. *J. Chem. Soc., Faraday Trans.* **1995**, *91*, 867–873.
- (381) Harada, A.; Li, J.; Kamachi, M. The Molecular Necklace: A Rotaxane Containing Many Threaded α -Cyclodextrins. *Nature* **1992**, *356*, 325–327.
- (382) Ghosh, S.; Mondal, S. K.; Sahu, K.; Bhattacharyya, K. Ultrafast Electron Transfer in a Nanocavity. Dimethylaniline to Coumarin Dyes in Hydroxypropyl γ -Cyclodextrin. *J. Phys. Chem. A* **2006**, *110*, 13139–13144.
- (383) Achermann, M. Exciton–Plasmon Interactions in Metal–Semiconductor Nanostructures. *J. Phys. Chem. Lett.* **2010**, *1*, 2837–2843.
- (384) Bellessa, J.; Bonnard, C.; Plenet, J. C.; Mugnier, J. Strong Coupling between Surface Plasmons and Excitons in an Organic Semiconductor. *Phys. Rev. Lett.* **2004**, *93*, 036404.
- (385) Sih, B. C.; Wolf, M. O. Metal Nanoparticle-Conjugated Polymer Nanocomposites. *Chem. Commun.* **2005**, 3375–3384.
- (386) Fan, C.; Wang, S.; Hong, J. W.; Bazan, G. C.; Plaxco, K. W.; Heeger, A. J. Beyond Superquenching: Hyper-Efficient Energy Transfer from Conjugated Polymers to Gold Nanoparticles. *Proc. Natl. Acad. Sci. U. S. A.* **2003**, *100*, 6297–6301.
- (387) Masuhara, A.; Kasai, H.; Okada, S.; Oikawa, H.; Terauchi, M.; Tanaka, M.; Nakanishi, H. Hybridized Microcrystals Composed of Metal Fine Particles and π -Conjugated Organic Microcrystals. *Jpn. J. Appl. Phys.* **2001**, *40*, L1129–L1131.
- (388) Guan, Z.; Polavarapu, L.; Xu, Q.-H. Enhanced Two-Photon Emission in Coupled Metal Nanoparticles Induced by Conjugated Polymers. *Langmuir* **2010**, *26*, 18020–18023.
- (389) Mahmoud, M. A.; Poncheri, A. J.; El-Sayed, M. A. Properties of π -Conjugated Fluorescence Polymer–Plasmonic Nanoparticles Hybrid Materials. *J. Phys. Chem. C* **2012**, *116*, 13336–13342.
- (390) Heydari, E.; Pastoriza-Santos, I.; Flehr, R.; Liz-Marzán, L. M.; Stumpe, J. Nanoplasmonic Enhancement of the Emission of Semiconductor Polymer Composites. *J. Phys. Chem. C* **2013**, *117*, 16577–16583.
- (391) Kim, M. S.; Park, D. H.; Cho, E. H.; Kim, K. H.; Park, Q. H.; Song, H.; Kim, D.-C.; Kim, J.; Joo, J. Complex Nanoparticle of Light-Emitting MEH-PPV with Au: Enhanced Luminescence. *ACS Nano* **2009**, *3*, 1329–1334.
- (392) O’Carroll, D. M.; Hofmann, C. E.; Atwater, H. A. Conjugated Polymer/Metal Nanowire Heterostructure Plasmonic Antennas. *Adv. Mater.* **2010**, *22*, 1223–1227.
- (393) Bhattacharyya, S.; Sen, T.; Patra, A. Host-Guest Energy Transfer: Semiconducting Polymer Nanoparticles and Au Nanoparticles. *J. Phys. Chem. C* **2010**, *114*, 11787–11795.
- (394) Bhattacharyya, S.; Patra, A. Photoluminescence Quenching of Semiconducting Polymer Nanoparticles in Presence of Au Nanoparticles. *Bull. Mater. Sci.* **2012**, *35*, 719–725.
- (395) Vijayakumar, C.; Balan, B.; Saeki, A.; Tsuda, T.; Kuwabata, S.; Seki, S. Gold Nanoparticle Assisted Self-Assembly and Enhancement of Charge Carrier Mobilities of a Conjugated Polymer. *J. Phys. Chem. C* **2012**, *116*, 17343–17350.
- (396) Jana, B.; Bhattacharyya, S.; Patra, A. Conjugated Polymer P3HT-Au Hybrid Nanostructures for Enhancing Photocatalytic Activity. *Phys. Chem. Chem. Phys.* **2015**, *17*, 15392–15399.
- (397) Wang, B.; Wang, K.; Lu, W.; Wang, H.; Li, Z.; Yang, J.; Hou, J. G. Effects of Discrete Energy Levels on Single-Electron Tunneling in Coupled Metal Particles. *Appl. Phys. Lett.* **2003**, *82*, 3767–3769.
- (398) Steiner, D.; Mokari, T.; Banin, U.; Millo, O. Electronic Structure of Metal–Semiconductor Nanojunctions in Gold CdSe Nanodumbbells. *Phys. Rev. Lett.* **2005**, *95*, 056805.
- (399) Guardia, P.; Korobchevskaya, K.; Casu, A.; Genovese, A.; Manna, L.; Comin, A. Plasmon Dynamics in Colloidal Au_2Cd Alloy–CdSe Core/Shell Nanocrystals. *ACS Nano* **2013**, *7*, 1045–1053.
- (400) Vasa, P.; Pomraenke, R.; Schwieger, S.; Mazur, Y. I.; Kunets, V.; Srinivasan, P.; Johnson, E.; Kihm, J. E.; Kim, D. S.; Runge, E.; et al. Coherent Exciton–Surface-Plasmon-Polariton Interaction in Hybrid Metal–Semiconductor Nanostructures. *Phys. Rev. Lett.* **2008**, *101*, 116801.
- (401) Wang, Y.; Yang, T.; Tuominen, M. T.; Achermann, M. Radiative Rate Enhancements in Ensembles of Hybrid Metal–Semiconductor Nanostructures. *Phys. Rev. Lett.* **2009**, *102*, 163001.
- (402) Zhang, J.; Tang, Y.; Lee, K.; Ouyang, M. Nonepitaxial Growth of Hybrid Core–Shell Nanostructures with Large Lattice Mismatches. *Science* **2010**, *327*, 1634–1638.
- (403) Figuerola, A.; Huis, M. v.; Zanella, M.; Genovese, A.; Marras, S.; Falqui, A.; Zandbergen, H. W.; Cingolani, R.; Manna, L. Epitaxial CdSe–Au Nanocrystal Heterostructures by Thermal Annealing. *Nano Lett.* **2010**, *10*, 3028–3036.
- (404) Tian, Z.-Q.; Zhang, Z.-L.; Jiang, P.; Zhang, M.-X.; Xie, H.-Y.; Pang, D.-W. Core/Shell Structured Noble Metal (Alloy)/Cadmium Selenide Nanocrystals. *Chem. Mater.* **2009**, *21*, 3039–3041.
- (405) Khon, E.; Hewa-Kasakarage, N. N.; Nemitz, I.; Acharya, K.; Zamkov, M. Tuning the Morphology of Au/CdS Nanocomposites through Temperature-Controlled Reduction of Gold-Oleate Complexes. *Chem. Mater.* **2010**, *22*, 5929–5936.
- (406) Li, M.; Yu, X.-F.; Liang, S.; Peng, X.-N.; Yang, Z.-J.; Wang, Y.-L.; Wang, Q.-Q. Synthesis of Au–CdS Core–Shell Hetero-Nanorods with Efficient Exciton–Plasmon Interactions. *Adv. Funct. Mater.* **2011**, *21*, 1788–1794.
- (407) Khon, E.; Mereshchenko, A.; Tarnovsky, A. N.; Acharya, K.; Klinkova, A.; Hewa-Kasakarage, N. N.; Nemitz, I.; Zamkov, M. Suppression of the Plasmon Resonance in Au/CdS Colloidal Nanocomposites. *Nano Lett.* **2011**, *11*, 1792–1799.
- (408) Shi, W.; Zeng, H.; Sahoo, Y.; Ohulchansky, T. Y.; Ding, Y.; Wang, Z. L.; Swihart, M.; Prasad, P. N. A General Approach to Binary and Ternary Hybrid Nanocrystals. *Nano Lett.* **2006**, *6*, 875–881.
- (409) Talapin, D. V.; Yu, H.; Shevchenko, E. V.; Lobo, A.; Murray, C. B. Synthesis of Colloidal PbSe/PbS Core–Shell Nanowires and PbS/Au Nanowire–Nanocrystal Heterostructures. *J. Phys. Chem. C* **2007**, *111*, 14049–14054.
- (410) Carbone, L.; Kudera, S.; Giannini, C.; Ciccarella, G.; Cingolani, R.; Cozzoli, P. D.; Manna, L. Selective Reactions on the Tips of Colloidal Semiconductor Nanorods. *J. Mater. Chem.* **2006**, *16*, 3952–3956.
- (411) Menagen, G.; Macdonald, J. E.; Shemesh, Y.; Popov, L.; Banin, U. Au Growth on Semiconductor Nanorods: Photoinduced Versus

- Thermal Growth Mechanisms. *J. Am. Chem. Soc.* **2009**, *131*, 17406–17411.
- (412) Mokari, T.; Rothenberg, E.; Popov, I.; Costi, R.; Banin, U. Selective Growth of Metal Tips onto Semiconductor Quantum Rods and Tetrapods. *Science* **2004**, *304*, 1787–1790.
- (413) Lee, J.; Govorov, A. O.; Dulka, J.; Kotov, N. A. Bioconjugates of CdTe Nanowires and Au Nanoparticles: Plasmon-Exciton Interactions, Luminescence Enhancement, and Collective Effects. *Nano Lett.* **2004**, *4*, 2323–2330.
- (414) AbouZeid, K. M.; Mohamed, M. B.; El-Shall, M. S. Hybrid Au–CdSe and Ag–CdSe Nanoflowers and Core–Shell Nanocrystals via One-Pot Heterogeneous Nucleation and Growth. *Small* **2011**, *7*, 3299–3307.
- (415) Yang, J.; Sargent, E.; Kelley, S.; Ying, J. Y. A General Phase-Transfer Protocol for Metal Ions and Its Application in Nanocrystal Synthesis. *Nat. Mater.* **2009**, *8*, 683–689.
- (416) Lee, J.; Hernandez, P.; Lee, J.; Govorov, A. O.; Kotov, N. A. Exciton-Plasmon Interactions in Molecular Spring Assemblies of Nanowires and Wavelength-Based Protein Detection. *Nat. Mater.* **2007**, *6*, 291–295.
- (417) Kanta Haldar, K.; Kundu, S.; Patra, A. Non-Radiative Relaxation and Rectification Behavior of Metal/Semiconductor Tetrapod Heterostructures. *Appl. Phys. Lett.* **2014**, *104*, 063110.
- (418) Hosoki, K.; Tayagaki, T.; Yamamoto, S.; Matsuda, K.; Kanemitsu, Y. Direct and Stepwise Energy Transfer from Excitons to Plasmons in Close-Packed Metal and Semiconductor Nanoparticle Monolayer Films. *Phys. Rev. Lett.* **2008**, *100*, 207404.
- (419) Pu, Y.; Grange, R.; Hsieh, C.-L.; Psaltis, D. Nonlinear Optical Properties of Core–Shell Nanocavities for Enhanced Second-Harmonic Generation. *Phys. Rev. Lett.* **2010**, *104*, 207402.
- (420) Yang, Y.; Nogami, M.; Shi, J.; Chen, H.; Liu, Y.; Qian, S. Ultrafast Electron Dynamics and Enhanced Optical Nonlinearities of CdS-Capped Au/BaTiO₃ Composite Film. *J. Appl. Phys.* **2005**, *98*, 033528.
- (421) Singh, M. R. Enhancement of the Second-Harmonic Generation in a Quantum Dot–Metallic Nanoparticle Hybrid System. *Nanotechnology* **2013**, *24*, 125701.
- (422) Nan, F.; Liang, S.; Liu, X.-L.; Peng, X.-N.; Li, M.; Yang, Z.-J.; Zhou, L.; Hao, Z.-H.; Wang, Q.-Q. Sign-Reversed and Magnitude-Enhanced Nonlinear Absorption of Au–CdS Core–Shell Heteronanorods. *Appl. Phys. Lett.* **2013**, *102*, 163112.
- (423) Gong, H.-M.; Wang, X.-H.; Du, Y.-M.; Wang, Q.-Q. Optical Nonlinear Absorption and Refraction of CdS and CdS-Ag Core–Shell Quantum Dots. *J. Chem. Phys.* **2006**, *125*, 024707.
- (424) Fu, M.; Wang, K.; Long, H.; Yang, G.; Lu, P.; Hetsch, F.; Susha, A. S.; Rogach, A. L. Resonantly Enhanced Optical Nonlinearity in Hybrid Semiconductor Quantum Dot – Metal Nanoparticle Structures. *Appl. Phys. Lett.* **2012**, *100*, 063117.
- (425) Sreeramulu, V.; Haldar, K. K.; Patra, A.; Rao, D. N. Nonlinear Optical Switching and Enhanced Nonlinear Optical Response of Au–CdSe Heteronanostructures. *J. Phys. Chem. C* **2014**, *118*, 30333–30341.
- (426) Tian, Z.; Yu, J.; Wu, C.; Szymanski, C.; McNeill, J. Amplified Energy Transfer in Conjugated Polymer Nanoparticle Tags and Sensors. *Nanoscale* **2010**, *2*, 1999–2011.
- (427) Collini, E.; Scholes, G. D. Coherent Intrachain Energy Migration in a Conjugated Polymer at Room Temperature. *Science* **2009**, *323*, 369–373.
- (428) Beenken, W. J. D.; Pullerits, T. Spectroscopic Units in Conjugated Polymers: A Quantum Chemically Founded Concept? *J. Phys. Chem. B* **2004**, *108*, 6164–6169.
- (429) Hwang, I.; Scholes, G. D. Electronic Energy Transfer and Quantum-Coherence in π -Conjugated Polymers. *Chem. Mater.* **2011**, *23*, 610–620.
- (430) Kietzke, T.; Neher, D.; Landfester, K.; Montenegro, R.; Guntner, R.; Scherf, U. Novel Approaches to Polymer Blends Based on Polymer Nanoparticles. *Nat. Mater.* **2003**, *2*, 408–412.
- (431) Kietzke, T.; Neher, D.; Kumke, M.; Montenegro, R.; Landfester, K.; Scherf, U. A Nanoparticle Approach to Control the Phase Separation in Polyfluorene Photovoltaic Devices. *Macromolecules* **2004**, *37*, 4882–4890.
- (432) Chen, J.-T.; Hsu, C.-S. Conjugated Polymer Nanostructures for Organic Solar Cell Applications. *Polym. Chem.* **2011**, *2*, 2707–2722.
- (433) Feng, L.; Zhu, C.; Yuan, H.; Liu, L.; Lv, F.; Wang, S. Conjugated Polymer Nanoparticles: Preparation, Properties, Functionalization and Biological Applications. *Chem. Soc. Rev.* **2013**, *42*, 6620–6633.
- (434) Pecher, J.; Mecking, S. Nanoparticles of Conjugated Polymers. *Chem. Rev.* **2010**, *110*, 6260–6279.
- (435) Najafov, H.; Lee, B.; Zhou, Q.; Feldman, L. C.; Podzorov, V. Observation of Long-Range Exciton Diffusion in Highly Ordered Organic Semiconductors. *Nat. Mater.* **2010**, *9*, 938–943.
- (436) Mikhnenko, O. V.; Blom, P. W. M.; Nguyen, T.-Q. Exciton Diffusion in Organic Semiconductors. *Energy Environ. Sci.* **2015**, *8*, 1867–1888.
- (437) Xing, G.; Mathews, N.; Sun, S.; Lim, S. S.; Lam, Y. M.; Grätzel, M.; Mhaisalkar, S.; Sum, T. C. Long-Range Balanced Electron- and Hole-Transport Lengths in Organic-Inorganic CH₃NH₃PbI₃. *Science* **2013**, *342*, 344–347.
- (438) Guzelturk, B.; Erdem, O.; Olutas, M.; Kelestemur, Y.; Demir, H. V. Stacking in Colloidal Nanoplatelets: Tuning Excitonic Properties. *ACS Nano* **2014**, *8*, 12524–12533.
- (439) Tamai, Y.; Matsuura, Y.; Ohkita, H.; Benten, H.; Ito, S. One-Dimensional Singlet Exciton Diffusion in Poly(3-Hexylthiophene) Crystalline Domains. *J. Phys. Chem. Lett.* **2014**, *5*, 399–403.
- (440) Guzelturk, B.; Demir, H. V. Organic–Inorganic Composites of Semiconductor Nanocrystals for Efficient Excitonics. *J. Phys. Chem. Lett.* **2015**, *6*, 2206–2215.
- (441) Stöferle, T.; Scherf, U.; Mahrt, R. F. Energy Transfer in Hybrid Organic/Inorganic Nanocomposites. *Nano Lett.* **2009**, *9*, 453–456.
- (442) Guzelturk, B.; Hernandez-Martinez, P. L.; Sharma, V. K.; Coskun, Y.; Ibrahimova, V.; Tuncel, D.; Govorov, A. O.; Sun, X. W.; Xiong, Q.; Demir, H. V. Study of Exciton Transfer in Dense Quantum Dot Nanocomposites. *Nanoscale* **2014**, *6*, 11387–11394.
- (443) Bhattacharyya, S.; Prashanthi, S.; Bangal, P. R.; Patra, A. Photophysics and Dynamics of Dye-Doped Conjugated Polymer Nanoparticles by Time-Resolved and Fluorescence Correlation Spectroscopy. *J. Phys. Chem. C* **2013**, *117*, 26750–26759.
- (444) Berberan-Santos, M. N.; Valeur, B. Fluorescence Depolarization by Electronic Energy Transfer in Donor–Acceptor Pairs of Like and Unlike Chromophores. *J. Chem. Phys.* **1991**, *95*, 8048–8055.
- (445) Enciso, E.; Costela, A.; Garcia-Moreno, I.; Martin, V.; Sastre, R. Conventional Unidirectional Laser Action Enhanced by Dye Confined in Nanoparticle Scatters. *Langmuir* **2010**, *26*, 6154–6157.
- (446) Grigalevicius, S.; Forster, M.; Ellinger, S.; Landfester, K.; Scherf, U. Excitation Energy Transfer from Semi-Conducting Polymer Nanoparticles to Surface-Bound Fluorescent Dyes. *Macromol. Rapid Commun.* **2006**, *27*, 200–202.
- (447) Dawson, K.; Lovera, P.; Iacopino, D.; O’Riordan, A.; Redmond, G. Multi-Colour Emission from Dye Doped Polymeric Nanotubes by Host-Guest Energy Transfer. *J. Mater. Chem.* **2011**, *21*, 15995–16000.
- (448) Zhu, M.-Q.; Zhu, L.; Han, J. J.; Wu, W.; Hurst, J. K.; Li, A. D. Q. Spiropyran-Based Photochromic Polymer Nanoparticles with Optically Switchable Luminescence. *J. Am. Chem. Soc.* **2006**, *128*, 4303–4309.
- (449) Harbron, E. J.; Davis, C. M.; Campbell, J. K.; Allred, R. M.; Kovary, M. T.; Economou, N. J. Photochromic Dye-Doped Conjugated Polymer Nanoparticles: Photomodulated Emission and Nanoenvironmental Characterization. *J. Phys. Chem. C* **2009**, *113*, 13707–13714.
- (450) Davis, C. M.; Childress, E. S.; Harbron, E. J. Ensemble and Single-Particle Fluorescence Photomodulation in Diarylethene-Doped Conjugated Polymer Nanoparticles. *J. Phys. Chem. C* **2011**, *115*, 19065–19073.

- (451) Jin, Y.; Ye, F.; Zeigler, M.; Wu, C.; Chiu, D. T. Near-Infrared Fluorescent Dye-Doped Semiconducting Polymer Dots. *ACS Nano* **2011**, *5*, 1468–1475.
- (452) Chan, Y.-H.; Gallina, M. E.; Zhang, X.; Wu, I. C.; Jin, Y.; Sun, W.; Chiu, D. T. Reversible Photoswitching of Spiropyran-Conjugated Semiconducting Polymer Dots. *Anal. Chem.* **2012**, *84*, 9431–9438.
- (453) Martin, C.; Bhattacharyya, S.; Patra, A.; Douhal, A. Single and Multistep Energy Transfer Processes within Doped Polymer Nanoparticles. *Photochem. Photobiol. Sci.* **2014**, *13*, 1241–1252.
- (454) Shen, X.; Li, L.; Wu, H.; Yao, S. Q.; Xu, Q.-H. Photosensitizer-Doped Conjugated Polymer Nanoparticles for Simultaneous Two-Photon Imaging and Two-Photon Photodynamic Therapy in Living Cells. *Nanoscale* **2011**, *3*, 5140–5146.
- (455) Scholes, G. D. Long-Range Resonance Energy Transfer in Molecular Systems. *Annu. Rev. Phys. Chem.* **2003**, *54*, 57–87.
- (456) Chen, L.; McBranch, D. W.; Wang, H.-L.; Helgeson, R.; Wudl, F.; Whitten, D. G. Highly Sensitive Biological and Chemical Sensors Based on Reversible Fluorescence Quenching in a Conjugated Polymer. *Proc. Natl. Acad. Sci. U. S. A.* **1999**, *96*, 12287–12292.
- (457) Grimland, J. L.; Wu, C.; Ramoutar, R. R.; Brumaghim, J. L.; McNeill, J. Photosensitizer-Doped Conjugated Polymer Nanoparticles with High Cross-Sections for One- and Two-Photon Excitation. *Nanoscale* **2011**, *3*, 1451–1455.
- (458) Bhattacharyya, S.; Barman, M. K.; Baidya, A.; Patra, A. Singlet Oxygen Generation from Polymer Nanoparticles—Photosensitizer Conjugates Using FRET Cascade. *J. Phys. Chem. C* **2014**, *118*, 9733–9740.
- (459) Olive, A. G. L.; Del Guerzo, A.; Schäfer, C.; Belin, C.; Raffy, G.; Giansante, C. Fluorescence Amplification in Self-Assembled Organic Nanoparticles by Excitation Energy Migration and Transfer. *J. Phys. Chem. C* **2010**, *114*, 10410–10416.
- (460) Ishida, Y.; Shimada, T.; Takagi, S. Artificial Light-Harvesting Model in a Self-Assembly Composed of Cationic Dyes and Inorganic Nanosheet. *J. Phys. Chem. C* **2013**, *117*, 9154–9163.
- (461) Woller, J. G.; Hannestad, J. K.; Albinsson, B. Self-Assembled Nanoscale DNA–Porphyrin Complex for Artificial Light Harvesting. *J. Am. Chem. Soc.* **2013**, *135*, 2759–2768.
- (462) Dutta, P. K.; Levenberg, S.; Loskutov, A.; Jun, D.; Saer, R.; Beatty, J. T.; Lin, S.; Liu, Y.; Woodbury, N. W.; Yan, H. A DNA-Directed Light-Harvesting/Reaction Center System. *J. Am. Chem. Soc.* **2014**, *136*, 16618–16625.
- (463) Niles, E. T.; Roehling, J. D.; Yamagata, H.; Wise, A. J.; Spano, F. C.; Moulé, A. J.; Grey, J. K. J-Aggregate Behavior in Poly(3-Hexylthiophene) Nanofibers. *J. Phys. Chem. Lett.* **2012**, *3*, 259–263.
- (464) Healy, A. T.; Boudouris, B. W.; Frisbie, C. D.; Hillmyer, M. A.; Blank, D. A. Intramolecular Exciton Diffusion in Poly(3-Hexylthiophene). *J. Phys. Chem. Lett.* **2013**, *4*, 3445–3449.
- (465) Ostrowski, D. P.; Lytwak, L. A.; Mejia, M. L.; Stevenson, K. J.; Holliday, B. J.; Vanden Bout, D. A. The Effects of Aggregation on Electronic and Optical Properties of Oligothiophene Particles. *ACS Nano* **2012**, *6*, 5507–5513.
- (466) Leclère, P.; Surin, M.; Viville, P.; Lazzaroni, R.; Kilbinger, A. F. M.; Henze, O.; Feast, W. J.; Cavallini, M.; Biscarini, F.; Schenning, A. P. H. J.; et al. About Oligothiophene Self-Assembly: From Aggregation in Solution to Solid-State Nanostructures. *Chem. Mater.* **2004**, *16*, 4452–4466.
- (467) Macchi, G.; Medina, B. M.; Zambianchi, M.; Tubino, R.; Cornil, J.; Barbarella, G.; Gierschner, J.; Meinardi, F. Spectroscopic Signatures for Planar Equilibrium Geometries in Methyl-Substituted Oligothiophenes. *Phys. Chem. Chem. Phys.* **2009**, *11*, 984–990.
- (468) Gao, J.; Stein, B. W.; Thomas, A. K.; Garcia, J. A.; Yang, J.; Kirk, M. L.; Grey, J. K. Enhanced Charge Transfer Doping Efficiency in J-Aggregate Poly(3-Hexylthiophene) Nanofibers. *J. Phys. Chem. C* **2015**, *119*, 16396–16402.
- (469) Bhattacharyya, S.; Jana, B.; Patra, A. Multichromophoric Organic Molecules Encapsulated in Polymer Nanoparticles for Artificial Light Harvesting. *ChemPhysChem* **2015**, *16*, 796–804.
- (470) Bhattacharyya, S.; Jana, B.; Sain, S.; Barman, M. K.; Pradhan, S. K.; Patra, A. Photoswitching and Thermoresponsive Properties of Conjugated Multi-Chromophore Nanostructured Materials. *Small* **2015**, *11*, 6317–6324.
- (471) Tabachnyk, M.; Ehrl, B.; Gélinas, S.; Böhm, M. L.; Walker, B. J.; Musselman, K. P.; Greenham, N. C.; Friend, R. H.; Rao, A. Resonant Energy Transfer of Triplet Excitons from Pentacene to PbSe Nanocrystals. *Nat. Mater.* **2014**, *13*, 1033–1038.
- (472) Thompson, N. J.; Wilson, M. W. B.; Congreve, D. N.; Brown, P. R.; Scherer, J. M.; Bischoff, Thomas, S.; Wu, M.; Geva, N.; Welborn, M.; Voorhis, T. V.; et al. Energy Harvesting of Non-Emissive Triplet Excitons in Tetracene by Emissive PbS Nanocrystals. *Nat. Mater.* **2014**, *13*, 1039–1043.
- (473) Rao, K. V.; Jain, A.; George, S. J. Organic-Inorganic Light-Harvesting Scaffolds for Luminescent Hybrids. *J. Mater. Chem. C* **2014**, *2*, 3055–3064.
- (474) Huynh, W. U.; Dittmer, J. J.; Alivisatos, A. P. Hybrid Nanorod-Polymer Solar Cells. *Science* **2002**, *295*, 2425–2427.
- (475) Lutich, A. A.; Jiang, G.; Susha, A. S.; Rogach, A. L.; Stefani, F. D.; Feldmann, J. Energy Transfer Versus Charge Separation in Type-II Hybrid Organic–Inorganic Nanocomposites. *Nano Lett.* **2009**, *9*, 2636–2640.
- (476) Achermann, M.; Petruska, M. A.; Kos, S.; Smith, D. L.; Koleske, D. D.; Klimov, V. I. Energy-Transfer Pumping of Semiconductor Nanocrystals Using an Epitaxial Quantum Well. *Nature* **2004**, *429*, 642–646.
- (477) Basko, D.; La Rocca, G. C.; Bassani, F.; Agranovich, V. M. Förster Energy Transfer from a Semiconductor Quantum Well to an Organic Material Overlayer. *Eur. Phys. J. B* **1999**, *8*, 353–362.
- (478) Nguyen, T.-Q.; Kwong, R. C.; Thompson, M. E.; Schwartz, B. J. Improving the Performance of Conjugated Polymer-Based Devices by Control of Interchain Interactions and Polymer Film Morphology. *Appl. Phys. Lett.* **2000**, *76*, 2454–2456.
- (479) Hong, S.-K.; Yeon, K.-H. Energy Transfer from a Conjugated Polymer to a Quantum Dot in the Semiclassical Approach. *J. Korean Phys. Soc.* **2005**, *46*, 1157–1162.
- (480) Erdem, T.; Ibrahimova, V.; Jeon, D.-W.; Lee, I.-H.; Tuncel, D.; Demir, H. V. Morphology-Dependent Energy Transfer of Polyfluorene Nanoparticles Decorating InGaN/GaN Quantum-Well Nanopillars. *J. Phys. Chem. C* **2013**, *117*, 18613–18619.
- (481) Reiss, P.; Couderc, E.; De Girolamo, J.; Pron, A. Conjugated Polymers/Semiconductor Nanocrystals Hybrid Materials-Preparation, Electrical Transport Properties and Applications. *Nanoscale* **2011**, *3*, 446–489.
- (482) Choudhury, K. R.; Samoc, M.; Patra, A.; Prasad, P. N. Charge Carrier Transport in Poly(N-Vinylcarbazole):CdS Quantum Dot Hybrid Nanocomposite. *J. Phys. Chem. B* **2004**, *108*, 1556–1562.
- (483) Yong, C. K.; Noori, K.; Gao, Q.; Joyce, H. J.; Tan, H. H.; Jagadish, C.; Giustino, F.; Johnston, M. B.; Herz, L. M. Strong Carrier Lifetime Enhancement in GaAs Nanowires Coated with Semiconducting Polymer. *Nano Lett.* **2012**, *12*, 6293–6301.
- (484) Morgenstern, F. S. F.; Rao, A.; Böhm, M. L.; Kist, R. J. P.; Vaynzof, Y.; Greenham, N. C. Ultrafast Charge- and Energy-Transfer Dynamics in Conjugated Polymer: Cadmium Selenide Nanocrystal Blends. *ACS Nano* **2014**, *8*, 1647–1654.
- (485) Strein, E.; deQuilettes, D. W.; Hsieh, S. T.; Colbert, A. E.; Ginger, D. S. Hot Hole Transfer Increasing Polaron Yields in Hybrid Conjugated Polymer/PbS Blends. *J. Phys. Chem. Lett.* **2014**, *5*, 208–211.
- (486) Colbert, A. E.; Janke, E. M.; Hsieh, S. T.; Subramanyan, S.; Schlenker, C. W.; Jenekhe, S. A.; Ginger, D. S. Hole Transfer from Low Band Gap Quantum Dots to Conjugated Polymers in Organic/Inorganic Hybrid Photovoltaics. *J. Phys. Chem. Lett.* **2013**, *4*, 280–284.
- (487) O’Carroll, D. M.; Petoukhoff, C. E.; Kohl, J.; Yu, B.; Carter, C. M.; Goodman, S. Conjugated Polymer-Based Photonic Nanostructures. *Polym. Chem.* **2013**, *4*, 5181–5196.
- (488) Bhattacharyya, S.; Paramanik, B.; Kundu, S.; Patra, A. Energy/Hole Transfer Phenomena in Hybrid α -Sexithiophene (α -STH) Nanoparticle-CdTe Quantum-Dot Nanocomposites. *ChemPhysChem* **2012**, *13*, 4155–4162.

- (489) Kundu, S.; Bhattacharyya, S.; Patra, A. Photoinduced Energy Transfer in Dye Encapsulated Polymer Nanoparticle-CdTe Quantum Dot Light Harvesting Assemblies. *Mater. Horiz.* **2015**, *2*, 60–67.
- (490) Clafon, S. N.; Beattie, D. A.; Mierczynska-Vasilev, A.; Acres, R. G.; Morgan, A. C.; Kee, T. W. Chemical Defects in the Highly Fluorescent Conjugated Polymer Dots. *Langmuir* **2010**, *26*, 17785–17789.
- (491) Verma, S.; Ghosh, H. N. Exciton Energy and Charge Transfer in Porphyrin Aggregate/Semiconductor (TiO_2) Composites. *J. Phys. Chem. Lett.* **2012**, *3*, 1877–1884.
- (492) Bai, F.; Sun, Z.; Wu, H.; Haddad, R. E.; Coker, E. N.; Huang, J. Y.; Rodriguez, M. A.; Fan, H. Porous One-Dimensional Nanostructures through Confined Cooperative Self-Assembly. *Nano Lett.* **2011**, *11*, 5196–5200.
- (493) Ikeda, M.; Takeuchi, M.; Shinkai, S. Unusual Emission Properties of a Triphenylene-Based Organogel System. *Chem. Commun.* **2003**, 1354–1355.
- (494) Chen, L.; Revel, S.; Morris, K.; Adams, D. J. Energy Transfer in Self-Assembled Dipeptide Hydrogels. *Chem. Commun.* **2010**, *46*, 4267–4269.
- (495) Ryu, J.-H.; Lee, M. Transformation of Isotropic Fluid to Nematic Gel Triggered by Dynamic Bridging of Supramolecular Nanocylinders. *J. Am. Chem. Soc.* **2005**, *127*, 14170–14171.
- (496) Smith, K. M.; Falk, J. E. *Porphyrins and Metalloporphyrins*; Elsevier: Amsterdam, 1975.
- (497) Kasha, M. Energy Transfer Mechanisms and the Molecular Exciton Model for Molecular Aggregates. *Radiat. Res.* **1963**, *20*, 55–70.
- (498) Kasha, M.; Rawls, H. R.; Ashraf El-Bayoumi, M. Exciton Model in Molecular Spectroscopy. *Pure Appl. Chem.* **1965**, *11*, 371–392.
- (499) Pescitelli, G.; Di Bari, L.; Berova, N. Application of Electronic Circular Dichroism in the Study of Supramolecular Systems. *Chem. Soc. Rev.* **2014**, *43*, 5211–5233.
- (500) Latter, M. J.; Langford, S. J. Porphyrinic Molecular Devices: Towards Nanoscaled Processes. *Int. J. Mol. Sci.* **2010**, *11*, 1878–1887.
- (501) Hasobe, T. Porphyrin-Based Supramolecular Nanoarchitectures for Solar Energy Conversion. *J. Phys. Chem. Lett.* **2013**, *4*, 1771–1780.
- (502) Nazeeruddin, M. K.; Humphry-Baker, R.; Officer, D. L.; Campbell, W. M.; Burrell, A. K.; Grätzel, M. Application of Metalloporphyrins in Nanocrystalline Dye-Sensitized Solar Cells for Conversion of Sunlight into Electricity. *Langmuir* **2004**, *20*, 6514–6517.
- (503) Gong, X.; Milic, T.; Xu, C.; Batteas, J. D.; Drain, C. M. Preparation and Characterization of Porphyrin Nanoparticles. *J. Am. Chem. Soc.* **2002**, *124*, 14290–14291.
- (504) Mandal, S.; Bhattacharyya, S.; Borovkov, V.; Patra, A. Porphyrin-Based Functional Nanoparticles: Conformational and Photophysical Properties of Bis-Porphyrin and Bis-Porphyrin Encapsulated Polymer Nanoparticles. *J. Phys. Chem. C* **2011**, *115*, 24029–24036.
- (505) Mandal, S.; Bhattacharyya, S.; Borovkov, V.; Patra, A. Photophysical Properties, Self-Assembly Behavior, and Energy Transfer of Porphyrin-Based Functional Nanoparticles. *J. Phys. Chem. C* **2012**, *116*, 11401–11407.
- (506) Shen, X.; He, F.; Wu, J.; Xu, G. Q.; Yao, S. Q.; Xu, Q.-H. Enhanced Two-Photon Singlet Oxygen Generation by Photosensitizer-Doped Conjugated Polymer Nanoparticles. *Langmuir* **2011**, *27*, 1739–1744.
- (507) Wu, C.; Bull, B.; Christensen, K.; McNeill, J. Ratiometric Single-Nanoparticle Oxygen Sensors for Biological Imaging. *Angew. Chem., Int. Ed.* **2009**, *48*, 2741–2745.
- (508) Prasad, P. N. *Introduction to Biophotonics*; John Wiley & Sons, 2004.
- (509) Mandal, S.; Kundu, S.; Bhattacharyya, S.; Patra, A. Photophysical Properties of Ionic Liquid-Assisted Porphyrin Nanoaggregate-Nickel Phthalocyanine Conjugates and Singlet Oxygen Generation. *J. Mater. Chem. C* **2014**, *2*, 8691–8699.
- (510) Kakade, S.; Ghosh, R.; Palit, D. K. Excited State Dynamics of Zinc-Phthalocyanine Nanoaggregates in Strong Hydrogen Bonding Solvents. *J. Phys. Chem. C* **2012**, *116*, 15155–15166.
- (511) McHale, J. L. Hierarchical Light-Harvesting Aggregates and Their Potential for Solar Energy Applications. *J. Phys. Chem. Lett.* **2012**, *3*, 587–597.
- (512) Doan, S. C.; Shanmugham, S.; Aston, D. E.; McHale, J. L. Counterion Dependent Dye Aggregates: Nanorods and Nanorings of Tetra(P-Carboxyphenyl)Porphyrin. *J. Am. Chem. Soc.* **2005**, *127*, 5885–5892.
- (513) Friesen, B. A.; Wiggins, B.; McHale, J. L.; Mazur, U.; Hipps, K. W. A Self-Assembled Two-Dimensional Zwitterionic Structure: H_6TSPP Studied on Graphite. *J. Phys. Chem. C* **2011**, *115*, 3990–3999.
- (514) Choi, M. Y.; Pollard, J. A.; Webb, M. A.; McHale, J. L. Counterion-Dependent Excitonic Spectra of Tetra(P-Carboxyphenyl)-Porphyrin Aggregates in Acidic Aqueous Solution. *J. Am. Chem. Soc.* **2003**, *125*, 810–820.
- (515) Friesen, B. A.; Wiggins, B.; McHale, J. L.; Mazur, U.; Hipps, K. W. Differing HOMO and LUMO Mediated Conduction in a Porphyrin Nanorod. *J. Am. Chem. Soc.* **2010**, *132*, 8554–8556.
- (516) Satake, A.; Kobuke, Y. Artificial Photosynthetic Systems: Assemblies of Slipped Cofacial Porphyrins and Phthalocyanines Showing Strong Electronic Coupling. *Org. Biomol. Chem.* **2007**, *5*, 1679–1691.
- (517) Würthner, F.; Kaiser, T. E.; Saha-Möller, C. R. J-Aggregates: From Serendipitous Discovery to Supramolecular Engineering of Functional Dye Materials. *Angew. Chem., Int. Ed.* **2011**, *50*, 3376–3410.
- (518) Verma, S.; Ghosh, A.; Das, A.; Ghosh, H. N. Exciton-Coupled Charge-Transfer Dynamics in a Porphyrin J-Aggregate/ TiO_2 Complex. *Chem. - Eur. J.* **2011**, *17*, 3458–3464.
- (519) Radivojevic, I.; Bazzan, G.; Burton-Pye, B. P.; Ithisuphalap, K.; Saleh, R.; Durstock, M. F.; Francesconi, L. C.; Drain, C. M. Zirconium(IV) and Hafnium(IV) Porphyrin and Phthalocyanine Complexes as New Dyes for Solar Cell Devices. *J. Phys. Chem. C* **2012**, *116*, 15867–15877.
- (520) Zhong, Y.; Wang, J.; Zhang, R.; Wei, W.; Wang, H.; Lü, X.; Bai, F.; Wu, H.; Haddad, R.; Fan, H. Morphology-Controlled Self-Assembly and Synthesis of Photocatalytic Nanocrystals. *Nano Lett.* **2014**, *14*, 7175–7179.
- (521) Guo, P.; Chen, P.; Ma, W.; Liu, M. Morphology-Dependent Supramolecular Photocatalytic Performance of Porphyrin Nanoassemblies: From Molecule to Artificial Supramolecular Nanoantenna. *J. Mater. Chem.* **2012**, *22*, 20243–20249.
- (522) Kano, H.; Kobayashi, T. Time-Resolved Fluorescence and Absorption Spectroscopies of Porphyrin J-Aggregates. *J. Chem. Phys.* **2002**, *116*, 184–195.
- (523) Bera, R.; Mandal, S.; Mondal, B.; Jana, B.; Nayak, S. K.; Patra, A. Graphene-Porphyrin Nanorod Composites for Solar Light Harvesting. *ACS Sustainable Chem. Eng.* **2016**, *4*, 1562–1568.
- (524) Ji, H.-X.; Hu, J.-S.; Wan, L.-J. ZnOEP Based Phototransistor: Signal Amplification and Light-Controlled Switch. *Chem. Commun.* **2008**, 2653–2655.
- (525) Fernández-Argüelles, M. T.; Yakovlev, A.; Sperling, R. A.; Lucardini, C.; Gaillard, S.; Sanz Medel, A.; Mallet, J.-M.; Brochon, J.-C.; Feltz, A.; Oheim, M.; et al. Synthesis and Characterization of Polymer-Coated Quantum Dots with Integrated Acceptor Dyes as FRET-Based Nanoprobes. *Nano Lett.* **2007**, *7*, 2613–2617.
- (526) Zhang, X.; Liu, Z.; Ma, L.; Hossu, M.; Chen, W. Interaction of Porphyrins with CdTe Quantum Dots. *Nanotechnology* **2011**, *22*, 195501.
- (527) Mandal, S.; Rahaman, M.; Sadhu, S.; Nayak, S. K.; Patra, A. Fluorescence Switching of Quantum Dot in Quantum Dot-Porphyrin-Cucurbit [7] Uril Assemblies. *J. Phys. Chem. C* **2013**, *117*, 3069–3077.
- (528) Doust, A. B.; Wilk, K. E.; Curmi, P. M. G.; Scholes, G. D. The Photophysics of Cryptophyte Light-Harvesting. *J. Photochem. Photobiol. A* **2006**, *184*, 1–17.
- (529) Blaudeck, T.; Zenkevich, E. I.; Abdel-Mottaleb, M.; Szwarcowska, K.; Kowerko, D.; Cichos, F.; von Borczyskowski, C.

Formation Principles and Ligand Dynamics of Nanoassemblies of CdSe Quantum Dots and Functionalised Dye Molecules. *ChemPhysChem* **2012**, *13*, 959–972.

(530) Zenkevich, E.; Cichos, F.; Shulga, A.; Petrov, E. P.; Blaudeck, T.; von Borczyskowski, C. Nanoassemblies Designed from Semiconductor Quantum Dots and Molecular Arrays. *J. Phys. Chem. B* **2005**, *109*, 8679–8692.

(531) Kang, S.; Yasuda, M.; Miyasaka, H.; Hayashi, H.; Kawasaki, M.; Umeyama, T.; Matano, Y.; Yoshida, K.; Isoda, S.; Imahori, H. Light Harvesting and Energy Transfer in Multiporphyrin-Modified CdSe Nanoparticles. *ChemSusChem* **2008**, *1*, 254–261.

(532) Bakalova, R.; Ohba, H.; Zhelev, Z.; Nagase, T.; Jose, R.; Ishikawa, M.; Baba, Y. Quantum Dot Anti-Cd Conjugates: Are They Potential Photosensitizers or Potentiators of Classical Photosensitizing Agents in Photodynamic Therapy of Cancer? *Nano Lett.* **2004**, *4*, 1567–1573.

(533) Blaudeck, T.; Zenkevich, E. I.; Cichos, F.; von Borczyskowski, C. Probing Wave Functions at Semiconductor Quantum-Dot Surfaces by Non-FRET Photoluminescence Quenching. *J. Phys. Chem. C* **2008**, *112*, 20251–20257.

(534) Shi, L.; Hernandez, B.; Selke, M. Singlet Oxygen Generation from Water-Soluble Quantum Dot–Organic Dye Nanocomposites. *J. Am. Chem. Soc.* **2006**, *128*, 6278–6279.

(535) Tsay, J. M.; Trzoss, M.; Shi, L.; Kong, X.; Selke, M.; Jung, M. E.; Weiss, S. Singlet Oxygen Production by Peptide-Coated Quantum Dot–Photosensitizer Conjugates. *J. Am. Chem. Soc.* **2007**, *129*, 6865–6871.

(536) Zen'kevich, É. I.; Sagun, E. I.; Yarovoī, A. A.; Shul'ga, A. M.; Knyukshto, V. N.; Stupak, A. P.; von Borczyskowski, C. Photoinduced Relaxation Processes in Complexes Based on Semiconductor CdSe Nanocrystals and Organic Molecules. *Opt. Spectrosc.* **2007**, *103*, 958–968.

(537) Vaishnavi, E.; Renganathan, R. "Turn-on-Off-on" Fluorescence Switching of Quantum Dots-Cationic Porphyrin Nanohybrid: A Sensor for DNA. *Analyst* **2014**, *139*, 225–234.

(538) Lemon, C. M.; Karnas, E.; Bawendi, M. G.; Nocera, D. G. Two-Photon Oxygen Sensing with Quantum Dot-Porphyrin Conjugates. *Inorg. Chem.* **2013**, *52*, 10394–10406.

(539) Xu, Z.; Gao, F.; Makarova, E. A.; Heikal, A. A.; Nemykin, V. N. Energy Transfer from Colloidal Quantum Dots to near-Infrared-Absorbing Tetraazaporphyrins for Enhanced Light Harvesting. *J. Phys. Chem. C* **2015**, *119*, 9754–9761.